Weierstraß-Institut
für Angewandte Analysis und Stochastik

Leibniz-Institut im Forschungsverbund Berlin e. V.

Preprint ISSN 2198-5855

A model for SEI-growth based on non-equilibrium thermodynamics

Manuel Landstorfer[1], Christoph Pohl[1], Ferran Brosa Planella[2], Kawa Manmi[2]

submitted: December 19, 2025

[1] Weierstrass Institute
Anton-Wilhelm-Amo Str. 39
10117 Berlin
Germany
E-Mail: manuel.landstorfer@wias-berlin.de

[2] Mathematics Institute
University of Warwick
Coventry, CV4 7AL
United Kingdom

No. 3250
Berlin 2025

2020 *Mathematics Subject Classification.* 78A57, 35Q92, 80A22, 35R37, 74A15.

Key words and phrases. Battery modelling, moving interface, solid electrolyte interphase, non-equilibrium thermodynamics, electrochemistry.

M. L. and C.P acknowledge funding by the Deutsche Forschungsgemeinschaft (DFG, German Research Foundation) under Germany´s Excellence Strategy – The Berlin Mathematics Research Center MATH+ (EXC-2046/1, project ID: 390685689) in project *PaA-2*. F. B-P. and K. M. acknowledge funding by The Faraday Institution in project *Multi-Scale Modelling* (EP/S003053/1 grant number FIRG059).

Edited by
Weierstraß-Institut für Angewandte Analysis und Stochastik (WIAS)
Leibniz-Institut im Forschungsverbund Berlin e. V.
Anton-Wilhelm-Amo-Straße 39
10117 Berlin
Germany

Fax: +49 30 20372-303
E-Mail: preprint@wias-berlin.de
World Wide Web: http://www.wias-berlin.de/

A model for SEI-growth based on non-equilibrium thermodynamics

Manuel Landstorfer, Christoph Pohl, Ferran Brosa Planella, Kawa Manmi

Abstract

The growth of the solid electrolyte interphase (SEI) is a dominant degradation mechanism in lithium-ion batteries, governing capacity fade, coulombic efficiency, and long-term performance. Despite extensive experimental investigation, quantitative understanding of SEI formation and evolution remains limited by its nanoscale thickness, complex chemistry, and strong sensitivity to operating conditions. Existing zero-dimensional models capture individual rate-limiting mechanisms but typically treat the SEI as an idealized interface layer, neglecting spatially resolved transport, solvent consumption, and dynamic interface motion.

In this work, we present a continuum-level model for SEI growth grounded in non-equilibrium thermodynamics. The SEI is treated as a distinct thermodynamic domain and modeled as a mixed ion–electron conductor, while the SEI–electrolyte interface is described as a moving boundary. The framework systematically derives transport laws and reaction kinetics from electrochemical potentials and interfacial free energies, ensuring thermodynamic consistency. A finite electrolyte reservoir is explicitly included, allowing solvent depletion to emerge naturally as a limiting mechanism for SEI growth.

The general formulation consists of coupled partial differential equations for all domains and interfaces. Under open-circuit voltage conditions, the system reduces to a tractable set of ordinary differential equations describing lithium concentration in the active material, solvent concentration, and SEI thickness. Numerical simulations under charging, rest, and cycling conditions reproduce experimentally observed features such as linear and $\sqrt{t}$ growth regimes, voltage shifts due to parasitic current consumption, capacity contributions from lithium stored in the SEI, and self-discharge during rest. Two distinct termination mechanisms—active lithium depletion and solvent exhaustion—are identified.

Overall, the proposed framework unifies multiple SEI growth mechanisms within a single thermodynamically consistent model and provides a mechanistic basis for improved lifetime prediction and optimization of battery formation and operating protocols.

DOI 10.20347/WIAS.PREPRINT.3250 Berlin 2025

1 Introduction

1.1 Batteries and Their Degradation Challenges

Batteries have become a critical component in modern energy systems, with their performance and longevity being crucial for cost-effective decarbonization of both energy grids and transport sectors. Understanding battery degradation is particularly critical as it directly impacts the economic viability and reliability of these applications. The development of high-capacity, durable, and fast-charging batteries has been instrumental in driving the adoption of electric vehicles (EVs) and enabling reliable renewable energy integration. Among various battery technologies for electric vehicles, lithium-ion batteries (LIBs) have emerged as the dominant choice, offering superior characteristics including high energy density (110-160 Wh/kg), excellent power density (1800 W/kg), and longer cycle life (500-1000 cycles) compared to conventional battery types [27, 17, 49, 63].

Battery degradation, defined as the progressive loss of capacity and power capability over time, manifests through multiple observable effects including capacity fade and power fade [17, 54]. The degradation mechanisms are particularly complex, involving three main external stress factors: temperature, state of charge (SoC) and load profile [38, 33], whose relative importance varies depending on the cell chemistry and operating conditions. These degradation effects have significant practical implications. From a user's perspective, capacity fade represents a reduction in the usable capacity of the cell, while power fade reduces the deliverable power after degradation [6]. The rapid market expansion for LIBs drives the need for improved understanding of degradation mechanisms [17, 72], as making LIBs last longer is crucial for improving lifetime economics and reducing environmental impacts. Understanding and accurately predicting battery degradation becomes key to increasing operational lifetime and enabling better battery management strategies [24].

Amongst all these degradation mechanisms, the formation and growth of the solid electrolyte interphase (SEI) represents one of the most fundamental and critical processes affecting battery life. The SEI forms initially on the first cycle of the cell, resulting in a 10% reduction in capacity, and continues to grow throughout the battery's life. The SEI layer growth has been found to approximately correlate with the square root of time, as solvent molecule diffusion slows down with increasing thickness [54, 41, 30, 41].

1.2 What is the SEI?

The solid electrolyte interphase (SEI) is a passive layer a few nanometres thick that forms instantaneously upon contact between the electrode and electrolyte, with its initial thickness governed by electron-tunneling range [51]. This layer has a significant growth during the first few cycles after assembling the battery, known as formation/ageing, but also continues to grow slowly throughout the battery's lifetime. The layer is thermodynamically unstable at both low and very high potentials versus $\mathrm{Li/Li^+}$, and forms through competing and parallel solvent and salt reduction processes [64] when the electrode potential falls below the electrochemical stability window of the electrolyte. These reduction processes result in the deposition of various organic and inorganic decomposition products on the electrode surface, causing the capacity and power of the battery to fade over time.

The resulting SEI exhibits a characteristic dual-layer nanostructure: a dense inorganic inner layer composed primarily of $\mathrm{Li_2CO_3}$, $\mathrm{Li_2O}$, and LiF nearest to the electrode surface, and a porous organic outer layer consisting mainly of lithium alkyl carbonates and other polymeric compounds facing the electrolyte. At the submicron level, this structure forms a complex mosaic where organic and inorganic

components are intimately mixed, creating what is known as a "polyhetero microphaseärchitecture [51]. The distribution of these components is highly dependent on factors including the type of carbon material used, electrolyte composition, and operating conditions [64]. The SEI layer serves as a crucial protective barrier that prevents further electrolyte decomposition while selectively allowing lithium ion transport, making it essential for long-term battery stability and performance.[40, 71, 1, 50, 5]

The SEI growth and characteristics evolve differently during formation and regular operation [17, 4]. During regular cycling, the battery experiences dynamic operating conditions including varying current rates, temperatures, and mechanical stresses from electrode volume changes, which significantly influence both SEI growth and properties [65]. The evolution of the SEI layer is governed by multiple factors: the electrolyte composition, including salt anions, solvents, and additives, determines its chemical composition and stability [70, 21]; the operating parameters such as current density affect formation rates [4]; and temperature impacts both formation kinetics and structure [25]. Throughout the battery's life, the SEI demonstrates a characteristic growth pattern that correlates approximately with the square root of time, as increasing thickness slows solvent molecule diffusion [54, 41].

The significance of SEI lies in both manufacturing economics and battery longevity. During production, establishing the initial SEI layer requires carefully controlled formation and aging protocols that account for 20% to 30% of total production costs [16, 8]. The process demands precise control of voltage ranges and temperatures to establish optimal protective layers. Beyond manufacturing, SEI growth represents one of the most fundamental degradation mechanisms in batteries, causing an initial capacity loss of approximately 10% and contributing to ongoing capacity fade [30, 41]. Understanding and optimizing SEI formation and growth thus presents a dual opportunity: reducing manufacturing costs while extending battery lifetime, both of which are crucial for improving the economic viability of battery technology [69, 48].

1.3 Experimental Approach

Studying SEI experimentally presents several significant challenges, including its complex structural composition, nanoscale dimensions, and high reactivity with air [1]. A key challenge in physical characterization is the substantial variation in measured SEI properties - for example, initial SEI film thickness can range from 450 to 980 nm depending on surface features and measurement technique [74]. For accurate characterization, researchers have developed and adapted numerous analytical techniques including X-ray Photoelectron Spectroscopy (XPS), X-ray Diffraction (XRD), Surface-Enhanced Raman scattering (SERS), Atomic Force Microscopy (AFM), and various other spectroscopic and microscopic methods [9, 51, 26]. However, these physical characterization methods must be carefully applied, as the exposure of SEI to moisture and oxygen during the teardown can lead to structural and chemical changes during analysis [20]. Current experimental techniques face fundamental limitations in achieving the necessary spatial resolution for nanometric structure analysis, temporal resolution for evolution studies, and compositional accuracy for complex chemistry characterization simultaneously [9]. Recent advances in operando techniques have enabled real-time monitoring of SEI evolution [17], with studies showing that formation conditions strongly influence interfacial stability [4]. High-precision coulometry studies have revealed that SEI growth kinetics follow approximately $t^{1/2}$ behaviour, with time and temperature being more influential than cycle count [61]. The integration of multiple complementary techniques has revealed that SEI properties show strong dependencies on factors such as electrolyte composition and cycling parameters [65, 9]. Recent studies have revealed that SEI growth shows complex dependencies on cycling parameters, with growth rates increasing with C-rate and exhibiting asymmetric behaviour between lithiation and delithiation [4]. While

SEI growth has traditionally been modeled using $t^{1/2}$ kinetics based on simple diffusion-limited surface layer growth assumptions, recent critical analysis suggests this relationship may be oversimplified. The time dependence appears to vary significantly between storage and cycling conditions, with different scaling relationships potentially dominating under different operating conditions [4]. This evolving understanding highlights the need for more sophisticated experimental techniques and models to accurately capture SEI formation and growth mechanisms.

1.4 Atomistic and Continuum Approaches

The modelling of SEI growth requires a multi-scale approach to capture both atomic-level reactions and macroscopic growth phenomena. At the atomic scale, density functional theory (DFT) and *ab initio* molecular dynamics (AIMD) have proven invaluable for understanding initial reduction mechanisms and electron transfer processes at the electrode-electrolyte interface. These methods can accurately predict reduction potentials and map complex reaction networks of electrolyte decomposition through simulations of solvent molecules, lithium ions, and electrode surfaces. However, they are computationally intensive and limited to simulating small systems and short timescales on the order of picoseconds [66, 9, 67].

To bridge this temporal and spatial gap, continuum models have been developed to describe SEI growth and properties at battery-relevant scales. Continuum-level models treat the SEI as a continuous medium and describe its growth through partial differential equations that incorporate transport phenomena, reaction kinetics, and thermodynamic considerations [7, 68, 59, 66]. These models often employ significant simplifications, treating the SEI as a uniform, homogeneous layer and reducing the complex physicochemical processes to rate-limiting mechanisms such as reaction kinetics or diffusion limitations. While these models can capture phenomena like ion transport and film growth kinetics over longer timescales, they necessarily make approximations that overlook atomic-scale complexity and chemical specificity. This highlights a fundamental challenge in SEI modelling - the need to balance computational tractability with physical accuracy across multiple time and length scales while maintaining sufficient resolution to capture the critical formation period.

Zero-dimensional models represent a deliberate simplification that ignores most of the SEI's complex morphology and detailed transport processes. These models focus on one or a few rate-limiting mechanisms, typically related to reactions occurring at the SEI-electrode or SEI-electrolyte interface [58, 73, 53, 43, 62, 52, 60, 62, 29, 32]. While such simplifications might seem limiting, strategic choices about which physical processes to include can maintain strong predictive capability with minimal parameters. For instance, models using as few as four fitted parameters have successfully predicted capacity fade across multiple temperatures and operating conditions by focusing on key SEI formation mechanisms [18, 33]. They can be categorized into two primary groups: solvent-limited and electron-limited models. Solvent-limited models encompass mechanisms like solvent diffusion and reaction limitations, while electron-limited models consider phenomena such as electron migration, tunnelling, and interstitial diffusion [73, 53, 56]. Some advanced approaches have demonstrated that combining multiple limiting mechanisms - such as coupling solvent diffusion with reaction kinetics - can successfully predict capacity fade across different operating modes while maintaining model simplicity [56, 32]. These models have been extensively studied for long-term SEI growth. However, their applicability to the formation period, where complex multi-phase growth and rapid chemical evolution occur, remains largely unexplored [42]. Most zero-dimensional models have been developed with a focus on long-term capacity fade over hundreds or thousands of cycles, rather than the initial formation period [39, 3]. Early modelling work showed that continuous SEI formation during charging could be captured through

coupled reaction-transport equations, though like many subsequent models, it emphasized long-term behavior over initial formation dynamics [55, 31]. This creates a significant gap in our understanding, as the formation cycle involves distinct physicochemical processes and typically exhibits much higher capacity loss compared to subsequent cycles [1, 2, 44]. The challenge lies in developing models that can accurately capture both the rapid initial SEI formation and the slower long-term growth while maintaining computational efficiency [42].

1.5 Non-equilibrium Thermodynamics Approaches

In this work, we present a comprehensive continuum-level model for solid electrolyte interphase (SEI) growth based on non-equilibrium thermodynamics, building upon Landstorfer's foundational work on boundary conditions for electrochemical interfaces [36] and cell voltage analysis [35]. This theoretical framework derives constitutive equations from fundamental principles of non-equilibrium thermodynamics, where transport processes and chemical reactions are governed by gradients in electrochemical potentials and affinities. The framework treats interfaces as distinct thermodynamic domains with their own free energy functionals, enabling systematic derivation of surface chemical potentials and reaction affinities that lead to thermodynamically consistent descriptions of interfacial processes.

Building on this foundation, we model the SEI as a thermodynamic domain characterized by its own free energy functional, incorporating both chemical and electrical contributions. The coupling between the SEI, electrode, and electrolyte domains is derived systematically through interface conditions that emerge from the non-equilibrium thermodynamic treatment of surface reactions and transport processes. The framework establishes clear relationships between surface chemical potentials and measurable quantities like cell voltage and reaction rates [35], while enabling natural incorporation of multiple reaction pathways and transport mechanisms. This approach provides a rigorous basis for developing Butler-Volmer-type equations that account for concentration dependencies and surface effects in battery system [37].

1.6 Outline

In section 2 we derive the general model for SEI growth, which couples ion and electron transport in the various phases, intercalation and formation reactions reactions as well as solid state diffusion of intercalated ions in the active phase. After sketching the domain setups and stating the specific species in each domain, we state in section 2.1 the general balance equations for charged species, and in section 2.2 their closure by non-equilibrium thermodynamics, i.e. flux relations expressed in gradients of electro-chemical potentials. In section 2.3 we discuss the impact of space charge layers, which may arise at all interfaces, and employ some simplifications for the subsequent paper. In sections 2.4 to 2.6 we state the material models for the electrolyte, the active phase, and the SEI as mixed ion-electron conductor, respectively, and formulate in section 2.7 the interface conditions for the SEI-electrolyte interface, including the moving interface description, followed by interface conditions of the SEI-active phase interface in section 2.8. In section 2.9 we derive the relation for the measurable cell voltage of the considered half cell and state in section 2.10 the initial conditions.

Section 3 then simplifies the derived equation system to a 1D geometrical setup, where we further apply a non-dimensionalization with respect to the C-rate. This allows us to systematically deduce open circuit voltage conditions, yielding an ODE system for the SEI growth in section 3.4. We discuss our findings of the three coupled ODEs, which are connected via the SEI formation reaction, cf. section 3.4.4.

In section 4 we provide finally various numerical examples of the derived SEI growth model.

We consider in section 4.1 a transient current profile where the electrode is charged until a certain cell voltage, and then disconnected from the external circuit. However, due to the internal reconfiguration, e.g. self-discharge, we can show that the SEI keeps growing, and we discuss this aspect for various scaling limits of the SEI formation reaction rate. In addition, we show the impact of the electrolyte domain on the SEI formation reaction and discuss the consumption of (bulk) solvent. Subsequently, we discuss in section 4.2 periodic cycling conditions, which requires are careful re-formulation of the cycle numbers and the corresponding transient current profile when SEI growth is present. In section 4.3 we compare finally our results to experimental results and draw in section 5 conclusions on our modeling and simulation work.

2 Modeling of SEI Growth Based on Non-equilibrium Thermodynamics

In this section we present a comprehensive 3D model for solid electrolyte interphase (SEI) growth based on non-equilibrium thermodynamics. The model is derived from fundamental principles of continuum thermodynamics, where transport processes and chemical reactions are governed by gradients in electrochemical potentials and affinities. We consider three domains for the transport equations: the intercalation electrode $\Omega^{\mathtt{A}}$, the SEI $\Omega^{\mathtt{I}}$, and the electrolyte $\Omega_{\mathtt{E}}$. We will also consider a lithium metal counter electrode to close the electrochemical system, but its behavior will be only represented via a boundary condition. The geometry of each domain can be arbitrarily complex, with the only constraint that the active material and the electrolyte do not share a boundary (i.e. all the lithium interchange between them is via the SEI layer), and we denote as $\Sigma^{\mathtt{AI}}$ the interface between active material and SEI, and as $\Sigma^{\mathtt{IE}}$ the interface between SEI and electrolyte. The 1D sketch in fig. 1 is thus illustrative. Each domain is composed of several species defined as the set $\mathcal{I}^i$ for $i \in \mathtt{A}, \mathtt{I}, \mathtt{E}$.

The model derivation is structured as follows. First, in sections 2.1 to 2.3, we present the general modelling framework based on non-equilibrium thermodynamics. Then, in sections 2.4 to 2.10, we apply this framework to each domain to derive their governing equations. Although the notation is introduced as needed in each section, there are a couple of general aspects worth discussing at this stage. First, we will use subscripts in the variables and parameters of the problem to distinguish the various species and domains. As some species are common to several domains, we introduce a nested subscript notation: for example, the molar density of lithium ions in the electrolyte is denoted by $n_{\mathtt{E}_C}$ (note we drop any further subscripts in the species for simplicity). Second, the evaluation of some quantity u at the j-side of an interface Σ_i will be written as $u\big|_i^j$, for instance $u\big|_{\mathtt{AI}}^{\mathtt{I}}$.

2.1 General Transport Equations

We consider each domain Ω as a mixture of species $\alpha \in \mathcal{I}$ for which we have balance equations

$$\frac{\partial n_\alpha}{\partial t} = -\operatorname{div}\left(n_\alpha \mathbf{v} + \mathbf{J}_\alpha\right), \tag{1}$$

where $n_\alpha(\mathbf{x}, t)$ denotes the molar density and $\mathbf{J}_\alpha$ the molar flux of constituent α. The velocity field $\mathbf{v}$ is the barycentric velocity of the mixture, which usually serves as reference for diffusional fluxes. Note, however, that other reference velocities can also be considered. The mass density $\rho = \sum_\alpha m_\alpha$, where

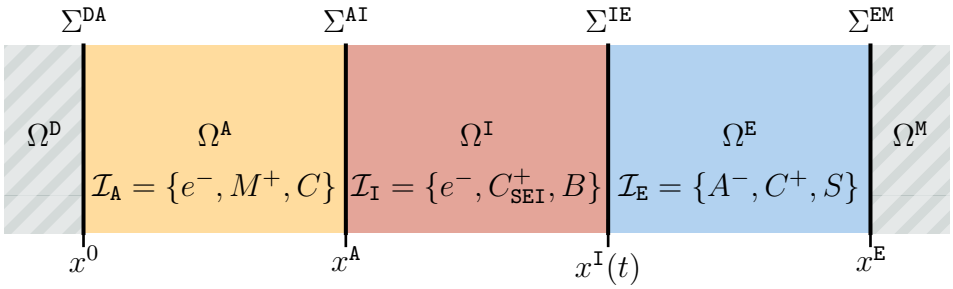

Figure 1: Sketch of the electrode setup, consisting of current collector | intercalation electrode | SEI | electrolyte | counter electrode.

m_α is the molar mass of constituent $\alpha \in \mathcal{I}$ satisfies,

$$\frac{\partial \rho}{\partial t} = -\operatorname{div}(\rho \mathbf{v}) , \tag{2}$$

whereby [22]

$$\sum_{\alpha \in \mathcal{I}} m_\alpha \mathbf{J}_\alpha = \mathbf{0}. \tag{3}$$

Since we consider charged matter, this is accompanied with Poisson's equation

$$-\operatorname{div}(\varepsilon_0(1+\chi)\nabla\varphi) = e_0 \sum_{\alpha \in \mathcal{I}} z_\alpha n_\alpha =: q , \tag{4}$$

where φ denotes the electrostatic potential, χ the dielectric susceptibility, e_0 the elementary charge, z_α the charge number, and q the charge density. Poisson's equation is complemented by the charge balance which, in its general form, reads

$$\frac{\partial q}{\partial t} = -\operatorname{div}(q\mathbf{v} + \mathbf{J}_{\mathtt{q}}) \tag{5}$$

and

$$\mathbf{J}_{\mathtt{q}} = e_0 \sum_{\alpha \in \mathcal{I}} z_\alpha \mathbf{J}_\alpha \tag{6}$$

the (free) charge flux.

Throughout this work, we consider stationary momentum balance, i.e.

$$\nabla p = -q\nabla\varphi , \tag{7}$$

which reflects the balance between the (electrostatic) Lorentz force and the mechanical counterforce by a gradient of the (mechanical) pressure p.

We refer to [15, 23, 45, 46, 22] for details on the full non-equilibrium thermodynamics of charged matter.

2.2 Free Energy Densities and Chemical Potential Functions

The transport equations introduced in the previous section only tell that the various species are conserved. We now need to discuss how species move around and react with each other. The mixtures in each domain Ω_α are modelled by continuum non-equilibrium thermodynamics [22]. We denote with

$\rho\psi = \rho\psi(T, (n_\alpha)_{\alpha\in\mathcal{I}})$ the free energy density of the mixture and with

$$\mu_\alpha = \frac{\partial \rho\psi}{\partial n_\alpha} \qquad \alpha \in \mathcal{I} \tag{8}$$

the chemical potential (function) of constituent $\alpha \in \mathcal{I}$.

A core ingredient of non-equilibrium thermodynamics is to state necessary conditions for fluxes and reaction rates to ensure the second law of thermodynamics, i.e. a non-negative entropy production. For the molar fluxes $\mathbf{J}_\alpha$, this essentially means

$$\mathbf{J}_\alpha = -\sum_{\beta\in\mathcal{I}} \mathbf{M}_{\alpha\beta}\nabla\tilde{\mu}_\beta \qquad \tilde{\mu}_\beta := \mu_\beta + e_0 z_\beta \varphi \,, \tag{9}$$

with a symmetric, positive semi-definite matrix $\mathbf{M} = (\mathbf{M}_{\alpha\beta})_{\alpha\beta}$, whereby the entropy production due to diffusional fluxes satisfies [22]

$$\sigma^{\mathbf{J}} := -\sum_{\alpha\in\mathcal{I}} \mathbf{J}_\alpha^T \cdot \nabla\tilde{\mu}_\alpha = \sum_{\alpha\in\mathcal{I}}\sum_{\beta\in\mathcal{I}} (\nabla\tilde{\mu}_\beta)^T \cdot \mathbf{M}_{\alpha\beta} \cdot \nabla\tilde{\mu}_\alpha \geq 0 \,. \tag{10}$$

Note that the constraint

$$\sum_{\alpha\in\mathcal{I}} m_\alpha \mathbf{J}_\alpha = \mathbf{0} \tag{11}$$

actually reduces the number of independent fluxes by one.

Let's now turn our attention to how species react. Consider a chemical reaction $R_k (k = 1, \ldots, N_R)$, i.e.

$$\sum_{\alpha\in\mathcal{I}} \nu'_{\alpha,k} \mathrm{A}_\alpha \rightleftharpoons \sum_{\alpha\in\mathcal{I}} \nu''_{\alpha,k} \mathrm{A}_\alpha \,, \tag{12}$$

where

$$\lambda_k := -\sum_{\alpha\in\mathcal{I}} \nu_{\alpha,k}\mu_\alpha \quad \text{with} \quad \nu_{\alpha,k} := \nu''_{\alpha,k} - \nu'_{\alpha,k} \tag{13}$$

is the affinity[1] of the reaction R_k , the entropy production due to chemical reactions is [12, 46, 22]

$$\sigma^R = \sum_{k=1}^{N_R} \lambda_k \cdot R_k \geq 0 \,. \tag{14}$$

Hence,

$$R_k = L_k \cdot f_{\mathtt{BV}}(\lambda_k) \quad \text{with} \quad f_{\mathtt{BV}}(z) := \mathsf{e}^{\alpha\frac{z}{k_\mathtt{B}T}} - \mathsf{e}^{-(1-\alpha)\frac{z}{k_\mathtt{B}T}} \,, \tag{15}$$

ensures $\sigma^R \geq 0$. We call $f_{\mathtt{BV}}$ a Butler-Volmer-type relation with the charge transfer coefficient α and emphasize that $f_{\mathtt{BV}}(z) > 0$ for $z > 0$. Since charge is conserved in chemical reactions, we have

$$\lambda_k = -\sum_{\alpha\in\mathcal{I}} \nu_{\alpha,k}\mu_\alpha = -\sum_{\alpha\in\mathcal{I}} \nu_{\alpha,k}\tilde{\mu}_\alpha \,. \tag{16}$$

2.3 Electro-Neutrality and Space Charge Layers at Interfaces

Before we can write the specific equations for each domain, we need to discuss what occurs at the interfaces. A common and very useful simplification in the coupled equation system is the (strong)

[1] We follow the IUPAC definition of reaction affinity here. Note, however, that among the literature also definitions with a plus sign are found.

electro-neutrality condition

$$q = \sum_{\alpha} e_0 z_\alpha n_\alpha = 0 \,, \tag{17}$$

which holds outside of space charge layers that form at the interface between two phases Ω_i and Ω_j, where mobile charge carriers are present. The following discussion is supposed to hold for the active phase–SEI interface as well as for the SEI–electrolyte interface.

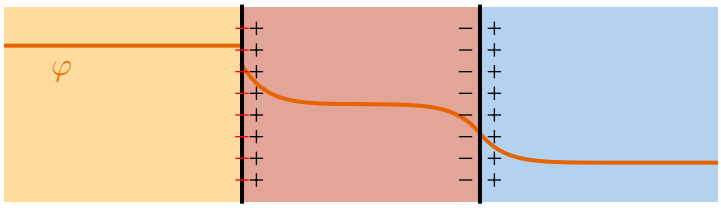

Figure 2: Space charge layers inside the electrode

The electro-neutrality condition can be derived through an asymptotic expansion of the balance equations at the interface Σ_{ij}, introducing the Debye-length as a small scale parameter. We briefly summarize the key conclusions and refer to [47, 34, 36, 13, 14, 35] for further details on the modeling, validation, and asymptotic derivation.

In principle, we have in all regions space charge layers, where we denote by x_{ij}^i the respective point out of the space charge layer, e.g. in the electrolyte at the interface $\mathtt{IE}$ we have $x_{\mathtt{IE}}^{\mathtt{E}}$ where a charge $Q_{\mathtt{IE}}^{\mathtt{E}}$ is stored and a potential drop $\underset{s}{\varphi}|_{\mathtt{IE}} - \varphi|_{x_{\mathtt{IE}}^{\mathtt{E}}} =: U_{\mathtt{IE}}^{\mathtt{E}}$ occurs. The syntax holds true for the four space charge layers we expect, i.e. the two space charge layers (SCL) at $\mathtt{AI}$ and the two at $\mathtt{IE}$. With the resolved double layer, we assume that electric potential at the interface is continuous, i.e. $[\![\underset{s}{\varphi}]\!] = 0$.

The domains Ω_i and Ω_j denote electro-neutral domains whereas $\Sigma_{ij}^{\mathtt{DL}}$ denotes the interfaces between Ω_i and Ω_j which covers the actual (singular) surface Σ_{ij} as well as the space charge layers where $q \neq 0$, denoted by $\Omega_i^{\mathtt{SCL}}$ and $\Omega_j^{\mathtt{SCL}}$, adjacent to the surface, i.e. $\Sigma_{ij}^{\mathtt{DL}} = \Sigma_{ij} \cup \Omega_i^{\mathtt{SCL}} \cup \Omega_j^{\mathtt{SCL}}$. The typeface $^{\mathtt{DL}}$ accounts for the fact that the interface $\Sigma_{ij}^{\mathtt{DL}}$ captures the double layer, formed by the two space charge layers, at the interface. We denote with we x_{ij}^k, $k \in \{i, j\}$ the respective point out of the space charge layer and the with $\underset{s}{x_{ij}}$ the position of the actual surface Σ_{ij}. If it is clear from the context, we drop the subscript ij for clarity. Note that we sketch in the following the 1D-planar case, which implicitly assumes that the curvature of the interface is small compared to the Debye length, but emphasize that the discussion is also possible for generally curved interfaces [11].

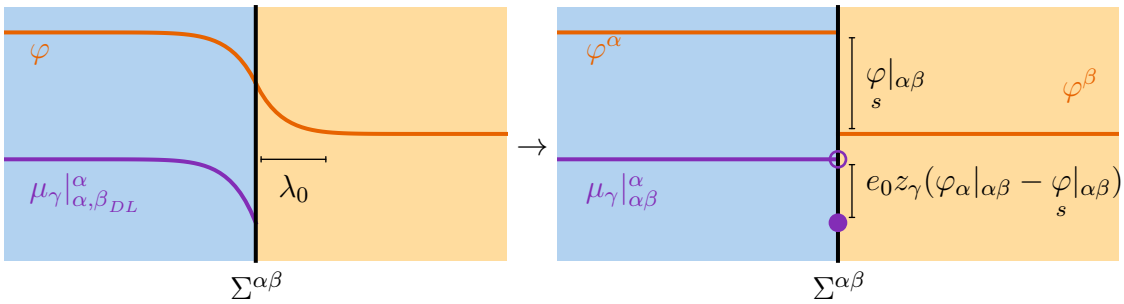

Figure 3: Asymptotic behaviour for $\lambda_0 \ll |x^{\mathtt{A}} - x^0|$.

We now define

$$Q^k = \int_{\underset{s}{x}}^{x^k} q^k \, \mathrm{d}x \tag{18}$$

as the (surface) charge store in the space charger layer $[x_{ij}, x_{ij}^k]$ and

$$\underset{s}{\varphi} - \varphi|_{x^k} =: U^k \tag{19}$$

as the potential drop across the space charge layer $\Omega_k^{\mathtt{SCL}}$, both for $k = i, j$. The electro-neutrality condition is derived by effectively decomposing the phase in the electro-neutral domain and in space charge layers. For the electro-neutral domain, effective boundary conditions can thus be derived by integrating the charge balance along the space charge layer, i.e.

$$\partial_t q_k = -\partial_x J_{k_q} \quad \Rightarrow -J_{k_q}|_{\underset{s}{x}} + J_{k_q}|_{x^k} = \frac{\mathrm{d}Q^k}{\mathrm{d}t} \tag{20}$$

where the term $J_{k_q}|_{\underset{s}{x}}$ is substituted by the actual chemical reactions occuring at the surface (cf. sections 2.7 and 2.8). For the charge Q^k stored in the space charge layer, a representation $Q^k = \hat{Q}^k(U^k)$ can be derived which introduces the capacitive charge flow

$$\frac{\mathrm{d}Q^k}{\mathrm{d}t} = \hat{C}^k(U^k) \cdot \frac{\mathrm{d}U^k}{\mathrm{d}t} \qquad \text{with} \qquad \hat{C}^k(U^k) := \frac{\mathrm{d}Q^k}{\mathrm{d}U^k}, \tag{21}$$

and we refer to [36] for details. Hence, for electro-neutral domains Ω^k we do have in general boundary conditions of the type

$$J_{k_q}|_{x^k} = J_{k_q}|_{\underset{s}{x}} + \hat{C}^k(U^k) \cdot \frac{\mathrm{d}U^k}{\mathrm{d}t} \, . \tag{22}$$

However, since capacitive effects essentially scale with the transient potential variation $\frac{\mathrm{d}U^k}{\mathrm{d}t}$, we consider throughout this work that capactive contributions are neglible [19, 35]. Note, however, that space charge layers are nevertheless present and the charge stored in the respective layer can still be computed from $Q^k = \hat{Q}^k(U^k)$.

It can be shown using asymptotic methods that the double layer remains in diffusional equilibrium, even when current passes through the space charge layer, whereby

$$\nabla \mu_\alpha + e_0 z_\alpha \nabla \varphi = 0 \qquad \mathbf{x} \in \Omega_k^{\mathtt{SCL}} \, . \tag{23}$$

This has an impact in two directions. First, it allows the determination of the function $\hat{Q}^k(U^k)$ since eq. (23) serves to determine the mole fractions y_α in terms of φ and p. Incompressibility relates n_α to y_α, whereby the charge density q can be written as $q = \hat{q}(\varphi, p)$. This allows to solve the coupled Poisson-Momentum equation system (4) and (7), which finally yields $Q^k = \hat{Q}^k(U^k)$. We refer to [34] for the detailed derivation, but emphasize here again that the mechanical pressure is a key component in space charge layers.

Secondly, eq. (23) allows to trace back the chemical potential function $\underset{s}{\mu_\alpha}$ on the surface Σ_{ij} to the chemical potential $\mu_\alpha|_{x^k}$ outside the space charge layer, i.e.

$$\underset{s}{\mu_\alpha} = \mu_\alpha|_{x^k} - e_0 z_\alpha (\underset{s}{\varphi} - \varphi|_{x^k}) \, . \tag{24}$$

This is of special importance for surface reactions which occur actually *at* a surface, while we seek expressions of the reaction rates in terms of (electro-)chemical potential functions *outside* of the adjacent space charge layers, in order to be compatible with the balance equations stated in electro-neutral domains. This is explained in more detail in section 2.7.

2.4 Electrolyte

Now that we have introduced the general modelling framework, we can focus on the specific equations for each domain, starting with the electrolyte. The electrolyte is a mixture $\mathcal{I}_{\mathrm{E}} = \{\mathrm{E}_S, \mathrm{E}_A, \mathrm{E}_C\}$ of solvent E_S, anions E_A and cations E_C with their corresponding molar densities n_α in the domain Ω^{E}. We consider the electrolyte to be an incompressible solvation mixture [10, 34], i.e. an incompressible liquid where each ion $\alpha \in \mathcal{I}_{\mathrm{E}}^0 = \{\mathrm{E}_A, \mathrm{E}_C\}$ binds κ_α solvent molecules. The solvation effect has various impacts on the mixture theory, and we refer to [10, 34] for detailed discussions.

The chemical potential functions of the electrolyte species are [10, 34]

$$\mu_\alpha = g_\alpha + k_{\mathrm{B}} T \ln y_\alpha + v_\alpha p \qquad \alpha \in \mathcal{I}_{\mathrm{E}}\,, \tag{25}$$

where g_α is the (constant) molar Gibbs energy, k_{B} the Boltzmann constant, T the temperature, y_α the mole fraction, satisfying

$$y_\alpha = \frac{n_\alpha}{n_{\mathrm{E}_{\mathrm{tot}}}}, \quad n_{\mathrm{E}_{\mathrm{tot}}} = n_{\mathrm{E}_S} + n_{\mathrm{E}_A} + n_{\mathrm{E}_C}, \quad \sum_{\alpha \in \mathcal{I}_{\mathrm{E}}} y_\alpha = 1\,, \tag{26}$$

and v_α being the partial molar volume.

The second term of the chemical potential corresponds to the entropy of mixing [10], while the third term is the mechanical contribution due to the incompressibility. Note that v_α captures also the solvation effect, whereby in general $v_{\mathrm{E}_A,\mathrm{E}_C} \gg v_S$.

The incompressibility entails the constraint [10]

$$\sum_{\alpha \in \mathcal{I}_{\mathrm{E}}} n_\alpha v_\alpha = 1\,, \tag{27}$$

whereby we can write

$$n_\alpha = \frac{y_\alpha}{\sum_{\beta \in \mathcal{I}_{\mathrm{E}}} v_\beta y_\beta}\,, \tag{28}$$

as well as the electrolyte pressure p_{E} as an independent variable.

We assume throughout this work that

$$\frac{m_\alpha}{m_{\mathrm{E}_S}} = \frac{v_\alpha}{v_{\mathrm{E}_S}}\,, \qquad \alpha \in \{\mathrm{E}_A, \mathrm{E}_C\}\,, \tag{29}$$

whereby not only mass, but also volume is conserved during solvation reactions. This simplifies the resulting equation system a bit, but is not a neccessary constraint in general.

The molar mass of a solvated ion is $m_\alpha = \hat{m}_\alpha + \kappa_\alpha m_{\mathrm{E}_S}$, where $\hat{m}_\alpha$ is the molar mass of the central ion, κ_α the solvation number, and m_{E_S} the molar mass of the solvent. Hence

$$\frac{m_\alpha}{m_{\mathrm{E}_S}} = \frac{\hat{m}_\alpha}{m_{\mathrm{E}_S}} + \kappa_\alpha\,, \qquad v_\alpha = \frac{\hat{m}_\alpha}{m_{\mathrm{E}_S}} v_{\mathrm{E}_S} + \kappa_\alpha v_{\mathrm{E}_S}\,. \tag{30}$$

If $m_{\mathrm{E}_S} \gg \hat{m}_\alpha$, we can approximate $v_\alpha \approx \kappa_\alpha v_{\mathrm{E}_S}$, which we consider for the rest of this work. Further, we consider a monovalent salt, whereby $z_{\mathrm{E}_A} = -z_{\mathrm{E}_C}$ and similar solvation numbers of cations and anions, i.e. $\kappa_{\mathrm{E}_A} = \kappa_{\mathrm{E}_C} =: \kappa_{\mathrm{E}}$.

For the electrolyte phase, we have the electric potential φ_{E}, the pressure p_{E}, the cation mole fraction y_{E_C} and the anion mole fraction y_{E_A} as a complete the set of independent variables, i.e. $(y_{\mathrm{E}_A}, y_{\mathrm{E}_C}, \varphi_{\mathrm{E}}, p_{\mathrm{E}})$.[2]

For an electrolyte consisting of three species, i.e. anions, cations and solvent, we have two independent

[2] Note that incompressibility yields $y_{\mathrm{E}_S} = 1 - y_{\mathrm{E}_A} - y_{\mathrm{E}_C}$.

fluxes ($\alpha \in \{\mathrm{E}_A, \mathrm{E}_C\}$),

$$\mathbf{J}_\alpha = -\boldsymbol{M}_{\alpha,\mathrm{E}_A}\nabla\hat{\mu}_{\mathrm{E}_A} - e_0 z_A \boldsymbol{M}_{\alpha,\mathrm{E}_A}\nabla\varphi_{\mathrm{E}} - \boldsymbol{M}_{\alpha,\mathrm{E}_C}\nabla\hat{\mu}_{\mathrm{E}_C} - e_0 z_C \boldsymbol{M}_{\alpha,\mathrm{E}_C}\nabla\varphi_{\mathrm{E}}\,, \tag{31}$$

where $\hat{\mu}_\alpha$ is the *effective* chemical potential of the ion in its solvated state, i.e.

$$\hat{\mu}_\alpha = \mu_\alpha - \kappa_\alpha \mu_{\mathrm{E}_S}\,, \tag{32}$$

and the solvent flux satisfies

$$\mathbf{J}_{\mathrm{E_s}} = -\sum_{\alpha\in\{\mathrm{E}_A,\mathrm{E}_C\}} \frac{m_\alpha}{m_{\mathrm{E}_S}}\mathbf{J}_\alpha\,. \tag{33}$$

Note that the solvent still satisfies the balance equation

$$\frac{\partial n_{\mathrm{E}_S}}{\partial t} = -\operatorname{div}\mathbf{J}_{\mathrm{E_s}}\,, \tag{34}$$

which is exploited in section 3.4.2.

The mobilities $\boldsymbol{M}_{\alpha,\beta} \in \mathbb{R}^{3\times3}$ are connected to the constant diffusion coefficients $\boldsymbol{D}_{\alpha,\alpha}$ and the friction $\boldsymbol{F}_{\mathrm{E}_A,\mathrm{E}_C} = \boldsymbol{F}_{\mathrm{E}_C,\mathrm{E}_A}$ via

$$\boldsymbol{M}_{\mathrm{E}_A,\mathrm{E}_A} = \frac{n_{\mathrm{E}_A}}{k_{\mathrm{B}}T}\boldsymbol{D}_{\mathrm{E}_A,\mathrm{E}_A}, \quad \boldsymbol{M}_{\mathrm{E}_C,\mathrm{E}_C} = \frac{n_{\mathrm{E}_C}}{k_{\mathrm{B}}T}\boldsymbol{D}_{\mathrm{E}_C,\mathrm{E}_C}\,, \quad \boldsymbol{M}_{\mathrm{E}_A,\mathrm{E}_C} = \frac{y_{\mathrm{E}_C}y_{\mathrm{E}_A}}{n_{\mathrm{E_{tot}}}k_{\mathrm{B}}T}\boldsymbol{F}_{\mathrm{E}_A,\mathrm{E}_C}\,. \tag{35}$$

Note that for the simpler Nernst–Planck flux approach [15, 57] the friction coefficients $F_{A,C}$ vanish, yielding

$$\mathbf{J}_\alpha = \boldsymbol{D}_{\alpha,\alpha}\frac{n_\alpha}{k_{\mathrm{B}}T}\nabla\tilde{\mu}_\alpha\,, \qquad \alpha = \mathrm{E}_A, \mathrm{E}_C\,, \tag{36}$$

with a constant diffusion coefficients $D_{\alpha,\alpha}$.

We consider for the electrolyte the strong electro-neutrality condition

$$q_{\mathrm{E}} = \sum_\alpha e_0 z_\alpha n_\alpha = 0 \quad \Leftrightarrow \qquad y_{\mathrm{E}_C} = -\frac{z_{\mathrm{E}_A}}{z_{\mathrm{E}_C}}y_{\mathrm{E}_A} =: y_{\mathrm{E}}\,, \tag{37}$$

which holds outside of potential space charge layers at electrode-electrolyte interfaces. More details on the electro-neutrality condition and the space charge layers forming at the respective interfaces are given in section 2.3.

The electro-neutrality ($y_{\mathrm{E}_A} = y_{\mathrm{E}_C}$) implies $\nabla\hat{\mu}_{\mathrm{E}_A} = \nabla\hat{\mu}_{\mathrm{E}_C}$ and we can compute

$$\nabla\hat{\mu}_{\mathrm{E}_C} = k_{\mathrm{B}}T\,\frac{1}{y_{\mathrm{E}}}\Gamma_{\mathrm{E}}\cdot\nabla y_{\mathrm{E}} \quad \text{with} \quad \Gamma_{\mathrm{E}} := 1 + \kappa_{\mathrm{E}_C}\frac{2y_{\mathrm{E}}}{(1-2y_{\mathrm{E}})}\,, \tag{38}$$

and call Γ_{E} thermodynamic factor [37, 28]. Hence we can write the cation flux $\mathbf{J}_{\mathrm{E_c}}$ and the electrolytic charge flux $\mathbf{J}_{\mathrm{E_q}}$ as

$$\begin{aligned}\mathbf{J}_{\mathrm{E_c}} =& -(\boldsymbol{D}_{C,C} + \boldsymbol{F}_{C,A})n_{\mathrm{E_{tot}}}\Gamma_{\mathrm{E}}\nabla y_{\mathrm{E}_C}\,,\\ &-\frac{e_0}{k_{\mathrm{B}}T}n_{\mathrm{E_{tot}}}y_{\mathrm{E}_C}(\boldsymbol{D}_{C,C} - \boldsymbol{F}_{C,A})\nabla\varphi_{\mathrm{E}}\,,\end{aligned} \tag{39a}$$

$$\begin{aligned}\mathbf{J}_{\mathrm{E_q}} =& -e_0(\boldsymbol{D}_{C,C} - \boldsymbol{D}_{A,A})n_{\mathrm{E_{tot}}}\Gamma_{\mathrm{E}}\nabla y_{\mathrm{E}_C}\,,\\ &-\frac{e_0^2}{k_{\mathrm{B}}T}n_{\mathrm{E_{tot}}}y_{\mathrm{E}_C}\big(\boldsymbol{D}_{C,C} + \boldsymbol{D}_{A,A} - 2\boldsymbol{F}_{A,C}\big)\nabla\varphi_{\mathrm{E}}\,.\end{aligned} \tag{39b}$$

An equivalent but more commonly used set of transport parameters is

$$\boldsymbol{\Lambda}_{\mathrm{E}} = \frac{e_0^2}{k_{\mathrm{B}}T}\left(\boldsymbol{D}_{A,A} + \boldsymbol{D}_{C,C} - 2\boldsymbol{F}_{A,C}\right)\,, \tag{40a}$$

$$\boldsymbol{t}_{\mathtt{E}_C} = \frac{\boldsymbol{D}_{C,C} - \boldsymbol{F}_{C,A}}{\boldsymbol{D}_{C,C} + \boldsymbol{D}_{A,A} - 2\boldsymbol{F}_{A,C}}\,, \tag{40b}$$

$$\boldsymbol{D}_{\mathtt{E}} = \frac{2(\boldsymbol{D}_{A,A}\boldsymbol{D}_{C,C} - \boldsymbol{F}_{AC}^2)}{\boldsymbol{D}_{C,C} + \boldsymbol{D}_{A,A} - 2\boldsymbol{F}_{A,C}}\,, \tag{40c}$$

$$\boldsymbol{S}_{\mathtt{E}} = e_0(\boldsymbol{D}_{C,C} - \boldsymbol{D}_{A,A})\,, \tag{40d}$$

which satisfy the constraint

$$\frac{k_{\mathtt{B}}T}{e_0}(2\boldsymbol{t}_{\mathtt{E}_C} - 1) = \frac{\boldsymbol{S}_{\mathtt{E}}}{\boldsymbol{\Lambda}_{\mathtt{E}}}\,. \tag{41}$$

The fluxes from eq. (39) can then be written as

$$\mathbf{J}_{\mathtt{E_c}} = -\,(\boldsymbol{D}_{\mathtt{E}} + \boldsymbol{t}_{\mathtt{E}_C}\frac{\boldsymbol{S}_{\mathtt{E}}}{e_0})n_{\mathtt{E}_{\mathrm{tot}}}\Gamma_{\mathtt{E}}\nabla y_{\mathtt{E}_C} - n_{\mathtt{E}_{\mathrm{tot}}}y_{\mathtt{E}}\frac{1}{e_0}\boldsymbol{t}_{\mathtt{E}_C}\boldsymbol{\Lambda}_{\mathtt{E}}\nabla\varphi_{\mathtt{E}}\,, \tag{42a}$$

$$= -\,\boldsymbol{D}_{\mathtt{E}}n_{\mathtt{E}_{\mathrm{tot}}}\Gamma_{\mathtt{E}}\nabla y_{\mathtt{E}_C} + \frac{1}{e_0}\boldsymbol{t}_{\mathtt{E}_C}\mathbf{J}_{\mathtt{E_q}}\,, \tag{42b}$$

$$\mathbf{J}_{\mathtt{E_q}} = -\,\boldsymbol{S}_{\mathtt{E}}\cdot n_{\mathtt{E}_{\mathrm{tot}}}\Gamma_{\mathtt{E}}\nabla y_{\mathtt{E}_C} - n_{\mathtt{E}_{\mathrm{tot}}}y_{\mathtt{E}}\boldsymbol{\Lambda}_{\mathtt{E}}\nabla\varphi_{\mathtt{E}}\,. \tag{42c}$$

The balance equations for the ion concentration and electric potential in the electrolyte are

$$\frac{\partial n_{\mathtt{E}_C}}{\partial t} = -\,\mathrm{div}\;\mathbf{J}_{\mathtt{E_c}} \qquad \mathbf{x}\in\Omega^{\mathtt{E}}\,, \tag{43a}$$

$$0 = -\,\mathrm{div}\;\mathbf{J}_{\mathtt{E_q}} \qquad \mathbf{x}\in\Omega^{\mathtt{E}}\,. \tag{43b}$$

2.5 Active Material Phase

The active material consists of a lattice species $\mathtt{A}_M$, electrons $\mathtt{A}_e$ and the intercalated lithium $\mathtt{A}_C$, forming the index set $\mathcal{I}_{\mathtt{A}} = \{\mathtt{A}_M, \mathtt{A}_e, \mathtt{A}_C\}$. The chemical potential of the lithium in the active phase is

$$\mu_{\mathtt{A}_C} = g_{\mathtt{A}_C} + k_{\mathtt{B}}T\, f_{\mathtt{A}}(y_{\mathtt{A}_C})\,, \tag{44a}$$

$$f_{\mathtt{A}}(y_{\mathtt{A}_C}) = \ln\left(\frac{y_{\mathtt{A}_C}}{1+y_{\mathtt{A}_C}}\right) + \gamma_{\mathtt{A}_C}(2y_{\mathtt{A}_C} - 1)\,. \tag{44b}$$

We assume that changes in lithium and electron concentration do not result in volume changes, i.e. $v_{\mathtt{A}_C} = v_{\mathtt{A}_e} = 0$. Incompressibility $\left(\sum_{\alpha\in\mathcal{I}_{\mathtt{A}}} v_\alpha n_\alpha = 1\right)$ then results in $n_{\mathtt{A}_M} = n^0_{\mathtt{A}_M} = \text{const}$. Since we again assume electro-neutrality, $n_{\mathtt{A}_e} = n_{\mathtt{A}_M}$ (the lattice ions have $z_{\mathtt{A}_M} = +1$). Analogously to the electrolyte, electro-neutrality leads to $p_{\mathtt{A}} = \text{const}$. The remaining variables are then $(n_{\mathtt{A}_C}, \varphi_{\mathtt{A}})$. The mole fraction of the intercalated lithium is

$$y_{\mathtt{A}_C} = \frac{n_{\mathtt{A}_C}}{n_{\mathtt{A}_{\mathrm{lat}}}}\,, \tag{45}$$

where $n_{\mathtt{A}_{\mathrm{lat}}}$ is the number of available lattice sites, $n_{\mathtt{A}_{\mathrm{lat}}} = \omega_{\mathtt{A}} n_{\mathtt{A}_M}$, i.e. the active material can store up to $\omega_{\mathtt{A}}$ mole lithium for each mole of active material. As there is only one variable mole fraction remaining, we will set $y_{\mathtt{A}} := y_{\mathtt{A}_C}$.

Since the lithium in the active phase is uncharged, the lithium flux only contains a chemical potential gradient term,

$$\mathbf{J}_{\mathtt{A_c}} = -\boldsymbol{M}_{\mathtt{A}}\nabla\mu_{\mathtt{A}_C}\,. \tag{46}$$

The mobility as expressed using a diffusion coefficient is given by

$$\boldsymbol{M}_{\mathtt{A}} = \frac{n_{\mathtt{A}_C}}{k_{\mathtt{B}}T}\boldsymbol{D}_{\mathtt{A}}\,. \tag{47}$$

Inserting this into the flux, together with the chemical potential, results in

$$\mathbf{J}_{\mathtt{A_C}} = -n_{\mathtt{A_{lat}}} \boldsymbol{D}_{\mathtt{A}} y_{\mathtt{A}} \frac{\mathrm{d}f_{\mathtt{A}}}{\mathrm{d}y_{\mathtt{A}}} \nabla y_{\mathtt{A}} \,. \tag{48}$$

The term $y_{\mathtt{A}} \frac{\mathrm{d}f_{\mathtt{A}}}{\mathrm{d}y_{\mathtt{A}}}$ is called thermodynamic factor $\Gamma_{\mathtt{A}}(y_{\mathtt{A}})$. As both a completely filled lattice as well as an empty lattice hinder lithium migration, the diffusion coefficient depends on the concentration y_A,

$$\boldsymbol{D}_{\mathtt{A}} = \boldsymbol{D}^0_{\mathtt{A}} y_{\mathtt{A}} (1 - y_{\mathtt{A}}) \,. \tag{49}$$

We assume the active phase to be a conductor, and therefore $y_{\mathtt{A}_e} = \text{const.}$, resulting in the electron flux

$$\mathbf{J}_{\mathtt{A_e}} = -e_0 z_{\mathtt{A}_e} \boldsymbol{M}_{\mathtt{A}_e} \nabla \varphi_{\mathtt{A}} \,. \tag{50}$$

The charge flux is

$$\mathbf{J}_{\mathtt{A_q}} = e_0 z_{\mathtt{A}_e} \mathbf{J}_{\mathtt{A_e}} \,, \tag{51}$$

and the electron conductivity is related to the mobility by

$$\boldsymbol{\sigma}_{\mathtt{A}} = e_0^2 \boldsymbol{M}_{\mathtt{A}_e} \,. \tag{52}$$

The lithium flux and the charge flux can then be written as

$$\mathbf{J}_{\mathtt{A_C}} = -\boldsymbol{D}^0_{\mathtt{A}} y_{\mathtt{A}} (1 - y_{\mathtt{A}}) n_{\mathtt{A_{lat}}} \Gamma_{\mathtt{A}}(y_{\mathtt{A}}) \nabla y_{\mathtt{A}} \,, \tag{53a}$$

$$\mathbf{J}_{\mathtt{A_q}} = -\boldsymbol{\sigma}_{\mathtt{A}} \nabla \varphi_{\mathtt{A}} \,. \tag{53b}$$

The resulting balance equation for the lithium concentration and electric potential are

$$\frac{\partial n_{\mathtt{A}_C}}{\partial t} = -\operatorname{div} \mathbf{J}_{\mathtt{A_C}} \qquad \mathbf{x} \in \Omega^{\mathtt{A}} \,, \tag{54a}$$

$$0 = -\operatorname{div} \mathbf{J}_{\mathtt{A_q}} \qquad \mathbf{x} \in \Omega^{\mathtt{A}} \,. \tag{54b}$$

2.6 Mixed Ion-Electron Conductor

The SEI is modelled as a mixed ion-electron conductor, consisting of lattice species $\mathtt{I}_B$, intercalated lithium ions $\mathtt{I}_C$ and electrons $\mathtt{I}_e$, forming the index set $\mathcal{I}_{\mathtt{I}} = \{\mathtt{I}_B, \mathtt{I}_C, \mathtt{I}_e\}$. The lattice forming species $\mathtt{I}_B$ are considered to be immobile, while the electrons and the ions are mobile.

We consider the SEI domain also to be electro-neutral and account for potential space charge layers in the boundary conditions, cf. section 2.3. The set of independent variables is thus $(y_{\mathtt{I}_C}, \varphi_{\mathtt{I}})$ since electro-neutrality requires $y_{\mathtt{I}_C} = y_{\mathtt{I}_e} =: y_{\mathtt{I}}$ and $p_{\mathtt{I}} = \text{const.}$ As an example[3], we consider the following chemical potential functions,

$$\mu_{\mathtt{I}_C} = g_{\mathtt{I}_C} + k_{\mathtt{B}} T \, f_{\mathtt{I}_C}(y_{\mathtt{I}_C}) \qquad \text{with } f_{\mathtt{I}_C}(y_{\mathtt{I}_C}) = \ln \frac{y_{\mathtt{I}_C}}{1 + y_{\mathtt{I}_C}} \,, \tag{55a}$$

$$\mu_{\mathtt{I}_e} = g_{\mathtt{I}_e} + k_{\mathtt{B}} T \, f_{\mathtt{I}_e}(y_{\mathtt{I}_e}) \qquad \text{with } f_{\mathtt{I}_e}(y_{\mathtt{I}_e}) = \ln \frac{y_{\mathtt{I}_e}}{1 + y_{\mathtt{I}_e}} \,, \tag{55b}$$

$$\mu_{\mathtt{I}_B} = g_{\mathtt{I}_B} \,, \tag{55c}$$

where we consider for electrons and ions a (respective) lattice mixing entropy, which, however, do not entropically interact[4].

[3] We emphasize here that different chemical potential functions can of course be used, for instance other entropy of mixing contributions or enthalpic contributions between ions and electrons. However, discussing various chemical potential functions is not the main scope of this work.

[4] An alternative for entropic interaction would be $f_{\mathtt{I}_e} = \ln \frac{y_{\mathtt{I}_e}}{1 + y_{\mathtt{I}_e} + y_{\mathtt{I}_C}}$ and $f_{\mathtt{I}_C} = \ln \frac{y_{\mathtt{I}_C}}{1 + y_{\mathtt{I}_e} + y_{\mathtt{I}_C}}$.

As with the active material, we assume an effective molar volume of zero for the intercalated lithium and for the electrons, i.e. $v_{\mathtt{I}_C} = v_{\mathtt{I}_e} = 0$. This assumption leads, together with incompressibility $\big(\sum_{\alpha\in\mathcal{I}_\mathtt{I}} v_\alpha n_\alpha = 1\big)$, to $n_{\mathtt{I}_B} = n^0_{\mathtt{I}_B} = \text{const.}$

The mole fraction of the intercalated lithium is

$$y_{\mathtt{I}_C} = \frac{n_{\mathtt{I}_C}}{n_{\mathtt{I}_{\text{lat}}}}\,, \tag{56}$$

with $n_{\mathtt{I}_{\text{lat}}} = \omega_\mathtt{I} n_{\mathtt{I}_B}$.

The fluxes of electrons and ions follow the general expression of non-equilibrium thermodynamics (cf. eq. (9)) and depend on the chemical and the electrostatic potential gradients:

$$\mathbf{J}_{\mathtt{I}_\mathtt{c}} = -\boldsymbol{M}_{\mathtt{I}_C,\mathtt{I}_C}\nabla\mu_{\mathtt{I}_C} - e_0\boldsymbol{M}_{\mathtt{I}_C,\mathtt{I}_C}\nabla\varphi_\mathtt{I} - \boldsymbol{M}_{\mathtt{I}_C,\mathtt{I}_e}\nabla\mu_{\mathtt{I}_e} + e_0\boldsymbol{M}_{\mathtt{I}_C,\mathtt{I}_e}\nabla\varphi_\mathtt{I}\,, \tag{57a}$$

$$\mathbf{J}_{\mathtt{I}_\mathtt{e}} = -\boldsymbol{M}_{\mathtt{I}_e,\mathtt{I}_e}\nabla\mu_{\mathtt{I}_e} + e_0\boldsymbol{M}_{\mathtt{I}_e,\mathtt{I}_e}\nabla\varphi_\mathtt{I} - \boldsymbol{M}_{\mathtt{I}_e,\mathtt{I}_C}\nabla\mu_{\mathtt{I}_C} - e_0\boldsymbol{M}_{\mathtt{I}_e,\mathtt{I}_C}\nabla\varphi_\mathtt{I}\,. \tag{57b}$$

We express again the mobilities in terms of diffusion coefficients an friction terms

$$\boldsymbol{M}_{\mathtt{I}_C,\mathtt{I}_C} = \frac{n_{\mathtt{I}_C}}{k_\mathtt{B}T}\boldsymbol{D}_{\mathtt{I}_C,\mathtt{I}_C}\,, \qquad \boldsymbol{M}_{\mathtt{I}_e,\mathtt{I}_e} = \frac{n_{\mathtt{I}_e}}{k_\mathtt{B}T}\boldsymbol{D}_{\mathtt{I}_e,\mathtt{I}_e} \quad\text{and}\quad \boldsymbol{M}_{\mathtt{I}_C,\mathtt{I}_e} = n_{\mathtt{I}_{\text{lat}}}\frac{y_{\mathtt{I}_e}y_{\mathtt{I}_C}}{k_\mathtt{B}T}\boldsymbol{F}_{\mathtt{I}_C,\mathtt{I}_e}\,. \tag{58}$$

We introduce again the thermodynamic factor Γ_α ($\alpha = \mathtt{I}_e, \mathtt{I}_C$), which is

$$\Gamma_\alpha := y_\alpha\frac{\mathrm{d}f_\alpha}{\mathrm{d}y_\alpha} = 1 + \frac{y_\alpha}{1-y_\alpha}\,. \tag{59}$$

We consider the diffusion coefficients $\boldsymbol{D}_{\alpha,\alpha}$ ($\alpha = \mathtt{I}_e, \mathtt{I}_C$) analogously to the active phase to be

$$\boldsymbol{D}_{\alpha,\alpha} = (1-y_\alpha)\boldsymbol{D}^0_{\alpha,\alpha}\,, \tag{60}$$

where the $(1-y_\alpha)$ term accounts for blocking effects. Note that

$$\boldsymbol{M}_{\alpha,\alpha}\Gamma_\mathtt{I} = \frac{n_{\mathtt{I}_{\text{lat}}}}{k_\mathtt{B}T} \qquad\text{and}\qquad \boldsymbol{M}_{\mathtt{I}_C,\mathtt{I}_e}\Gamma_\mathtt{I} = \frac{n_{\mathtt{I}_{\text{lat}}}}{k_\mathtt{B}T}\frac{y_\mathtt{I}y_\mathtt{I}}{1-y_\mathtt{I}}\boldsymbol{F}_{\mathtt{I}_C,\mathtt{I}_e}\,, \tag{61}$$

so the fluxes simplify to

$$\mathbf{J}_{\mathtt{I}_\mathtt{c}} = -n_{\mathtt{I}_{\text{lat}}}(\boldsymbol{D}^0_{\mathtt{I}_C,\mathtt{I}_C} + \frac{y_\mathtt{I}y_\mathtt{I}}{1-y_\mathtt{I}}\boldsymbol{F}_{\mathtt{I}_C,\mathtt{I}_e})\nabla y_\mathtt{I} - \frac{e_0}{k_\mathtt{B}T}n_{\mathtt{I}_{\text{lat}}}y_\mathtt{I}\big((1-y_\mathtt{I})\boldsymbol{D}^0_{\mathtt{I}_C,\mathtt{I}_C} - y_\mathtt{I}\boldsymbol{F}_{\mathtt{I}_C,\mathtt{I}_e}\big)\nabla\varphi_\mathtt{I}\,, \tag{62a}$$

$$\mathbf{J}_{\mathtt{I}_\mathtt{e}} = -n_{\mathtt{I}_{\text{lat}}}(\boldsymbol{D}^0_{\mathtt{I}_e,\mathtt{I}_e} + \frac{y_\mathtt{I}y_\mathtt{I}}{1-y_\mathtt{I}}\boldsymbol{F}_{\mathtt{I}_C,\mathtt{I}_e})\nabla y_\mathtt{I} - \frac{e_0}{k_\mathtt{B}T}n_{\mathtt{I}_{\text{lat}}}y_\mathtt{I}\big((1-y_\mathtt{I})\boldsymbol{D}^0_{\mathtt{I}_e,\mathtt{I}_e} - y_\mathtt{I}\boldsymbol{F}_{\mathtt{I}_C,\mathtt{I}_e}\big)\nabla\varphi_\mathtt{I}\,. \tag{62b}$$

Similarly to the electrolyte, eq. (40), an equivalent set of transport parameters can be considered, i.e.

$$\boldsymbol{\Lambda}_\mathtt{I} = \frac{e_0^2}{k_\mathtt{B}T}\left(\boldsymbol{D}_{\mathtt{I}_C,\mathtt{I}_C} + \boldsymbol{D}_{\mathtt{I}_e,\mathtt{I}_e} - 2\boldsymbol{F}_{\mathtt{I}_C,\mathtt{I}_e}\right)\,, \tag{63a}$$

$$\boldsymbol{t}_{\mathtt{I}_C} = \frac{\boldsymbol{D}_{\mathtt{I}_C,\mathtt{I}_C} - \boldsymbol{F}_{\mathtt{I}_C,\mathtt{I}_e}}{\boldsymbol{D}_{\mathtt{I}_C,\mathtt{I}_C} + \boldsymbol{D}_{\mathtt{I}_e,\mathtt{I}_e} - 2\boldsymbol{F}_{\mathtt{I}_C,\mathtt{I}_e}}\,, \tag{63b}$$

$$\boldsymbol{D}_\mathtt{I} = \frac{2(\boldsymbol{D}_{\mathtt{I}_e,\mathtt{I}_e}\boldsymbol{D}_{\mathtt{I}_C,\mathtt{I}_C} - \boldsymbol{F}^2_{\mathtt{I}_C,\mathtt{I}_e})}{\boldsymbol{D}_{\mathtt{I}_C,\mathtt{I}_C} + \boldsymbol{D}_{\mathtt{I}_e,\mathtt{I}_e} - 2\boldsymbol{F}_{\mathtt{I}_C,\mathtt{I}_e}}\,, \tag{63c}$$

$$\boldsymbol{S}_\mathtt{I} = e_0(\boldsymbol{D}_{\mathtt{I}_C,\mathtt{I}_C} - \boldsymbol{D}_{\mathtt{I}_e,\mathtt{I}_e})\,, \tag{63d}$$

which satisfy the constraint

$$\frac{k_\mathtt{B}T}{e_0}(2\boldsymbol{t}_{\mathtt{I}_C} - 1) = \frac{\boldsymbol{S}_\mathtt{I}}{\boldsymbol{\Lambda}_\mathtt{I}}\,. \tag{64}$$

The cation and the charge flux in the SEI can then be written as

$$\mathbf{J}_{\mathtt{I_c}} = -\left(\boldsymbol{D}_{\mathtt{I}} + \boldsymbol{t}_{\mathtt{I}_C}\frac{\boldsymbol{S}_{\mathtt{I}}}{e_0}\right) n_{\mathtt{I}_{\mathsf{lat}}}\Gamma_{\mathtt{E}}\nabla y_{\mathtt{I}} - n_{\mathtt{I}_{\mathsf{lat}}} y_{\mathtt{I}}\frac{1}{e_0}\boldsymbol{t}_{\mathtt{I}_C}\boldsymbol{\Lambda}_{\mathtt{I}}\nabla\varphi_{\mathtt{I}}\,, \tag{65a}$$

$$= -\boldsymbol{D}_{\mathtt{I}} n_{\mathtt{I}_{\mathsf{lat}}}\Gamma_{\mathtt{I}}\nabla y_{\mathtt{I}_C} + \frac{1}{e_0}\boldsymbol{t}_{\mathtt{I}_C}\mathbf{J}_{\mathtt{I_q}}\,, \tag{65b}$$

$$\mathbf{J}_{\mathtt{I_q}} = -\boldsymbol{S}_{\mathtt{I}}\cdot n_{\mathtt{I}_{\mathsf{lat}}}\Gamma_{\mathtt{I}}\nabla y_{\mathtt{I}} - n_{\mathtt{I}_{\mathsf{lat}}} y_{\mathtt{I}}\boldsymbol{\Lambda}_{\mathtt{I}}\nabla\varphi_{\mathtt{I}}\,, \tag{65c}$$

which serve the balance equations for the ion concentration and and charge density

$$\frac{\partial n_{\mathtt{I}_C}}{\partial t} = -\operatorname{div}\mathbf{J}_{\mathtt{I_c}} \qquad \mathbf{x}\in\Omega^{\mathtt{I}}\,, \tag{66a}$$

$$0 = -\operatorname{div}\mathbf{J}_{\mathtt{I_q}} \qquad \mathbf{x}\in\Omega^{\mathtt{I}}\,, \tag{66b}$$

in order to determine $(y_{\mathtt{I}}, \varphi_{\mathtt{I}})$.

2.7 SEI–Electrolyte Interface

Two reactions occur at the interface $\Sigma_{\mathtt{IE}}$: the SEI formation reaction and the intercalation reaction. For the SEI formation, we assume that a cation and a solvent molecule out of the electrolyte react with an electron coming from the SEI to form a new, electro-neutral species B,

$$\mathrm{C}^+\big|^{\mathtt{E}} + \mathrm{e}^-\big|^{\mathtt{I}} + \mathrm{S}\big|^{\mathtt{E}} \rightleftharpoons \mathrm{B}\big|^{\mathtt{I}} + \kappa_{\mathtt{E_C}}\mathrm{S}\big|^{\mathtt{E}}\,. \tag{67}$$

In accordance with the entropy principle (cf. section 2.2), the reaction rate of this formation reaction is

$$R^{\mathsf{fo}}_{\mathtt{IE}} = L^{\mathsf{fo}}_{\mathtt{IE}} f_{\mathtt{BV}}(\lambda^{\mathsf{fo}}_{\mathtt{IE}})\,, \tag{68}$$

where $L^{\mathsf{fo}}_{\mathtt{IE}}$ is the reaction rate coefficient, $\lambda^{\mathsf{fo}}_{\mathtt{IE}}$ is the surface affinity

$$\lambda^{\mathsf{fo}}_{\mathtt{IE}} := -\big(\underset{s}{\mu}_{\mathtt{I}_B} - \underset{s}{\mu}_{\mathtt{E}_C} - \underset{s}{\mu}_{\mathtt{I}_e} + \kappa_{\mathtt{E_C}}\underset{s}{\mu}_{\mathtt{E}_S} - \underset{s}{\mu}_{\mathtt{E}_S}\big)\,, \tag{69}$$

and $f_{\mathtt{BV}}$ is a Butler-Volmer-type relation (cf. eq. (15))

$$f_{\mathtt{BV}}(z) := \mathsf{e}^{\left(\alpha\frac{z}{k_{\mathtt{B}}T}\right)} - \mathsf{e}^{-\left((1-\alpha)\frac{z}{k_{\mathtt{B}}T}\right)}\,, \tag{70}$$

with the charge transfer coefficient α, satisfying $f_{\mathtt{BV}}(z)|_{z>0} > 0$. Pulling back the surface chemical potentials towards points outside of the respective space charge layers (cf. section 2.3),

$$\underset{s}{\mu}_{\alpha}\big|_{\mathtt{IE}} = \mu_{\alpha}\big|^{\mathtt{E}}_{\mathtt{IE}} + e_0 z_{\alpha}(\varphi_{\mathtt{E}}\big|_{\mathtt{IE}} - \underset{s}{\varphi}\big|^{\mathtt{E}}_{\mathtt{IE}})\,, \qquad \alpha\in\mathcal{I}_{\mathtt{E}}\,, \tag{71a}$$

$$\underset{s}{\mu}_{\alpha}\big|_{\mathtt{IE}} = \mu_{\alpha}\big|^{\mathtt{I}}_{\mathtt{IE}} + e_0 z_{\alpha}(\varphi_{\mathtt{I}}\big|_{\mathtt{IE}} - \underset{s}{\varphi}\big|^{\mathtt{I}}_{\mathtt{IE}})\,, \qquad \alpha\in\mathcal{I}_{\mathtt{I}}\,, \tag{71b}$$

yields thus for the formation reaction affinity

$$\frac{\lambda^{\mathsf{fo}}_{\mathtt{IE}}}{k_{\mathtt{B}}T} = -\Delta g^{\mathsf{fo}}_{\mathtt{IE}} - \frac{e_0}{k_{\mathtt{B}}T}(\varphi_{\mathtt{I}}\big|_{\mathtt{IE}} - \varphi_{\mathtt{E}}\big|_{\mathtt{IE}}) + f_{\mathtt{E}_C}(y_{\mathtt{E}}\big|_{\mathtt{IE}}) + \ln(1-2y_{\mathtt{E}}\big|_{\mathtt{IE}}) + f_{\mathtt{I}_e}(y_{\mathtt{I}}\big|_{\mathtt{IE}})\,, \tag{72}$$

with

$$\Delta g^{\mathsf{fo}}_{\mathtt{IE}} := \frac{1}{k_{\mathtt{B}}T}(g_{\mathtt{I}_B} + \kappa_{\mathtt{E_C}} g_{\mathtt{E}_S} - g_{\mathtt{E}_C} - g_{\mathtt{I}_e} - g_{\mathtt{E}_S})\,. \tag{73}$$

The intercalation reaction into the SEI is

$$\mathrm{C}^+\big|^{\mathtt{E}} \rightleftharpoons \mathrm{C}^+_{\mathtt{I}}\big|^{\mathtt{I}} + \kappa_{\mathtt{E_C}}\mathrm{S}\big|^{\mathtt{E}}, \tag{74}$$

with a reaction rate

$$R^{\text{in}}_{\text{IE}} = L^{\text{in}}_{\text{IE}} f_{\text{BV}}(\lambda^{\text{in}}_{\text{IE}})\,, \tag{75}$$

where $L^{\text{in}}_{\text{IE}}$ is again the reaction rate cofficient, and the surface affinity for the intercalation reaction

$$\lambda^{\text{in}}_{\text{IE}} := -\big(\underset{s}{\mu}_{\text{I}_C} + \kappa_{\text{E}_\text{C}} \underset{s}{\mu}_{\text{E}_S} - \underset{s}{\mu}_{\text{E}_C}\big)\,, \tag{76}$$

or equivalently

$$\frac{\lambda^{\text{in}}_{\text{IE}}}{k_\text{B}T} = -\Delta g^{\text{in}}_{\text{IE}} - \frac{e_0}{k_\text{B}T}(\varphi_\text{I}\big|_{\text{IE}} - \varphi_\text{E}\big|_{\text{IE}}) + f_{\text{E}_C}(y_\text{E}\big|_{\text{IE}}) - f_{\text{I}_C}(y_{\text{I}_C}\big|_{\text{IE}})\,, \tag{77a}$$

with

$$\Delta g^{\text{in}}_{\text{IE}} := \frac{1}{k_\text{B}T}(g_{\text{I}_C} + \kappa_{\text{E}_\text{C}} g_{\text{E}_S} - g_{\text{E}_C})\,, \tag{77b}$$

$$f_{\text{E}_C}(y_\text{E}) := \ln(y_\text{E}) - \kappa_{\text{E}_\text{C}} \ln(1-2y_\text{E})\,. \tag{77c}$$

This yields the species reaction rates on the surface Σ_{IE},

$$\underset{s}{r}_\alpha = \begin{cases} \kappa_{\text{E}_\text{C}} R^{\text{in}}_{\text{IE}} + (\kappa_{\text{E}_\text{C}} - 1) R^{\text{fo}}_{\text{IE}} & \alpha = \text{E}_\text{S} \\ -R^{\text{in}}_{\text{IE}} - R^{\text{fo}}_{\text{IE}} & \alpha = \text{E}_\text{C}\,, \\ 0 & \alpha = \text{E}_\text{A}\,, \\ +R^{\text{fo}}_{\text{IE}} & \alpha = \text{I}_\text{B}\,, \\ +R^{\text{in}}_{\text{IE}} & \alpha = \text{I}_\text{C}\,, \\ -R^{\text{fo}}_{\text{IE}} & \alpha = \text{I}_\text{e}\,. \end{cases} \tag{78}$$

Mass conservation on the interface Σ_{IE} gives [12]

$$-\big(\mathbf{J}_\alpha + n_\alpha(\mathbf{v}-\mathbf{w})\big)\cdot\mathbf{n} = \underset{s}{r}_\alpha \qquad \alpha \in \mathcal{I}_\text{I}, \tag{79}$$

$$\big(\mathbf{J}_\alpha + n_\alpha(\mathbf{v}-\mathbf{w})\big)\cdot\mathbf{n} = \underset{s}{r}_\alpha \qquad \alpha \in \mathcal{I}_\text{E}, \tag{80}$$

where $\mathbf{J}_\alpha$ is the diffusive flux, $\mathbf{n}$ is the normal vector pointing from Ω^I to Ω^E, $\mathbf{v}$ is the barycentric velocity, $\mathbf{w}$ is the moving interface velocity of Σ_{IE}, and $\underset{s}{r}_\alpha$ is the molar surface production rate of the species α.

The interface condition for the species I_B,

$$-\left(\mathbf{J}_{\text{I}_\text{B}} + n_{\text{I}_B}(\mathbf{v}-\mathbf{w})\right)\cdot\mathbf{n} = R^{\text{fo}}_{\text{IE}}\,, \tag{81}$$

together with the definition of the diffusive flux $\mathbf{J}_\alpha = n_\alpha(\mathbf{v}_\alpha - \mathbf{v})$, leads to

$$-(\mathbf{v}_{\text{I}_B} - \mathbf{w})\cdot\mathbf{n} = v_{\text{I}_B} R^{\text{fo}}_{\text{IE}}\,. \tag{82}$$

We consider the species I_B to be immobile, i.e. $\mathbf{v}_{\text{I}_B} = \mathbf{0}$. The normal velocity of the interface is therefore determined by the formation reaction rate $R^{\text{fo}}_{\text{IE}}$ weighted by the molar volume v_{I_B} of the species I_B,

$$\mathbf{w}\cdot\mathbf{n} = v_{\text{I}_B} R^{\text{fo}}_{\text{IE}}\,. \tag{83}$$

Note, since we have $R^{\text{fo}}_{\text{IE}} > 0$ for $\lambda^{\text{fo}}_{\text{IE}} > 0$, we find that $\mathbf{w}\cdot\mathbf{n} > 0$, i.e. the SEI interface is moving *into* the electrolyte.

Summing the interface condition over all species on the electrolyte side of the interface and multiplying by their respective molar masses gives

$$\sum_{\alpha\in\mathcal{I}_\text{E}} m_\alpha(\mathbf{J}_\alpha + n_\alpha\mathbf{v} - n_\alpha\mathbf{w})\cdot\mathbf{n} = \sum_{\alpha\in\mathcal{I}_\text{E}} m_\alpha \underset{s}{r}_\alpha\,. \tag{84}$$

Utilizing the fact that diffusional flows have no global momentum ($\sum_\alpha m_\alpha \mathbf{J}_\alpha = 0$) and that the solvation reaction is volume conserving ($\frac{v_\alpha}{v_{\mathtt{E}_S}} = \frac{m_\alpha}{m_{\mathtt{E}_S}}$), we find thats the left-hand side reduces to

$$\frac{m_{\mathtt{E}_S}}{v_{\mathtt{E}_S}} \sum_{\alpha \in \mathcal{I}_\mathtt{E}} v_\alpha (n_\alpha \mathbf{v} - n_\alpha \mathbf{w}) \cdot \mathbf{n} = \sum_{\mathcal{I}_\mathtt{E}} m_\alpha r_{\underset{s}{\alpha}} \,. \tag{85}$$

Inserting the species reaction rates and the incompressibility of the electrolyte ($\sum_\alpha v_\alpha n_\alpha = 1$) then results in

$$(\mathbf{v} - \mathbf{w}) \cdot \mathbf{n} = -\frac{\widetilde{m}_{\mathtt{E}_C}}{m_{\mathtt{E}_S}} v_{\mathtt{E}_S} R^{\mathsf{in}}_{\mathtt{IE}} - v_{\mathtt{E}_S}(1 + \frac{\widetilde{m}_{\mathtt{E}_C}}{m_{\mathtt{E}_S}}) R^{\mathsf{fo}}_{\mathtt{IE}} \,. \tag{86}$$

For the SEI side of the interface, a similar argument leads to

$$-\rho^{\mathtt{I}} (\mathbf{v} - \mathbf{w}) \cdot \mathbf{n} = (\widetilde{m}_{\mathtt{E}_C} + m_{\mathtt{E}_S}) R^{\mathsf{fo}}_{\mathtt{IE}} + \widetilde{m}_{\mathtt{E}_C} R^{\mathsf{in}}_{\mathtt{IE}} \,, \tag{87}$$

where $\rho^{\mathtt{I}} = \sum_{\alpha \in \mathcal{I}_\mathtt{I}} m_\alpha n_\alpha$. Since the reaction rates are independent of the molar masses and molar volumes, the combination of eq. (86) and eq. (87) results in the conditions

$$\rho^I \frac{\widetilde{m}_{\mathtt{E}_C}}{m_{\mathtt{E}_S}} v_{\mathtt{E}_S} = \widetilde{m}_{\mathtt{E}_C} \quad \text{and} \quad \rho^I v_{\mathtt{E}_S} \left(1 + \frac{\widetilde{m}_{\mathtt{E}_C}}{m_{\mathtt{E}_S}}\right) = \widetilde{m}_{\mathtt{E}_C} + m_{\mathtt{E}_S} \,. \tag{88}$$

For the approximations $\frac{\widetilde{m}_{\mathtt{E}_C}}{m_{\mathtt{E}_S}} \approx 0$ and $\frac{m_{\mathtt{I}_e}}{m_{\mathtt{E}_S}} \approx 0$, i.e. ions and electrons are much lighter than solvent, this means

$$\rho^{\mathtt{I}} \approx m_{\mathtt{E}_S} n^0_{\mathtt{E}_S} \Leftrightarrow n_{\mathtt{I}_B} \approx n_{\mathtt{E}_S} \Leftrightarrow v_{\mathtt{I}_B} \approx v_{\mathtt{E}_S} \,. \tag{89}$$

Inserting the expression for $\mathbf{w}$ back into eq. (86) leads to

$$\mathbf{v} \cdot \mathbf{n} = -\frac{\widetilde{m}_{\mathtt{E}_C}}{m_{\mathtt{E}_S}} v_{\mathtt{E}_S} R^{\mathsf{in}}_{\mathtt{IE}} \,. \tag{90}$$

Since to molar mass of lithium ($6.94\,\mathrm{g\,mol^{-1}}$) is much smaller than that of the solvent (e.g. DMC has a molar mass of $90.08\,\mathrm{g\,mol^{-1}}$), the normal velocity is

$$\mathbf{v} \cdot \mathbf{n} \approx 0 \tag{91}$$

for a moderate reaction rate $R^{\mathsf{in}}_{\mathtt{IE}}$. Together with $\operatorname{div} \mathbf{v} = 0$, the barycentric velocity becomes $\mathbf{v} = \mathbf{0}$ in the electrolyte. This reduces the interface conditions eqs. (79) and (80) on $\Sigma_{\mathtt{IE}}$ to

$$-\mathbf{J}_{\mathtt{I_c}} \cdot \mathbf{n} = L^{\mathsf{in}}_{\mathtt{IE}} f_{\mathtt{BV}}(\lambda^{\mathsf{in}}_{\mathtt{IE}}) - v_{\mathtt{E}_S} n_{\mathtt{I}_C} L^{\mathsf{fo}}_{\mathtt{IE}} f_{\mathtt{BV}}(\lambda^{\mathsf{fo}}_{\mathtt{IE}}) \,, \tag{92a}$$

$$-\mathbf{J}_{\mathtt{I_e}} \cdot \mathbf{n} = -L^{\mathsf{fo}}_{\mathtt{IE}} f_{\mathtt{BV}}(\lambda^{\mathsf{fo}}_{\mathtt{IE}}) - v_{\mathtt{E}_S} n_{\mathtt{I}_e} L^{\mathsf{fo}}_{\mathtt{IE}} f_{\mathtt{BV}}(\lambda^{\mathsf{fo}}_{\mathtt{IE}}) \,, \tag{92b}$$

$$\mathbf{J}_{\mathtt{E_C}} \cdot \mathbf{n} = -L^{\mathsf{in}}_{\mathtt{IE}} f_{\mathtt{BV}}(\lambda^{\mathsf{in}}_{\mathtt{IE}}) - (1 - v_{\mathtt{E}_S} n_{\mathtt{E}_C}) L^{\mathsf{fo}}_{\mathtt{IE}} f_{\mathtt{BV}}(\lambda^{\mathsf{fo}}_{\mathtt{IE}}) \,, \tag{92c}$$

$$\mathbf{J}_{\mathtt{E_A}} \cdot \mathbf{n} = n_{\mathtt{E}_A} v_{\mathtt{E}_S} L^{\mathsf{fo}}_{\mathtt{IE}} f_{\mathtt{BV}}(\lambda^{\mathsf{fo}}_{\mathtt{IE}}) \,, \tag{92d}$$

and the charge fluxes are

$$\mathbf{J}_{\mathtt{E_q}} \cdot \mathbf{n} = e_0 \mathbf{J}_{\mathtt{Ec}} \cdot \mathbf{n} - e_0 \mathbf{J}_{\mathtt{E_A}} \cdot \mathbf{n} = -e_0 (L^{\mathsf{in}}_{\mathtt{IE}} f_{\mathtt{BV}}(\lambda^{\mathsf{in}}_{\mathtt{IE}}) + L^{\mathsf{fo}}_{\mathtt{IE}} f_{\mathtt{BV}}(\lambda^{\mathsf{fo}}_{\mathtt{IE}})) \,, \tag{93a}$$

$$-\mathbf{J}_{\mathtt{I_q}} \cdot \mathbf{n} = -e_0 (\mathbf{J}_{\mathtt{I_c}} \cdot \mathbf{n} - \mathbf{J}_{\mathtt{I_e}} \cdot \mathbf{n}) = e_0 (L^{\mathsf{in}}_{\mathtt{IE}} f_{\mathtt{BV}}(\lambda^{\mathsf{in}}_{\mathtt{IE}}) + L^{\mathsf{fo}}_{\mathtt{IE}} f_{\mathtt{BV}}(\lambda^{\mathsf{fo}}_{\mathtt{IE}})) \,. \tag{93b}$$

2.8 Active Material–SEI Interface

At the interface between the active material and the SEI, $\Sigma_{\mathtt{AI}}$, only the intercalation reaction

$$\mathrm{C^+}\big|^{\mathtt{I}} + \mathrm{e^-}\big|^{\mathtt{A}} \rightleftharpoons \mathrm{C}\big|^{\mathtt{A}} \tag{94}$$

occurs, with a reaction rate

$$R^{\mathsf{in}}_{\mathtt{AI}} = L^{\mathsf{in}}_{\mathtt{AI}} f_{\mathtt{BV}}(\lambda^{\mathsf{in}}_{\mathtt{AI}}) \,, \tag{95}$$

where $L^{\mathsf{in}}_{\mathtt{AI}}$ is the reaction rate coefficient and the surface affinity is

$$\lambda^{\mathsf{in}}_{\mathtt{AI}} := -(\underset{s}{\mu}_{\mathtt{A}_C} - \underset{s}{\mu}_{\mathtt{I}_C} - \underset{s}{\mu}_{e^-}) \,. \tag{96}$$

Equivalently to the SEI–electrolyte interface, pulling back the surface chemical potentials to positions outside of the respective space charge layers yields

$$\underset{s}{\mu}_\alpha = \mu_\alpha\big|^{\mathtt{I}}_{\mathtt{AI}} + e_0 z_\alpha(\varphi_{\mathtt{I}}\big|_{\mathtt{AI}} - \underset{s}{\varphi}\big|^{\mathtt{I}}_{\mathtt{AI}}) \qquad \alpha \in \mathcal{I}_{\mathtt{I}} \,, \tag{97}$$

$$\underset{s}{\mu}_\alpha = \mu_\alpha\big|^{\mathtt{A}}_{\mathtt{AI}} + e_0 z_\alpha(\varphi_{\mathtt{A}}\big|_{\mathtt{AI}} - \underset{s}{\varphi}\big|^{\mathtt{A}}_{\mathtt{AI}}) \qquad \alpha \in \mathcal{I}_{\mathtt{A}} \,, \tag{98}$$

whereby the surface affinity of the intercalation reaction satisfies

$$\frac{\lambda^{\mathsf{in}}_{\mathtt{AI}}}{k_{\mathtt{B}}T} = -\Delta g^{\mathsf{in}}_{\mathtt{AI}} - \frac{e_0}{k_{\mathtt{B}}T}(\varphi_{\mathtt{A}}\big|_{\mathtt{AI}} - \varphi_{\mathtt{I}}\big|_{\mathtt{AI}}) - f_{\mathtt{A}}(y_{\mathtt{A}}\big|_{\mathtt{AI}}) + f_{\mathtt{I}_C}(y_{\mathtt{I}_C}\big|_{\mathtt{AI}}) \,. \tag{99}$$

with

$$\Delta g^{\mathsf{in}}_{\mathtt{AI}} := \frac{1}{k_{\mathtt{B}}T}(g_{\mathtt{A}_C} - g_{\mathtt{I}_C} - g_{\mathtt{A}_e}) \,. \tag{100}$$

For the electrons, an additional constraint arises, essentially stating the continuity of the (electro-)chemical potential at the active material–SEI interface, since the SEI is a mixed ion-electron conductor. This reads as

$$\mu_{\mathtt{A}_\mathrm{e}}\big|^{\mathtt{A}}_{\mathtt{AI}} - e_0(\varphi_{\mathtt{A}}\big|^{\mathtt{A}}_{\mathtt{AI}} - \underset{s}{\varphi}\big|^{\mathtt{A}}_{\mathtt{AI}}) = \underset{s}{\mu}_{\mathtt{A}_e} = \mu_{\mathtt{I}_\mathrm{e}}\big|^{\mathtt{I}}_{\mathtt{AI}} - e_0(\varphi_{\mathtt{I}}\big|^{\mathtt{I}}_{\mathtt{AI}} - \underset{s}{\varphi}\big|^{\mathtt{I}}_{\mathtt{AI}}) \,, \tag{101}$$

where $\underset{s}{\mu}_{\mathtt{A}_e}$ is essentially the constant work function of the electrode surface [34]. From the continuity condition, eq. (101), we obtain

$$e_0(\varphi_{\mathtt{A}}|^{\mathtt{A}}_{\mathtt{AI}} - \varphi_{\mathtt{I}}|^{\mathtt{I}}_{\mathtt{AI}}) = g_{\mathtt{A}_e} - g_{\mathtt{I}_e} - k_{\mathtt{B}}T\, f_{\mathtt{I}_e}(y_{\mathtt{I}}|^{\mathtt{I}}_{\mathtt{AI}}) \,. \tag{102}$$

The species reaction rates are

$$\underset{s}{r}_\alpha = \begin{cases} R^{\mathsf{in}}_{\mathtt{AI}} & \alpha = \mathtt{A_C} \,, \\ -R^{\mathsf{in}}_{\mathtt{AI}} & \alpha = \mathtt{A_e} \,, \\ -R^{\mathsf{in}}_{\mathtt{AI}} & \alpha = \mathtt{I_C} \,, \end{cases} \tag{103}$$

resulting in the following equations for the fluxes across $\Sigma_{\mathtt{AI}}$,

$$-\mathbf{J}_{\mathtt{A_C}} \cdot \mathbf{n} = \quad R^{\mathsf{in}}_{\mathtt{AI}} = \quad L^{\mathsf{in}}_{\mathtt{AI}}\, f_{\mathtt{BV}}(\lambda^{\mathsf{in}}_{\mathtt{AI}}) \,, \tag{104a}$$

$$\mathbf{J}_{\mathtt{I_C}} \cdot \mathbf{n} = -R^{\mathsf{in}}_{\mathtt{AI}} = -L^{\mathsf{in}}_{\mathtt{AI}}\, f_{\mathtt{BV}}(\lambda^{\mathsf{in}}_{\mathtt{AI}}) \,, \tag{104b}$$

$$(\mathbf{J}_{\mathtt{I_e}} - \mathbf{J}_{\mathtt{A_e}}) \cdot \mathbf{n} = -R^{\mathsf{in}}_{\mathtt{AI}} = -L^{\mathsf{in}}_{\mathtt{AI}}\, f_{\mathtt{BV}}(\lambda^{\mathsf{in}}_{\mathtt{AI}}) \,, \tag{104c}$$

where $\mathbf{n}$ is the outward normal vector to $\Omega^{\mathtt{A}}$, pointing into $\Omega^{\mathtt{E}}$. The charge flux across the interface is then

$$(\mathbf{J}_{\mathtt{I_q}} - \mathbf{J}_{\mathtt{A_q}}) \cdot \mathbf{n} = e_0 \mathbf{J}_{\mathtt{I_c}} \cdot \mathbf{n} - e_0(\mathbf{J}_{\mathtt{I_e}} - \mathbf{J}_{\mathtt{A_e}}) \cdot \mathbf{n} = 0 \,. \tag{105}$$

2.9 Cell Voltage and Counter Electrode

We consider a (working electrode)|SEI|electrolyte|(counter electrode) setup, where the counter electrode is considered to be a metallic lithium foil. At the surface $\Sigma_{\mathtt{EM}}$ of the lithium foil, we have a metallic dissolution reaction

$$\mathtt{M_C}\big|^{\mathtt{M}} + \kappa_{\mathtt{E}_C}\mathtt{E_S}\big|^{\mathtt{E}} \rightleftharpoons \mathtt{E_C}\big|^{\mathtt{E}} \,, \tag{106}$$

with a reaction rate $R^{\mathsf{di}}_{\mathtt{EM}}$ and a surface affinity

$$\lambda^{\mathsf{di}}_{\mathtt{EM}} = -(\mu_{\mathtt{E}_C}|^{\mathtt{E}}_{\mathtt{EM}} + e_0\varphi_{\mathtt{E}}|^{\mathtt{E}}_{\mathtt{EM}} - \mu_{\mathtt{M}_C}|^{\mathtt{M}}_{\mathtt{EM}} - e_0\varphi_{\mathtt{M}}|^{\mathtt{M}}_{\mathtt{EM}} - \kappa_{\mathtt{E}_C}\mu_{\mathtt{E}_S}|^{\mathtt{E}}_{\mathtt{EM}}) \,, \tag{107a}$$

$$= -k_{\mathtt{B}}T\left(\Delta g^{\mathsf{di}}_{\mathtt{EM}} + f_{\mathtt{E}}(y_{\mathtt{E}_C}|_{\mathtt{EM}}) + \frac{e_0}{k_{\mathtt{B}}T}(\varphi_{\mathtt{E}}|^{\mathtt{E}}_{\mathtt{EM}} - \varphi_{\mathtt{M}}|^{\mathtt{M}}_{\mathtt{EM}})\right) . \tag{107b}$$

We will assume throughout this work, that the lithium foil is so large compared to the active electrode, that we can assume reaction equilibrium, i.e.

$$\lambda^{\mathsf{di}}_{\mathtt{EM}} = 0 \Leftrightarrow \frac{e_0}{k_{\mathtt{B}}T}(\varphi_{\mathtt{E}}|^{\mathtt{E}}_{\mathtt{EM}} - \varphi_{\mathtt{M}}|^{\mathtt{M}}_{\mathtt{EM}}) = -\Delta g^{\mathsf{di}}_{\mathtt{EM}} - f_{\mathtt{E}}(y_{\mathtt{E}_C}|_{\mathtt{EM}}) \,. \tag{108}$$

Further, the electronic conductivity is considered to be very high, entailing $\nabla\varphi_{\mathtt{M}} = 0$ in the counter electrode $\Omega_{\mathtt{M}}$ and thus $\varphi_{\mathtt{M}}(\mathbf{x}, t) = \text{const.} = \varphi_{\mathtt{M}}$. Note that the whole mathematical problem is determined up to a constant shift in φ whereby we may set $\varphi^{\mathtt{M}} = 0$ and obtain the boundary condition

$$\frac{e_0}{k_{\mathtt{B}}T}\varphi_{\mathtt{E}}|^{\mathtt{E}}_{\mathtt{EM}} = -\Delta g^{\mathsf{di}}_{\mathtt{EM}} - f_{\mathtt{E}}(y_{\mathtt{E}_C}|_{\mathtt{EM}}) \,, \quad \text{and} \quad \mathbf{J}_{\mathtt{E_C}} \cdot \mathbf{n} = i \,. \tag{109}$$

The *cell voltage* is related to the electrochemical potential of the electrons in the different phases, which yields

$$E = \varphi^{\mathtt{A}}|_{\Sigma_{\mathtt{DA}}} - e_0(g_{\mathtt{A}_e} - g_{\mathtt{M}_e}) \tag{110}$$

since $\mu_{\mathtt{M}_e} = g_{\mathtt{M}_e}$ and $\mu_{\mathtt{A}_e}|_{\Sigma_{\mathtt{DA}}} = g_{\mathtt{A}_e}$.

At the current collector–active phase interface $\Sigma_{\mathtt{DA}}$, the electronic current I is entering the working electrode, which yields the boundary conditions

$$-e_0\mathbf{J}_{\mathtt{A_e}} \cdot \mathbf{n} = \frac{I}{|\Sigma_{\mathtt{DA}}|} =: i \,, \tag{111a}$$

$$\mathbf{J}_{\mathtt{A_C}} \cdot \mathbf{n} = 0 \,. \tag{111b}$$

2.10 Initial Conditions

We assume that the system is initially in equilibrium, so we impose the initial conditions

$$y_{\mathtt{A}}(\mathbf{x}, t = 0) = y^0_{\mathtt{A}} \qquad \mathbf{x} \in \Omega_{\mathtt{A}} \,, \tag{112a}$$

$$y_{\mathtt{I}}(\mathbf{x}, t = 0) = y^0_{\mathtt{I}} \qquad \mathbf{x} \in \Omega_{\mathtt{I}} \,, \tag{112b}$$

$$y_{\mathtt{E}}(\mathbf{x}, t = 0) = y^0_{\mathtt{E}} \qquad \mathbf{x} \in \Omega_{\mathtt{E}} \,. \tag{112c}$$

Mathematically, these conditions are sufficient to close the system. However, it is also useful to consider what the initial states of the potentials φ_j for ($j = \mathtt{A}, \mathtt{I}, \mathtt{E}, \mathtt{M}$) will be, which is useful for understanding the system's behaviour and defining accurate initial guesses for the numerical solver. We impose

$$\varphi_j(\mathbf{x}, t = 0) = \varphi^0_j \,, \qquad \mathbf{x} \in \Omega_{\mathtt{A}} \cup \Omega_{\mathtt{I}} \cup \Omega_{\mathtt{E}} \,. \tag{113}$$

Without any current flowing in the initial state, we can deduce the initial conditions for φ_j from the reaction equilibrium, i.e.

$$\lambda^{\mathsf{in}}_{\mathtt{IE}} \stackrel{!}{=} 0 \qquad \Leftrightarrow \qquad -\Delta g^{\mathsf{in}}_{\mathtt{IE}} + f_{\mathtt{E}}(y^0_{\mathtt{E}_C}) - f_{\mathtt{I}}(y^0_{\mathtt{I}_C}) = \frac{e_0}{k_{\mathtt{B}}T}(\varphi^0_{\mathtt{I}} - \varphi^0_{\mathtt{E}}) \,, \tag{114a}$$

$$\lambda^{\mathsf{in}}_{\mathtt{AI}} \stackrel{!}{=} 0 \qquad \Leftrightarrow \qquad -\Delta g^{\mathsf{in}}_{\mathtt{AI}} + f_{\mathtt{I}_C}(y^0_{\mathtt{I}_C}) - f_{\mathtt{A}}(y^0_{\mathtt{A}_C}) = \frac{e_0}{k_{\mathtt{B}}T}(\varphi^0_{\mathtt{A}} - \varphi^0_{\mathtt{I}}) \,, \tag{114b}$$

$$\lambda^{\mathtt{M}}_{\mathsf{di}} \stackrel{!}{=} 0 \qquad \Leftrightarrow \qquad -\Delta g^{\mathsf{di}}_{\mathtt{EM}} - f_{\mathtt{E}}(y^0_{\mathtt{E}_C}) = \frac{e_0}{k_{\mathtt{B}}T}(\varphi^0_{\mathtt{E}} - \varphi^0_{\mathtt{M}}) \,. \tag{114c}$$

Hence, the initial values for φ_j are determined as

$$\frac{e_0}{k_B T}\varphi^0_{\mathtt{M}} = 0\,, \tag{115a}$$

$$\frac{e_0}{k_B T}\varphi^0_{\mathtt{E}} = -\left(\Delta g^{\mathsf{di}}_{\mathtt{EM}} + f_{\mathtt{E}}(y^0_{\mathtt{E}_C})\right)\,, \tag{115b}$$

$$\frac{e_0}{k_B T}\varphi^0_{\mathtt{I}} = -\left(\Delta g^{\mathsf{in}}_{\mathtt{IE}} + \Delta g^{\mathsf{di}}_{\mathtt{EM}} + f_{\mathtt{I}}(y^0_{\mathtt{I}_C})\right)\,, \tag{115c}$$

$$\frac{e_0}{k_B T}\varphi^0_{\mathtt{A}} = -\left(\Delta g^{\mathsf{in}}_{\mathtt{AI}} + \Delta g^{\mathsf{in}}_{\mathtt{IE}} + \Delta g^{\mathsf{di}}_{\mathtt{EM}} + f_{\mathtt{A}}(y^0_{\mathtt{A}_C})\right)\,. \tag{115d}$$

We now introduce the variable transformations ($j = \mathtt{A}, \mathtt{I}, \mathtt{E}, \mathtt{M}$)

$$\tilde{\varphi}_j := \frac{e_0}{k_B T}(\varphi_j - \varphi^0_j)\,, \tag{116}$$

which yields the convenient[5] expressions

$$\frac{\lambda^{\mathsf{in}}_{\mathtt{IE}}}{k_B T} = -(f_{\mathtt{I}}(y_{\mathtt{I}_C}|^{\mathtt{I}}_{\mathtt{IE}}) - f_{\mathtt{I}}(y^0_{\mathtt{I}_C})) + (f_{\mathtt{E}}(y_{\mathtt{E}_C}|^{\mathtt{E}}_{\mathtt{IE}}) - f_{\mathtt{E}}(y^0_{\mathtt{E}_C})) - \tilde{\varphi}_{\mathtt{I}}|^{\mathtt{I}}_{\mathtt{IE}} + \tilde{\varphi}_{\mathtt{E}}|^{\mathtt{E}}_{\mathtt{IE}}\,, \tag{117a}$$

$$\frac{\lambda^{\mathsf{in}}_{\mathtt{AI}}}{k_B T} = -(f_{\mathtt{A}}(y_{\mathtt{A}_C}|^{\mathtt{A}}_{\mathtt{AI}}) - f_{\mathtt{A}}(y^0_{\mathtt{A}_C})) + (f_{\mathtt{I}_C}(y_{\mathtt{I}_C}|^{\mathtt{A}}_{\mathtt{AI}}) - f_{\mathtt{I}_C}(y^0_{\mathtt{I}_C})) - \tilde{\varphi}_{\mathtt{A}}|^{\mathtt{A}}_{\mathtt{AI}} + \tilde{\varphi}_{\mathtt{I}}|^{\mathtt{I}}_{\mathtt{AI}}\,, \tag{117b}$$

and

$$\begin{aligned}\frac{\lambda^{\mathsf{fo}}_{\mathtt{IE}}}{k_B T} = &-\Delta g^{\mathsf{fo}} + (f_{\mathtt{E}}(y_{\mathtt{E}_C}|^{\mathtt{E}}_{\mathtt{IE}}) - f_{\mathtt{E}}(y^0_{\mathtt{E}_C})) + (\ln(y_{\mathtt{E}_S}|^{\mathtt{E}}_{\mathtt{IE}}) - \ln(y^0_{\mathtt{E}_S}))\\ &+ (f_{\mathtt{I}_e}(y_{\mathtt{I}_e}|_{\mathtt{IE}}) - f_{\mathtt{I}}(y^0_{\mathtt{I}_C})) - \tilde{\varphi}_{\mathtt{I}}|^{\mathtt{I}}_{\mathtt{IE}} + \tilde{\varphi}_{\mathtt{E}}|^{\mathtt{E}}_{\mathtt{IE}}\,,\end{aligned} \tag{117c}$$

where

$$\Delta g^{\mathsf{fo}} := \frac{e_0}{k_B T}(\Delta g^{\mathsf{fo}}_{\mathtt{IE}} - \Delta g^{\mathsf{in}}_{\mathtt{IE}}) - \ln(y^0_{\mathtt{E}_S})\,, \tag{118a}$$

$$y_{\mathtt{E}_S} = 1 - 2y_{\mathtt{E}_C}\,, \tag{118b}$$

In order to achieve initial SEI growth, $\Delta g^{\mathsf{fo}} < 0$ is required.

Note further that the continuity condition for the electrons, eq. (101) also holds for the initial values, i.e.

$$\frac{e_0}{k_B T}(\varphi^0_{\mathtt{A}} - \varphi^0_{\mathtt{I}}) = \frac{1}{k_B T}(g_{\mathtt{A}_e} - g_{\mathtt{I}_e}) - f_{\mathtt{I}_e}(y^0_{\mathtt{I}})\,. \tag{119}$$

In addition, we have

$$\frac{e_0}{k_B T}(\varphi^0_{\mathtt{A}} - \varphi^0_{\mathtt{A}}) = -\Delta g^{\mathsf{in}}_{\mathtt{AI}} + f_{\mathtt{I}_C}(y^0_{\mathtt{I}_C}) - f_{\mathtt{A}}(y^0_{\mathtt{A}_C})\,, \tag{120}$$

and therefore

$$\frac{1}{k_B T}(g_{\mathtt{A}_C} - g_{\mathtt{I}_C} - g_{\mathtt{I}_e}) + f_{\mathtt{A}}(y^0_{\mathtt{A}_C}) = f_{\mathtt{I}_e}(y^0_{\mathtt{I}}) + f_{\mathtt{I}_C}(y^0_{\mathtt{I}_C})\,. \tag{121}$$

This constraint allows the consistent determination of the initial values $y^0_{\mathtt{I}}$. Further, it allows us to rewrite the continuity of the electron electro-chemical potential, eq. (101), as

$$(\tilde{\varphi}_{\mathtt{A}}|^{\mathtt{A}}_{\mathtt{AI}} - \tilde{\varphi}_{\mathtt{I}}|^{\mathtt{I}}_{\mathtt{AI}}) = -(f_{\mathtt{I}_e}(y_{\mathtt{I}}|^{\mathtt{I}}_{\mathtt{AI}}) - f_{\mathtt{I}_e}(y^0_{\mathtt{I}}))\,. \tag{122}$$

Note further that the constraint $\lambda^{\mathsf{di}}_{\mathtt{EM}} = 0$ yields the boundary condition

$$\tilde{\varphi}_{\mathtt{E}}|^{\mathtt{E}}_{\mathtt{EM}} = -(f_{\mathtt{E}}(y_{\mathtt{E}}|_{\mathtt{EM}}) - f_{\mathtt{E}}(y^0_{\mathtt{E}}))\,. \tag{123}$$

[5]The affinities are expressed in terms of the initial conditions, yielding directly $\lambda^{\mathsf{in}}_{\mathtt{IE}} = 0$ and $\lambda^{\mathsf{in}}_{\mathtt{AI}} = 0$ for the initial state. This is also an important aspect for numerical implementations.

The *cell voltage* can be finally be written as

$$E = \frac{k_{\mathrm{B}}T}{e_0}\big(\tilde{\varphi}^{\mathtt{A}}|_{\Sigma_{\mathtt{DA}}} - f_{\mathtt{A}}(y^0_{\mathtt{A}_C})\big) + E^0 \quad \text{with} \quad E^0 := e_0(g_{\mathtt{M}_C} + g_{\mathtt{M}_e} - g_{\mathtt{A}_C})\,. \tag{124}$$

3 One-Dimensional Equation System

We consider now a 1D approximation of the problem. The structure of this section is the following. After stating the 1D version of the governing equations, we introduce proper non-dimensionalizations of the overall problem and introduce the C-Rate C_h as a central scaling factor. We show how open-circuit voltage (OCV) conditions can be achieved for $C_h \to 0$ and derive a coupled ODE system to determine the evolution of $(y_{\mathtt{A}}, y_{\mathtt{I}}, y_{\mathtt{E}}, \ell_{\mathtt{I}})$ under OCV conditions, which is particularly relevant for battery calendar aging.

3.1 Balance Equations

We now write the governing equations and boundary conditions in each domain in a compact way, exploiting that notation can be simplified when considering a 1D planar geometry. We consider the variable transformations $\tilde{\varphi}_j = \frac{e_0}{k_{\mathrm{B}}T}(\varphi_{\mathtt{E}} - \varphi^0_{\mathtt{E}}), j = \mathtt{A}, \mathtt{I}, \mathtt{E}$ in the following. For the electrolyte domain $\Omega_{\mathtt{E}}$, with interfaces $\Sigma_{\mathtt{IE}}$ and $\Sigma_{\mathtt{EM}}$, we need to solve the balance equations (cf. eqs. (42) and (43)) for the variables $(y_{\mathtt{E}}, \tilde{\varphi}_{\mathtt{E}})$,

$$h_{\mathtt{E}}\frac{\partial y_{\mathtt{E}}}{\partial t} = -\frac{\partial J_{\mathtt{E}_C}}{\partial x}\,, \tag{125a}$$

$$0 = -\frac{\partial J_{\mathtt{E}_q}}{\partial x}\,. \tag{125b}$$

The corresponding fluxes are

$$J_{\mathtt{E}_C} = -(D_{\mathtt{E}} + t_{\mathtt{E}_C}\frac{S_{\mathtt{E}}}{e_0})n_{\mathtt{E}_{\mathrm{tot}}}\Gamma_{\mathtt{E}}\frac{\partial y_{\mathtt{E}_C}}{\partial x} - n_{\mathtt{E}_{\mathrm{tot}}}y_{\mathtt{E}}\frac{k_{\mathrm{B}}T}{(e_0)^2}t_{\mathtt{E}_C}\Lambda_{\mathtt{E}}\frac{\partial\tilde{\varphi}_{\mathtt{E}}}{\partial x}\,, \tag{125c}$$

$$= -D_{\mathtt{E}}n_{\mathtt{E}_{\mathrm{tot}}}\Gamma_{\mathtt{E}}\frac{\partial y_{\mathtt{E}}}{\partial x} + \frac{k_{\mathrm{B}}T}{(e_0)^2}\boldsymbol{t}_{\mathtt{E}_C}J_{\mathtt{E}_q}\,, \tag{125d}$$

$$J_{\mathtt{E}_q} = -S_{\mathtt{E}}\cdot n_{\mathtt{E}_{\mathrm{tot}}}\Gamma_{\mathtt{E}}\frac{\partial y_{\mathtt{E}}}{\partial x} - n_{\mathtt{E}_{\mathrm{tot}}}y_{\mathtt{E}}\Lambda_{\mathtt{E}}\frac{k_{\mathrm{B}}T}{e_0}\frac{\partial\tilde{\varphi}_{\mathtt{E}}}{\partial x}\,, \tag{125e}$$

with

$$n_{\mathtt{E}_{\mathrm{tot}}} = \tilde{n}_{\mathtt{E}_{\mathrm{tot}}}(y_{\mathtt{E}})n^0_{\mathtt{E}_S}\,, \qquad \tilde{n}_{\mathtt{E}_{\mathrm{tot}}}(y_{\mathtt{E}}) := \frac{1}{1-2(\kappa_{\mathtt{E}}-1)y_{\mathtt{E}}}\,, \tag{125f}$$

$$h_{\mathtt{E}} = \frac{\partial n_{\mathtt{E}_C}}{\partial y_{\mathtt{E}}} = n^0_{\mathtt{E}_S}\tilde{h}_{\mathtt{E}}, \qquad \tilde{h}_{\mathtt{E}}(y_{\mathtt{E}}) := 1 + \frac{2y_{\mathtt{E}}(\kappa_{\mathtt{E}}-1)}{(1-2(\kappa_{\mathtt{E}}-1)y_{\mathtt{E}})^2}\,. \tag{125g}$$

Note that both flux representations of $J_{\mathtt{E}_C}$ are useful, either for theoretical or numerical aspects.

For the SEI domain $\Omega_{\mathtt{I}}$, with interfaces $\Sigma_{\mathtt{AI}}$ and $\Sigma_{\mathtt{IE}}$, we need to solve the balance equations (cf. eqs. (65) and (66)) for the variables $(y_{\mathtt{I}}, \tilde{\varphi}_{\mathtt{I}}, x_{\mathtt{I}}(t))$,

$$n_{\mathtt{I}_{\mathrm{lat}}}\frac{\partial y_{\mathtt{I}}}{\partial t} = -\frac{\partial J_{\mathtt{I}_C}}{\partial x}\,, \tag{126a}$$

$$0 = -\frac{\partial J_{\mathtt{I}_q}}{\partial x}\,, \tag{126b}$$

as well as the ODE

$$\frac{\mathrm{d}x_{\mathtt{I}}(t)}{\mathrm{d}t} = v_{\mathtt{E}_S} L^{\mathsf{fo}}_{\mathtt{IE}} \cdot f_{\mathtt{BV}}(\lambda^{\mathsf{fo}}_{\mathtt{IE}}) \tag{126c}$$

for the moving SEI interface. The corresponding fluxes are

$$J_{\mathtt{I}_C} = -\,(D_{\mathtt{I}} + t_{\mathtt{I}_C}\frac{S_{\mathtt{I}}}{e_0}) n_{\mathtt{E}_{\mathsf{tot}}} \Gamma_{\mathtt{E}} \frac{\partial y_{\mathtt{I}}}{\partial x} - n_{\mathtt{I}_{\mathsf{lat}}} y_{\mathtt{I}} \frac{k_{\mathtt{B}}T}{(e_0)^2} t_{\mathtt{I}_C} \Lambda_{\mathtt{E}} \frac{\partial \tilde{\varphi}_{\mathtt{I}}}{\partial x}\,, \tag{126d}$$

$$= -\,D_{\mathtt{I}} n_{\mathtt{I}_{\mathsf{lat}}} \Gamma_{\mathtt{I}} \frac{\partial y_{\mathtt{I}}}{\partial x} + \frac{1}{e_0} t_{\mathtt{I}_C} J_{\mathtt{I}_q}\,, \tag{126e}$$

$$J_{\mathtt{I}_q} = -\,S_{\mathtt{I}} \cdot n_{\mathtt{I}_{\mathsf{lat}}} \Gamma_{\mathtt{I}} \frac{\partial y_{\mathtt{I}}}{\partial x} - n_{\mathtt{I}_{\mathsf{lat}}} y_{\mathtt{I}} \frac{k_{\mathtt{B}}T}{e_0} \Lambda_{\mathtt{I}} \frac{\partial \tilde{\varphi}_{\mathtt{I}}}{\partial x}\,. \tag{126f}$$

In the active active phase $\Omega_{\mathtt{A}}$, with interfaces $\Sigma_{\mathtt{DA}}$ and $\Sigma_{\mathtt{AI}}$, we need to solve the balance equations (cf. (53) and (54)) for the variables $(y_{\mathtt{A}}, \tilde{\varphi}_{\mathtt{A}})$,

$$n_{\mathtt{A}_{\mathsf{lat}}} \frac{\partial y_{\mathtt{A}}}{\partial t} = -\frac{\partial J_{\mathtt{A}_C}}{\partial x}\,, \tag{127a}$$

$$0 = -\frac{\partial J_{\mathtt{A}_q}}{\partial x}\,. \tag{127b}$$

The corresponding fluxes are

$$J_{\mathtt{A}_C} = -\underbrace{D^0_{\mathtt{A}} y_{\mathtt{A}}(1-y_{\mathtt{A}}) \cdot n_{\mathtt{A},\mathsf{lat}}\, \Gamma_{\mathtt{A}}(y_{\mathtt{A}})}_{=:D^{\mathsf{eff}}_{\mathtt{A}}(y_{\mathtt{A}})} \frac{\partial y_{\mathtt{A}}}{\partial x}\,, \tag{127c}$$

$$J_{\mathtt{A}_q} = -\sigma_{\mathtt{A}} \frac{k_{\mathtt{B}}T}{e_0} \frac{\partial \tilde{\varphi}_{\mathtt{A}}}{\partial x}\,. \tag{127d}$$

3.2 Boundary Conditions

At the electrolyte–SEI interface $x_{\mathtt{I}}(t)$, we have

$$-J_{I_C} = +R^{\mathsf{in}}_{\mathtt{IE}} = L^{\mathsf{in}}_{\mathtt{IE}} \cdot f_{\mathtt{BV}}(\lambda^{\mathsf{in}}_{\mathtt{IE}}) - n_{\mathtt{I}_C} v_{\mathtt{E}_S} L^{\mathsf{fo}}_{\mathtt{IE}} \cdot f_{\mathtt{BV}}(\lambda^{\mathsf{fo}}_{\mathtt{IE}}) \quad \text{on } \Sigma^{\mathtt{I}}_{\mathtt{IE}}\,, \tag{128a}$$

$$-J_{\mathtt{I}_q} = e_0 L^{\mathsf{in}}_{\mathtt{IE}} \cdot f_{\mathtt{BV}}(\lambda^{\mathsf{in}}_{\mathtt{IE}}) + e_0 L^{\mathsf{fo}}_{\mathtt{IE}} \cdot f_{\mathtt{BV}}(\lambda^{\mathsf{fo}}_{\mathtt{IE}}) \quad \text{on } \Sigma^{\mathtt{I}}_{\mathtt{IE}}\,, \tag{128b}$$

$$J_{E_C} = -L^{\mathsf{in}}_{\mathtt{IE}} \cdot f_{\mathtt{BV}}(\lambda^{\mathsf{in}}_{\mathtt{IE}}) - L^{\mathsf{fo}}_{\mathtt{IE}} \cdot f_{\mathtt{BV}}(\lambda^{\mathsf{fo}}_{\mathtt{IE}}) + n_{\mathtt{E}_C} v_{\mathtt{E}_S} L^{\mathsf{fo}}_{\mathtt{IE}} \cdot f_{\mathtt{BV}}(\lambda^{\mathsf{fo}}_{\mathtt{IE}}) \quad \text{on } \Sigma^{\mathtt{E}}_{\mathtt{IE}}\,, \tag{128c}$$

$$J_{E_q} = +e_0 L^{\mathsf{in}}_{\mathtt{IE}} \cdot f_{\mathtt{BV}}(\lambda^{\mathsf{in}}_{\mathtt{IE}}) + e_0 L^{\mathsf{fo}}_{\mathtt{IE}} \cdot f_{\mathtt{BV}}(\lambda^{\mathsf{fo}}_{\mathtt{IE}}) \quad \text{on } \Sigma^{\mathtt{E}}_{\mathtt{IE}}\,, \tag{128d}$$

and at the active phase–SEI Interface $x_{\mathtt{A}}$

$$-J_{\mathtt{A}_C} = R^{\mathsf{in}}_{\mathtt{AI}} = L^{\mathsf{in}}_{\mathtt{AI}} \cdot f_{\mathtt{BV}}(\lambda^{\mathsf{in}}_{\mathtt{AI}}) \quad \text{on } \Sigma^{\mathtt{A}}_{\mathtt{AI}}\,, \tag{129a}$$

$$J_{\mathtt{I}_C} = -R^{\mathsf{in}}_{\mathtt{AI}} = -L^{\mathsf{in}}_{\mathtt{AI}} \cdot f_{\mathtt{BV}}(\lambda^{\mathsf{in}}_{\mathtt{AI}}) \quad \text{on } \Sigma^{\mathtt{I}}_{\mathtt{AI}}\,, \tag{129b}$$

$$(J_{\mathtt{I}_q} - J_{\mathtt{A}_q}) = 0 \quad \text{on } \Sigma_{\mathtt{AI}}\,, \tag{129c}$$

with $f_{\mathtt{BV}}$ according to eq. (15) and the surface affinities $(\lambda^{\mathsf{in}}_{\mathtt{IE}}, \lambda^{\mathsf{fo}}_{\mathtt{IE}}, \lambda^{\mathsf{in}}_{\mathtt{AI}})$ according to eq. (117).

At the current collector–active phase interface x_0, we have

$$J_{\mathtt{A}_q} = i \qquad \text{and} \qquad J_{\mathtt{A}_C} = 0\,, \tag{130}$$

and at the electrolyte–counter electrode $x_{\mathtt{M}}$ interface

$$\tilde{\varphi}_{\mathtt{E}} = -(f_{\mathtt{E}}(y_{\mathtt{E}}|_{\mathtt{EM}}) - f_{\mathtt{E}}(y^0_{\mathtt{E}})) \qquad \text{and} \qquad J_{\mathtt{E}_q}|_{x_{\mathtt{E}}} = i\,. \tag{131}$$

Note that $J_{\mathrm{E}_q}|_{x_\mathrm{E}} = i$ also implies

$$J_{\mathrm{E}_C}|_{x_\mathrm{E}} = i(e_0)^{-1} \qquad \text{and} \qquad J_{\mathrm{E}_S}|_{x_\mathrm{E}} = -\kappa i(e_0)^{-1}\,. \tag{132}$$

3.3 Non-dimensionalization

We non-dimensionalize the whole system of equations with respect to the following scalings:

$$\begin{aligned}
\mathcal{L} &:= |x_\mathrm{A} - x_0|\,, \qquad \xi := \frac{(x-x_0)}{\mathcal{L}}\,, \qquad \tilde{\ell}_\mathrm{I} := \frac{\ell_\mathrm{I}(t)}{\mathcal{L}}\,,\\
\eta_{\mathrm{AI}} &:= \frac{n_{\mathrm{A}_{\mathrm{lat}}}}{n_{\mathrm{I}_{\mathrm{lat}}}}\,, \qquad \eta_{\mathrm{IE}} := \frac{n_{\mathrm{I}_{\mathrm{lat}}}}{n^0_{\mathrm{E}_S}}\,, \qquad \eta_{\mathrm{EA}} := \frac{n^0_{\mathrm{E}_S}}{n_{\mathrm{A}_{\mathrm{lat}}}}\,,\\
Q^0_\mathrm{A} &:= e_0 n_{\mathrm{A}_{\mathrm{lat}}}\mathcal{L}\,, \qquad i := i^0\cdot C_h\cdot \tilde{i}(\tau)\,, \qquad i^0 := \frac{Q^0_\mathrm{A}}{1[h]}\,,\\
\tau &:= C_h\frac{t}{[h]}\,, \qquad \tilde{\varphi}_j := \frac{k_\mathrm{B}T}{e_0}(\varphi_j - \varphi^0_j)\,,
\end{aligned} \tag{133}$$

where C_h is called the C-rate. We then define the dimensionless parameters

$$\begin{aligned}
\tilde{D}^y_\mathrm{E} &:= \frac{[h]}{\mathcal{L}^2}(D_\mathrm{E} + t_{\mathrm{E}_C}\frac{S_\mathrm{E}}{e_0})\tilde{n}_{\mathrm{E}_{\mathrm{tot}}}\Gamma_\mathrm{E}\,, \quad \tilde{D}^\varphi_\mathrm{E} := \frac{[h]}{\mathcal{L}^2}\tilde{n}_{\mathrm{E}_{\mathrm{tot}}}(y_\mathrm{E})y_\mathrm{E}\frac{k_\mathrm{B}T}{(e_0)^2}t_{\mathrm{E}_C}\Lambda_\mathrm{E}\,,\\
\tilde{S}_\mathrm{E} &:= \frac{[h]}{\mathcal{L}^2}\frac{1}{e_0}S_\mathrm{E}\cdot\tilde{n}_{\mathrm{E}_{\mathrm{tot}}}\Gamma_\mathrm{E}\,, \qquad \tilde{\sigma}_\mathrm{E} := \frac{[h]}{\mathcal{L}^2}\tilde{n}_{\mathrm{E}_{\mathrm{tot}}}y_\mathrm{E}\Lambda_\mathrm{E}\frac{k_\mathrm{B}T}{(e_0)^2}\,,\\
\tilde{D}^y_\mathrm{I} &:= \frac{[h]}{\mathcal{L}^2}(D_\mathrm{I} + t_{\mathrm{I}_C}\frac{S_\mathrm{I}}{e_0})\Gamma_\mathrm{I}\,, \qquad \tilde{D}^\varphi_\mathrm{I} := \frac{[h]}{\mathcal{L}^2}y_\mathrm{I}\frac{k_\mathrm{B}T}{(e_0)^2}t_{\mathrm{I}_C}\Lambda_\mathrm{I}\,,\\
\tilde{S}_\mathrm{I} &:= \frac{[h]}{\mathcal{L}^2}\frac{1}{e_0}S_\mathrm{I}\cdot\Gamma_\mathrm{I}\,, \qquad \tilde{\sigma}_\mathrm{I} := \frac{[h]}{\mathcal{L}^2}y_\mathrm{I}\frac{k_\mathrm{B}T}{(e_0)^2}\Lambda_\mathrm{I}\,,\\
\tilde{D}_\mathrm{A} &:= \frac{[h]}{\mathcal{L}^2}D^0_\mathrm{A}y_\mathrm{A}(1-y_\mathrm{A})\Gamma_\mathrm{A}(y_\mathrm{A})\,, \quad \tilde{\sigma}_\mathrm{A} := \frac{[h]k_\mathrm{B}T}{e_0^2\mathcal{L}^2 n_{\mathrm{A}_{\mathrm{lat}}}}\sigma_\mathrm{A}\,,\\
\tilde{L}^{\mathsf{in}}_{\mathrm{IE}} &:= \frac{[h]}{\mathcal{L}n_{\mathrm{I}_{\mathrm{lat}}}}L^{\mathsf{in}}_{\mathrm{IE}}\,, \qquad \tilde{L}^{\mathsf{fo}}_{\mathrm{IE}} := \frac{[h]}{\mathcal{L}n^0_{\mathrm{E}_S}}L^{\mathsf{fo}}_{\mathrm{IE}}\,,\\
\tilde{L}^{\mathsf{in}}_{\mathrm{AI}} &:= \frac{[h]}{\mathcal{L}n_{\mathrm{A}_{\mathrm{lat}}}}L^{\mathsf{in}}_{\mathrm{AI}}\,.
\end{aligned} \tag{134}$$

3.3.1 Balance equations

We can now write the governing equations in section 3.1 in dimensionless form. The electrolyte with the variables $(y_\mathrm{E}, \tilde{\varphi}_\mathrm{E})$ is governed by

$$\tilde{h}_\mathrm{E}\frac{\partial y_\mathrm{E}}{\partial\tau} = -\frac{\partial\tilde{J}_{\mathrm{E}_C}}{\partial\xi} \qquad \text{with} \qquad \tilde{J}_{\mathrm{E}_C} = \frac{[h]}{\mathcal{L}n^0_{\mathrm{E}_S}C_h}J_{\mathrm{E}_C} = -\frac{1}{C_h}\tilde{D}^y_\mathrm{E}\frac{\partial y_\mathrm{E}}{\partial\xi} - \frac{1}{C_h}\tilde{D}^\varphi_\mathrm{E}\frac{\partial\tilde{\varphi}_\mathrm{E}}{\partial\xi}\,, \tag{135a}$$

$$0 = -\frac{\partial\tilde{J}_{\mathrm{E}_q}}{\partial\xi} \qquad \text{with} \qquad \tilde{J}_{\mathrm{E}_q} = \frac{[h]}{e_0\mathcal{L}n^0_{\mathrm{E}_S}C_h}J_{\mathrm{E}_q} = -\frac{1}{C_h}\tilde{S}_\mathrm{E}\frac{\partial y_\mathrm{E}}{\partial\xi} - \frac{1}{C_h}\tilde{\sigma}_\mathrm{E}\frac{\partial\tilde{\varphi}_\mathrm{E}}{\partial\xi}\,. \tag{135b}$$

The SEI with the variables $(y_\mathrm{I}, \tilde{\varphi}_\mathrm{I}, \ell_\mathrm{I})$ is governed by

$$\frac{\partial y_\mathrm{I}}{\partial\tau} = -\frac{\partial\tilde{J}_{\mathrm{I}_C}}{\partial\xi} \qquad \text{with} \qquad \tilde{J}_{\mathrm{I}_C} = \frac{[h]}{\mathcal{L}n_{\mathrm{I}_{\mathrm{lat}}}C_h}J_{\mathrm{I}_C} = -\frac{1}{C_h}\tilde{D}^y_\mathrm{I}\frac{\partial y_\mathrm{I}}{\partial\xi} - \frac{1}{C_h}\tilde{D}^\varphi_\mathrm{I}\frac{\partial\tilde{\varphi}_\mathrm{I}}{\partial\xi}\,, \tag{136a}$$

$$0 = -\frac{\partial \tilde{J}_{\mathtt{I}_q}}{\partial \xi} \qquad \text{with} \qquad \tilde{J}_{\mathtt{I}_q} = \frac{[h]}{e_0 n_{\mathtt{I}_{\mathsf{lat}}} C_h} J_{\mathtt{I}_q} = -\frac{1}{C_h}\tilde{S}_{\mathtt{I}} \frac{\partial y_{\mathtt{I}}}{\partial \xi} - \frac{1}{C_h}\tilde{\sigma}_{\mathtt{I}} \frac{\partial \tilde{\varphi}_{\mathtt{I}}}{\partial \xi}\,, \tag{136b}$$

(136c)

and

$$\frac{\mathrm{d}\tilde{\ell}_{\mathtt{I}}(t)}{\mathrm{d}\tau} = \frac{1}{C_h}\tilde{L}^{\mathsf{fo}}_{\mathtt{IE}}\, f_{\mathtt{BV}}(\lambda^{\mathsf{fo}}_{\mathtt{IE}})\,. \tag{136d}$$

The active phase with the variables $(y_{\mathtt{A}}, \tilde{\varphi}_{\mathtt{A}})$ is governed by

$$\frac{\partial y_{\mathtt{A}}}{\partial \tau} = -\frac{\partial \tilde{J}_{\mathtt{A}_C}}{\partial \xi} \qquad \text{with} \qquad \tilde{J}_{\mathtt{A}_C} = \frac{[h]}{\mathcal{L} n_{\mathtt{A}_{\mathsf{lat}}} C_h} J_{\mathtt{A}_C} = -\frac{1}{C_h}\tilde{D}_{\mathtt{A}} \frac{\partial y_{\mathtt{A}}}{\partial \xi}\,, \tag{137a}$$

$$0 = -\frac{\partial \tilde{J}_{\mathtt{A}_q}}{\partial \xi} \qquad \text{with} \qquad \tilde{J}_{\mathtt{A}_q} = \frac{[h]}{e_0 \mathcal{L} n_{\mathtt{A}_{\mathsf{lat}}} C_h} J_{\mathtt{A}_q} = -\frac{1}{C_h}\tilde{\sigma}_{\mathtt{A}} \frac{\partial \tilde{\varphi}_{\mathtt{A}}}{\partial \xi}\,. \tag{137b}$$

3.3.2 Boundary conditions

The dimensionless version of the boundary condition at the SEI–electrolyte interface reads

$$\tilde{J}_{\mathtt{E}_C} = -\eta_{\mathtt{IE}} \frac{1}{C_h}\tilde{L}^{\mathsf{in}}_{\mathtt{IE}} \cdot f_{\mathtt{BV}}(\lambda^{\mathsf{in}}_{\mathtt{IE}}) - \frac{1}{C_h}\tilde{L}^{\mathsf{fo}}_{\mathtt{IE}} \cdot f_{\mathtt{BV}}(\lambda^{\mathsf{fo}}_{\mathtt{IE}}) + y_{\mathtt{E}} \tilde{n}_{\mathtt{E}_{\mathsf{tot}}} \frac{1}{C_h}\tilde{L}^{\mathsf{fo}}_{\mathtt{IE}} \cdot f_{\mathtt{BV}}(\lambda^{\mathsf{fo}}_{\mathtt{IE}}) \quad \text{on } \Sigma^{\mathtt{E}}_{\mathtt{IE}}\,, \tag{138a}$$

$$\tilde{J}_{\mathtt{E}_q} = +\eta_{\mathtt{IE}} \frac{1}{C_h}\tilde{L}^{\mathsf{in}}_{\mathtt{IE}} \cdot f_{\mathtt{BV}}(\lambda^{\mathsf{in}}_{\mathtt{IE}}) + \frac{1}{C_h}\tilde{L}^{\mathsf{fo}}_{\mathtt{IE}} \cdot f_{\mathtt{BV}}(\lambda^{\mathsf{fo}}_{\mathtt{IE}}) \qquad \text{on } \Sigma^{\mathtt{E}}_{\mathtt{IE}}\,, \tag{138b}$$

and those at the active phase–SEI Interface are

$$-\tilde{J}_{\mathtt{A}_C} = \frac{1}{C_h}\tilde{L}^{\mathsf{in}}_{\mathtt{AI}} \cdot f_{\mathtt{BV}}(\lambda^{\mathsf{in}}_{\mathtt{AI}}) \qquad \text{on } \Sigma^{\mathtt{A}}_{\mathtt{AI}}\,, \tag{139a}$$

$$(\eta_{\mathtt{EA}} \tilde{J}_{\mathtt{E}_q} - \tilde{J}_{\mathtt{A}_q}) = 0 \qquad \text{on } \Sigma_{\mathtt{AI}}\,, \tag{139b}$$

with $f_{\mathtt{BV}}$ according to eq. (15) and the surface affinities $(\lambda^{\mathsf{in}}_{\mathtt{IE}}, \lambda^{\mathsf{fo}}_{\mathtt{IE}}, \lambda^{\mathsf{in}}_{\mathtt{AI}})$ according to the dimensionless versions of eq. (117), omitted here for compactness.

At the current collector–active phase interface, we have

$$\tilde{J}_{\mathtt{A}_q} = \tilde{i}(\tau)\,, \tag{140a}$$

$$\tilde{J}_{\mathtt{A}_C} = 0\,, \tag{140b}$$

and at the electrolyte–counter electrode interface

$$\tilde{\varphi}_{\mathtt{E}}|^{\mathtt{E}}_{\mathtt{EM}} = -(f_{\mathtt{E}}(y_{\mathtt{E}}|_{\mathtt{EM}}) - f_{\mathtt{E}}(y^0_{\mathtt{E}}))\,, \tag{141a}$$

$$\tilde{J}_{\mathtt{E}_q}|_{x_{\mathtt{E}}} = (\eta_{\mathtt{EA}})^{-1}\tilde{i}(\tau)\,. \tag{141b}$$

Note that eq. (141a) reflects that the counter electrode–electrolyte interface is to be in equilibrium, since $\tilde{\varphi}_{\mathtt{E}}|^{\mathtt{E}}_{\mathtt{EM}} = \frac{k_{\mathtt{B}}T}{e_0}\varphi_{\mathtt{E}}|^{\mathtt{E}}_{\mathtt{EM}} + \frac{k_{\mathtt{B}}T}{e_0}(\Delta\tilde{g}^{\mathsf{di}}_{\mathtt{EM}} + f_{\mathtt{E}}(y^0_{\mathtt{E}}))$.

3.4 Derivation of the ODE System

In this section we aim to determine balance equations for $(y_{\mathtt{I}}, y_{\mathtt{A}}, y_{\mathtt{E}})$.

3.4.1 Charge Balance

For the electro-neutral electrolyte, we have

$$J_{\mathtt{E}_q}|_{x_\mathtt{E}} = J_{\mathtt{E}_q}|_{\mathtt{IE}}^{\mathtt{E}} \,. \tag{142}$$

Note that

$$J_{\mathtt{E}_q}|_{\mathtt{IE}}^{\mathtt{E}} = e_0 L_{\mathtt{IE}}^{\mathsf{in}} \cdot f_{\mathtt{BV}}(\lambda_{\mathtt{IE}}^{\mathsf{in}}) + e_0 L_{\mathtt{IE}}^{\mathsf{fo}} \cdot f_{\mathtt{BV}}(\lambda_{\mathtt{IE}}^{\mathsf{fo}}) \,, \tag{143a}$$

$$J_{\mathtt{E}_q}|_{x_\mathtt{E}} = i(t) \,, \tag{143b}$$

where the second equation ensures electro-neutrality of the external circuit. Hence we obtain

$$i(t) = e_0 L_{\mathtt{IE}}^{\mathsf{in}} \cdot f_{\mathtt{BV}}(\lambda_{\mathtt{IE}}^{\mathsf{in}}) + e_0 L_{\mathtt{IE}}^{\mathsf{fo}} \cdot f_{\mathtt{BV}}(\lambda_{\mathtt{IE}}^{\mathsf{fo}}) \,, \tag{144}$$

which we can further exploit.

In order to determine $y_\mathtt{I}$, consider

$$\bar{y}_\mathtt{I} := \frac{1}{\ell_\mathtt{I}(t)} \int_{x_\mathtt{A}}^{x_\mathtt{I}(t)} y_\mathtt{I} \, \mathrm{d}x \,, \tag{145}$$

from which we can deduce

$$\frac{\mathrm{d}\bar{y}_\mathtt{I}}{\mathrm{d}t} = \frac{1}{n_{\mathtt{I}_{\mathsf{lat}}} \ell_\mathtt{I}(t)} \left(L_{\mathtt{IE}}^{\mathsf{in}} \cdot f_{\mathtt{BV}}(\lambda_{\mathtt{IE}}^{\mathsf{in}}) - n_{\mathtt{I}_C} v_{\mathtt{E}_S} L_{\mathtt{IE}}^{\mathsf{fo}} \cdot f_{\mathtt{BV}}(\lambda_{\mathtt{IE}}^{\mathsf{fo}}) - L_{\mathtt{AI}}^{\mathsf{in}} \cdot f_{\mathtt{BV}}(\lambda_{\mathtt{AI}}^{\mathsf{in}}) \right) \,. \tag{146}$$

Further, in order to determine $y_\mathtt{A}$, consider

$$\bar{y}_\mathtt{A} := \frac{1}{\mathcal{L}} \int_{x_0}^{x_\mathtt{A}} y_{\mathtt{A}_C} \, \mathrm{d}x \,, \tag{147}$$

which, using

$$n_{\mathtt{A}_{\mathsf{lat}}} \partial_t y_\mathtt{A} = -\partial_x J_{\mathtt{A}_C} \,, \tag{148a}$$

and

$$-J_{\mathtt{A}_C}|_{\mathtt{AI}}^{\mathtt{A}} = R_{\mathtt{AI}}^{\mathsf{in}} = L_{\mathtt{AI}}^{\mathsf{in}} \cdot f_{\mathtt{BV}}(\lambda_{\mathtt{AI}}^{\mathsf{in}}) \,, \tag{148b}$$

$$J_{\mathtt{A}_C}|_{x_0} = 0, \tag{148c}$$

yields the relation

$$\frac{\mathrm{d}\bar{y}_\mathtt{A}}{\mathrm{d}t} = \frac{1}{n_{\mathtt{A}_{\mathsf{lat}}} \mathcal{L}} L_{\mathtt{AI}}^{\mathsf{in}} \cdot f_{\mathtt{BV}}(\lambda_{\mathtt{AI}}^{\mathsf{in}}) \,. \tag{149}$$

Substituting $L_{\mathtt{AI}}^{\mathsf{in}} \cdot f_{\mathtt{BV}}(\lambda_{\mathtt{AI}}^{\mathsf{in}})$ in eq. (146) by eq. (149) yields

$$\frac{\mathrm{d}y_\mathtt{I}}{\mathrm{d}t} + \frac{n_{\mathtt{A}_{\mathsf{lat}}} \mathcal{L}}{n_{\mathtt{I}_{\mathsf{lat}}} \ell_\mathtt{I}(t)} \frac{\mathrm{d}\bar{y}_\mathtt{A}}{\mathrm{d}t} = \frac{1}{n_{\mathtt{I}_{\mathsf{lat}}} \ell_\mathtt{I}(t)} (L_{\mathtt{IE}}^{\mathsf{in}} \cdot f_{\mathtt{BV}}(\lambda_{\mathtt{IE}}^{\mathsf{in}}) - n_{\mathtt{I}_C} v_{\mathtt{E}_S} L_{\mathtt{IE}}^{\mathsf{fo}} \cdot f_{\mathtt{BV}}(\lambda_{\mathtt{IE}}^{\mathsf{fo}})) \,, \tag{150}$$

and substituting further $L_{\mathtt{IE}}^{\mathsf{in}} \cdot f_{\mathtt{BV}}(\lambda_{\mathtt{IE}}^{\mathsf{in}})$ via eq. (144), we obtain the evolution equation

$$\frac{\mathrm{d}\bar{y}_\mathtt{I}}{\mathrm{d}t} + \frac{n_{\mathtt{A}_{\mathsf{lat}}} \mathcal{L}}{n_{\mathtt{I}_{\mathsf{lat}}} \ell_\mathtt{I}(t)} \frac{\mathrm{d}\bar{y}_\mathtt{A}}{\mathrm{d}t} = \frac{1}{n_{\mathtt{I}_{\mathsf{lat}}} \ell_\mathtt{I}(t)} \Big(\frac{i(t)}{e_0} - (1 + n_{\mathtt{I}_C} v_{\mathtt{E}_S}) L_{\mathtt{IE}}^{\mathsf{fo}} \cdot f_{\mathtt{BV}}(\lambda_{\mathtt{IE}}^{\mathsf{fo}}) \Big) \,. \tag{151}$$

Equation (151) essentially relates the amount of intercalated lithium to the current $i(t)$ and the formation reaction $L_{\mathtt{IE}}^{\mathsf{fo}} \cdot f_{\mathtt{BV}}(\lambda_{\mathtt{IE}}^{\mathsf{fo}})$. Note that if no formation reaction were present, eq. (151) would simplify to

$$Q_\mathtt{A}^0 \frac{\mathrm{d}\bar{y}_\mathtt{A}}{\mathrm{d}t} = i(t) \,, \tag{152}$$

simply stating that the mole fraction of intercalated lithium (or the state of charge) $y_\mathtt{A}$ is directly determined by the current $i(t)$. However, when a formation reaction is present, the current does not

only change the state of charge, but it also contributes to the formation reaction.

Note that the formation reaction affinity $\lambda^{\text{fo}}_{\text{IE}}$, cf. eq. (117c), depends on the solvent concentration $y_{\text{E}_C}|^{\text{E}}_{\text{IE}}$, since solvent is consumed due to the formation reaction. Hence, we also have to take the solvent concentration variation into account, which we discuss in the next section.

3.4.2 Solvent Balance

Previously we used incompressibility so we did not have to solve the balance equation for the solvent species in the electrolyte domain $[x_{\text{I}}(t), x_{\text{E}}]$. However, it is now convenient to use solvent balance explicitly, which reads

$$\frac{\partial n_{\text{E}_S}}{\partial t} = -\partial_x J_{\text{E}_S}\,, \tag{153a}$$

together with the boundary conditions

$$(j_{\text{E}_S} - n_{\text{E}_S} w)|_{x_{\text{I}}(t)} = \kappa_{\text{E}_C} R^{\text{in}}_{\text{IE}} + (\kappa_{\text{E}_C} - 1) R^{\text{fo}}_{\text{IE}}\,, \tag{153b}$$

$$-j_{\text{E}_S}|_{x_{\text{E}}} = -\kappa_{\text{E}_C} i/e_0\,, \tag{153c}$$

and

$$w = \frac{\mathrm{d}x_{\text{I}}(t)}{\mathrm{d}t} = v_{\text{E}_S} L^{\text{fo}}_{\text{IE}} \cdot f_{\text{BV}}(\lambda^{\text{fo}}_{\text{IE}})\,. \tag{153d}$$

We denote with $\ell_{\text{E}}(t) = x_{\text{E}} - x_{\text{I}}(t)$ which yields (cf. appendix B)

$$\frac{\mathrm{d}\bar{n}_{\text{E}_S}}{\mathrm{d}t} = \frac{1}{\ell_{\text{E}}(t)}\big(\kappa_{\text{E}_C} R^{\text{in}}_{\text{IE}} + (\kappa_{\text{E}_C} - 1) R^{\text{fo}}_{\text{IE}} - \kappa_{\text{E}_C} i/e_0 - \bar{n}_{\text{E}_S} w\big)\,. \tag{154}$$

Note that we can rewrite $\ell_{\text{E}}(t) = \ell^0_{\text{E}} - (\ell_{\text{I}}(t) - \ell^0_{\text{I}})$. Further, for the cations we have

$$\frac{\partial n_{\text{E}_C}}{\partial t} = -\partial_x J_{\text{E}_C}\,, \tag{155a}$$

together with the boundary conditions

$$(j_{\text{E}_C} - n_{\text{E}_C} w)|_{x_{\text{I}}(t)} = -R^{\text{in}}_{\text{IE}} - R^{\text{fo}}_{\text{IE}}\,, \tag{155b}$$

$$j_{\text{E}_C}|_{x_{\text{E}}} = +i/e_0\,, \tag{155c}$$

which yields

$$\frac{\mathrm{d}\bar{n}_{\text{E}_C}}{\mathrm{d}t} = \frac{1}{\ell_{\text{E}}(t)}\big(i/e_0 - R^{\text{in}}_{\text{IE}} - R^{\text{fo}}_{\text{IE}} - \bar{n}_{\text{E}_C} w\big)\,. \tag{156}$$

Hence we obtain the balance equation for $\bar{n} = \sum_\beta \bar{n}_\beta$

$$\frac{\mathrm{d}\bar{n}}{\mathrm{d}t} = \frac{1}{\ell_{\text{E}}(t)}\big(-(\kappa_{\text{E}_C} - 1) i/e_0 + \kappa_{\text{E}_C} R^{\text{in}}_{\text{IE}} + (\kappa_{\text{E}_C} - 1) R^{\text{fo}}_{\text{IE}} - R^{\text{in}}_{\text{IE}} - R^{\text{fo}}_{\text{IE}} - \bar{n} w\big)\,, \tag{157}$$

and thus for $\bar{y}_{\text{E}_S}$ the balance equation (again, cf. appendix B)

$$\frac{\mathrm{d}\bar{y}_{\text{E}_S}}{\mathrm{d}t} = \frac{1}{\bar{n}\,\ell_{\text{E}}}(-(\kappa_{\text{E}_C} - y_{\text{E}_S}(\kappa_{\text{E}_C} - 1)) \cdot (i/e_0 - R^{\text{in}}_{\text{IE}}) + ((\kappa_{\text{E}_C} - 1)(1 - y_{\text{E}_S}) R^{\text{fo}}_{\text{IE}} + y_{\text{E}_S} R^{\text{fo}}_{\text{IE}})\,. \tag{158}$$

Next, we substitute $R^{\text{in}}_{\text{IE}}$ (cf. eq. (144)), i.e.

$$R^{\text{in}}_{\text{IE}} = e_0^{-1} i(t) - R^{\text{fo}}_{\text{IE}}\,, \tag{159}$$

whereby we obtain

$$\frac{\mathrm{d}}{\mathrm{d}t}\bar{y}_{\mathtt{E}_S} = -\frac{1}{\bar{n}\,\ell_{\mathtt{E}}}(1-y_{\mathtt{E}_S})R^{\mathsf{fo}}_{\mathtt{IE}}\,. \tag{160}$$

As expected, we find that the mole fraction of solvent species decreases by the formation reaction ($R^{\mathsf{fo}}_{\mathtt{IE}} > 0$).

The derived relations of the last sections hold true in general and we have not yet made any further assumptions. However, we will systematically apply some equilibrium conditions in order to simplify the resulting equation system.

3.4.3 OCV Conditions

Now we focus on the particular case of OCV-conditions, in which actually $C_h \to 0$, which implies for the transport parameters

$$(\partial_\xi y_{\mathtt{A}}, \partial_\xi \tilde{\varphi}_{\mathtt{A}}) \xrightarrow{\frac{(\tilde{D}_{\mathtt{A}},\tilde{\sigma}_{\mathtt{A}})}{C_h}\to\infty} 0\,, \tag{161a}$$

$$(\partial_\xi y_{\mathtt{E}}, \partial_\xi \tilde{\varphi}_{\mathtt{E}}) \xrightarrow{\frac{(\tilde{D}^y_{\mathtt{E}},\tilde{D}^\varphi_{\mathtt{E}},\tilde{S}_{\mathtt{E}},\tilde{\sigma}_{\mathtt{E}})}{C_h}\to\infty} 0\,, \tag{161b}$$

$$(\partial_\xi y_{\mathtt{I}}, \partial_\xi \tilde{\varphi}_{\mathtt{I}}) \xrightarrow{\frac{(\tilde{D}^y_{\mathtt{I}},\tilde{D}^\varphi_{\mathtt{I}},\tilde{S}_{\mathtt{I}},\tilde{\sigma}_{\mathtt{I}})}{C_h}\to\infty} 0\,, \tag{161c}$$

and for the reaction parameters

$$\lambda^{\mathsf{in}}_{\mathtt{IE}} \xrightarrow{\frac{\tilde{L}^{\mathsf{in}}_{\mathtt{IE}}}{C_h}\to\infty} 0, \qquad\qquad \lambda^{\mathsf{in}}_{\mathtt{AI}} \xrightarrow{\frac{\tilde{L}^{\mathsf{in}}_{\mathtt{AI}}}{C_h}\to\infty} 0\,. \tag{162}$$

The conditions from eq. (161) yield $\bar{y}_{\mathtt{A}} = y_{\mathtt{A}}$,$\bar{y}_{\mathtt{E}} = y_{\mathtt{E}}$ and $\bar{y}_{\mathtt{I}} = y_{\mathtt{I}}$, respectively, as well as

$$y_{\mathtt{A}}|^{\mathtt{A}}_{\mathtt{AI}} = y_{\mathtt{A}}\,, \quad y_{\mathtt{E}_S}|^{\mathtt{E}}_{\mathtt{IE}} = y_{\mathtt{E}_S} \quad \text{and} \quad y_{\mathtt{I}}|^{\mathtt{I}}_{\mathtt{AI}} = y_{\mathtt{I}}|^{\mathtt{I}}_{\mathtt{IE}} = y_{\mathtt{I}}\,, \tag{163}$$

and constant values (w.r.t. the space variable x) for $\varphi_{\mathtt{A}}$, $\varphi_{\mathtt{E}}$ and $\varphi_{\mathtt{I}}$.

The condition for $\lambda^{\mathsf{in}}_{\mathtt{IE}}$ in eq. (162) can be exploited to substitute $-\tilde{\varphi}_{\mathtt{I}}|^{\mathtt{I}}_{\mathtt{IE}} + \tilde{\varphi}_{\mathtt{E}}|^{\mathtt{E}}_{\mathtt{IE}}$ in $\lambda^{\mathsf{fo}}_{\mathtt{IE}}$ from eq. (117a), i.e.

$$0 = -(f_{\mathtt{I}}(y_{\mathtt{I}_C}|^{\mathtt{I}}_{\mathtt{IE}}) - f_{\mathtt{I}}(y^0_{\mathtt{I}_C})) + (f_{\mathtt{E}}(y_{\mathtt{E}_C}|^{\mathtt{E}}_{\mathtt{IE}}) - f_{\mathtt{E}}(y^0_{\mathtt{E}_C})) - \tilde{\varphi}_{\mathtt{I}}|^{\mathtt{I}}_{\mathtt{IE}} + \tilde{\varphi}_{\mathtt{E}}|^{\mathtt{E}}_{\mathtt{IE}}\,, \tag{164}$$

yielding the representation

$$\frac{\lambda^{\mathsf{fo}}_{\mathtt{IE}}}{k_{\mathtt{B}}T} = -\Delta g^{\mathsf{fo}} + (\ln(y_{\mathtt{E}_S}) - \ln(y^0_{\mathtt{E}_S})) + (f_{\mathtt{I}_e}(y_{\mathtt{I}}) - f_{\mathtt{I}_e}(y^0_{\mathtt{I}})) + (f_{\mathtt{I}_C}(y_{\mathtt{I}}) - f_{\mathtt{I}_C}(y^0_{\mathtt{I}}))\,. \tag{165}$$

The condition for $\lambda^{\mathsf{in}}_{\mathtt{AI}}$ in eq. (162) yields the constraint

$$0 = -(f_{\mathtt{A}}(y_{\mathtt{A}}) - f_{\mathtt{A}}(y^0_{\mathtt{A}_C})) + (f_{\mathtt{I}_C}(y_{\mathtt{I}}) - f_{\mathtt{I}_C}(y^0_{\mathtt{I}_C})) - \tilde{\varphi}_{\mathtt{A}}|^{\mathtt{A}}_{\mathtt{AI}} + \tilde{\varphi}_{\mathtt{I}}|^{\mathtt{I}}_{\mathtt{AI}}\,. \tag{166}$$

The continuity of the (electro-)chemical potential at the electrode–SEI interface, eq. (122), states that

$$(\tilde{\varphi}_{\mathtt{A}}|^{\mathtt{A}}_{\mathtt{AI}} - \tilde{\varphi}_{\mathtt{I}}|^{\mathtt{I}}_{\mathtt{AI}}) = -(f_{\mathtt{I}_e}(y_{\mathtt{I}}|^{\mathtt{I}}_{\mathtt{AI}}) - f_{\mathtt{I}_e}(y^0_{\mathtt{I}}))\,, \tag{167}$$

whereby eq. (166) yields the constraint

$$f_{\mathtt{I}_C}(y_{\mathtt{I}}) - f_{\mathtt{I}_C}(y^0_{\mathtt{I}}) + f_{\mathtt{I}_e}(y_{\mathtt{I}}) - f_{\mathtt{I}_e}(y^0_{\mathtt{I}_e}) = f_{\mathtt{A}}(y_{\mathtt{A}}) - f_{\mathtt{A}}(y^0_{\mathtt{A}})\,. \tag{168}$$

This condition allows us to write

$$y_{\mathtt{I}} = \hat{y}_{\mathtt{I}}(y_{\mathtt{A}})\,. \tag{169}$$

via the implicit function theorem, i.e. as a solution of

$$g(y_{\mathtt{I}}, y_{\mathtt{A}}) := f_{\mathtt{I}_C}(y_{\mathtt{I}}) - f_{\mathtt{I}_C}(y_{\mathtt{I}}^0) + f_{\mathtt{I}_e}(y_{\mathtt{I}}) - f_{\mathtt{I}_e}(y_{\mathtt{I}_e}^0) = f_{\mathtt{A}}(y_{\mathtt{A}}) - f_{\mathtt{A}}(y_{\mathtt{A}}^0) \stackrel{!}{=} 0\,, \tag{170}$$

and allows us further to substitute $(f_{\mathtt{I}_e}(y_{\mathtt{I}}) - f_{\mathtt{I}_e}(y_{\mathtt{I}}^0)) + (f_{\mathtt{I}_C}(y_{\mathtt{I}}) - f_{\mathtt{I}_C}(y_{\mathtt{I}_C}^0))$ in $\lambda_{\mathtt{IE}}^{\mathsf{fo}}$, yielding

$$\frac{\lambda_{\mathtt{IE}}^{\mathsf{fo}}}{k_{\mathtt{B}}T} = -\Delta g^{\mathsf{fo}} + (\ln(y_{\mathtt{E}_S}) - \ln(y_{\mathtt{E}_S}^0)) + f_{\mathtt{A}}(y_{\mathtt{A}}) - f_{\mathtt{A}}(y_{\mathtt{A}}^0)\,. \tag{171}$$

The actual values of the potential in the respective phases can be determined from eqs. (117a), (117b) and (141a) as

$$\tilde{\varphi}_{\mathtt{E}} = -(f_{\mathtt{E}}(y_{\mathtt{E}}) - f_{\mathtt{E}}(y_{\mathtt{E}}^0))\,, \tag{172a}$$
$$\tilde{\varphi}_{\mathtt{I}} = -(f_{\mathtt{I}}(\hat{y}_{\mathtt{I}_C}(y_{\mathtt{A}})) - f_{\mathtt{I}}(y_{\mathtt{I}_C}^0))\,, \tag{172b}$$
$$\tilde{\varphi}_{\mathtt{A}} = -(f_{\mathtt{A}}(y_{\mathtt{A}}) - f_{\mathtt{A}}(y_{\mathtt{A}_C}^0))\,, \tag{172c}$$

where the open-circuit voltage (OCV) is determined from eq. (124) as

$$E^{\mathsf{OCV}} = -\frac{k_{\mathtt{B}}T}{e_0} f_{\mathtt{A}}(y_{\mathtt{A}}) + E^0\,. \tag{173}$$

Note that $\lambda_{\mathtt{IE}}^{\mathsf{fo}}$ (cf. eq. (171)) is dependent on the OCV. Overall, to determine the variables $(y_{\mathtt{A}}, y_{\mathtt{E}_S}, \ell_{\mathtt{I}})$, we have the following coupled system of equations:

$$\frac{\mathrm{d}y_{\mathtt{A}}}{\mathrm{d}t} = \Big(\frac{\mathrm{d}\hat{y}_{\mathtt{I}}}{\mathrm{d}y_{\mathtt{A}}} + \frac{n_{\mathtt{A}_{\mathsf{lat}}}\mathcal{L}}{n_{\mathtt{I}_{\mathsf{lat}}}\ell_{\mathtt{I}}(t)}\Big)^{-1} \frac{1}{n_{\mathtt{I}_{\mathsf{lat}}}\ell_{\mathtt{I}}(t)} \Big(\frac{i(t)}{e_0} - (1 + n_{\mathtt{I}_C} v_{\mathtt{E}_S}) L_{\mathtt{IE}}^{\mathsf{fo}} \cdot f_{\mathtt{BV}}(\lambda_{\mathtt{IE}}^{\mathsf{fo}})\Big)\,, \tag{174a}$$

$$\frac{\mathrm{d}y_{\mathtt{E}_S}}{\mathrm{d}t} = -\frac{1}{\bar{n}\,(\ell_{\mathtt{E}}^0 - (\ell_{\mathtt{I}}(t) - \ell_{\mathtt{I}}^0))}(1 - y_{\mathtt{E}_S}) L_{\mathtt{IE}}^{\mathsf{fo}} \cdot f_{\mathtt{BV}}(\lambda_{\mathtt{IE}}^{\mathsf{fo}})\Big)\,, \tag{174b}$$

$$\frac{\mathrm{d}\ell_{\mathtt{I}}(t)}{\mathrm{d}t} = v_{\mathtt{E}_S} L_{\mathtt{IE}}^{\mathsf{fo}} \cdot f_{\mathtt{BV}}(\lambda_{\mathtt{IE}}^{\mathsf{fo}})\,, \tag{174c}$$

$$\frac{\lambda_{\mathtt{IE}}^{\mathsf{fo}}}{k_{\mathtt{B}}T} = -\Delta g^{\mathsf{fo}} + (\ln(y_{\mathtt{E}_S}) - \ln(y_{\mathtt{E}_S}^0)) + f_{\mathtt{A}}(y_{\mathtt{A}}) - f_{\mathtt{A}}(y_{\mathtt{A}}^0)\,. \tag{174d}$$

In non-dimensional form, the ODE system reads

$$\frac{\mathrm{d}y_{\mathtt{A}}}{\mathrm{d}\tau} = \frac{1}{1 + \tilde{\ell}_I(t)\eta_{\mathtt{AI}}^{-1}\frac{\mathrm{d}\hat{y}_{\mathtt{I}}}{\mathrm{d}y_{\mathtt{A}}}} \big(\tilde{i}(\tau) - (\eta_{\mathtt{EA}} + \eta_{\mathtt{IA}} y_{\mathtt{I}}(\tau)) \frac{1}{C_h} \tilde{L}_{\mathtt{IE}}^{\mathsf{fo}} \cdot f_{\mathtt{BV}}(\lambda_{\mathtt{IE}}^{\mathsf{fo}})\big)\,, \tag{175a}$$

$$\frac{\mathrm{d}y_{\mathtt{E}_S}}{\mathrm{d}\tau} = -\frac{1}{\tilde{n}_{\mathtt{E}_{\mathsf{tot}}}\,(\tilde{\ell}_{\mathtt{E}}^0 - \tilde{\ell}_{\mathtt{I}}(\tau)\,)}(1 - y_{\mathtt{E}_S}(\tau)) \frac{1}{C_h} \tilde{L}_{\mathtt{IE}}^{\mathsf{fo}} f_{\mathtt{BV}}(\lambda_{\mathtt{IE}}^{\mathsf{fo}})\,, \tag{175b}$$

$$\frac{\mathrm{d}\tilde{\ell}_{\mathtt{I}}(t)}{\mathrm{d}\tau} = \frac{1}{C_h} \tilde{L}_{\mathtt{IE}}^{\mathsf{fo}} \cdot f_{\mathtt{BV}}(\lambda_{\mathtt{IE}}^{\mathsf{fo}})\,, \tag{175c}$$

$$\frac{\lambda_{\mathtt{IE}}^{\mathsf{fo}}}{k_{\mathtt{B}}T} = -\Delta g^{\mathsf{fo}} + (\ln(y_{\mathtt{E}_S}) - \ln(y_{\mathtt{E}_S}^0)) + f_{\mathtt{A}}(y_{\mathtt{A}}) - f_{\mathtt{A}}(y_{\mathtt{A}}^0)\,. \tag{175d}$$

3.4.4 Representation of the Reaction Rate

Non-equilibrium thermodynamics initially treats each chemical reaction as *reversible*, which is also reflected in the notation A + B $\rightleftharpoons$ C and the formulation of the reaction rate

$$R = L \cdot f_{\mathtt{BV}}(\lambda) \qquad \text{with} \qquad f_{\mathtt{BV}}(z) = \mathrm{e}^{\alpha \frac{z}{k_{\mathtt{B}}T}} - \mathrm{e}^{-(1-\alpha)\frac{z}{k_{\mathtt{B}}T}} \tag{176}$$

$$\text{and} \qquad \lambda = -(\mu_C - \mu_A - \mu_B)\,, \tag{177}$$

which yields $R > 0$ for $\lambda > 0$ and $R < 0$ for $\lambda < 0$. However, if presumably (or approximately) only one direction occurs, e.g. A + B $\longrightarrow$ C, we can rewrite R in order to obtain some necessary restrictions on the reaction parameters.

In principle, each reaction has two independent parameters, (i) the Δg of the reaction, i.e.

$$\Delta g = g_C - g_A - g_B \tag{178}$$

which covers the *constant* parts of the chemical potentials $\mu_\alpha = g_\alpha + k_\mathrm{B} T \ln y_\alpha$, and (ii) the constant Onsager coefficient L. We decompose the reaction affinity

$$\lambda = -\Delta g + \tilde{\lambda}\,, \tag{179}$$

where $\tilde{\lambda}$ has then no *constant* terms. This can be exploited to rewrite $R = L \cdot f_{\mathtt{BV}}(\lambda)$ as

$$R = L \cdot \mathrm{e}^{-\alpha(\Delta g - \tilde{\lambda})} - L \cdot \mathrm{e}^{+(1-\alpha)(\Delta g - \tilde{\lambda})}\,, \tag{180}$$

$$= K^{\mathrm{fo}} \cdot \mathrm{e}^{\alpha\tilde{\lambda}} - K^{\mathrm{ba}} \cdot \mathrm{e}^{-(1-\alpha)\tilde{\lambda}}\,, \tag{181}$$

where $K^{\mathrm{fo}} = L \cdot \mathrm{e}^{-\alpha(\Delta g)}$ and $K^{\mathrm{ba}} = L \cdot \mathrm{e}^{(1-\alpha)(\Delta g)}$ can be considered as equivalent independent parameters to Δg and L. However, this representation is especially useful when a reaction considerably occurs only in one direction, i.e. $\Delta g \to -\infty$ implies $K^{ba} \to 0$ (while $K^{\mathrm{fo}} < \infty$ yields a constraint on L). Hence, for reactions occurring only in *forward direction*, we can consider K^{fo} as the single reaction rate parameter.

4 Numerical Examples under OCV conditions

In this section, we discuss several numerical examples of the derived SEI-growth model under OCV conditions. We consider three different kinds of numerical experiments, i.e.

1 Charge and rest,

2 periodic cycling between $(0\%$-$100\%)$ SOC and between $(20\%$-$80\%)$ SOC,

3 and various $\mu_\mathtt{A}$ functions (OCVs),

which are reflected in different time dependent current profiles $i(t)$. For each experiment we solve the ODE system (174) and compute the cell voltage $E(t)$, the lithium content $y_\mathtt{A}(t)$ in the electrode, the SEI thickness $\ell_\mathtt{I}(t)$ and the solvent concentration $y_{\mathtt{E}_S}(t)$.

If not stated otherwise, we consider DMC as solvent with $n^{\mathrm{ref}}_{\mathtt{E}_S} = 11.867\mathrm{mol\,L^{-1}}$, a salt concentration of $n^{\mathrm{ref}}_{\mathtt{E}_C} = 1\mathrm{mol\,L^{-1}}$ and a solvation number of $\kappa = 4$ [46, 35]. For the active phase material we consider a lattice site density of graphite, i.e. $n_{\mathtt{A}_{\mathrm{lat}}} = \frac{1}{\omega_\mathtt{A}} \frac{\rho_\mathtt{A}}{M_\mathtt{A}} = 31\mathrm{mol\,L^{-1}}$, where $\rho_\mathtt{A} = 2260\mathrm{g\,L^{-1}}$, $M_\mathtt{A} = 12.01\mathrm{g\,mol^{-1}}$, and $\omega_\mathtt{A} = 6$, reflecting LiC_6, i.e. one lattice site per six carbon atoms. This yields

$$y^0_{\mathtt{E}_S} = 0.6591 \qquad y^0_{\mathtt{E}_C} = 0.1704 \tag{182}$$

$$\eta_{\mathtt{EA}} = 0.3828 \qquad \eta_{\mathtt{IA}} = 1\,. \tag{183}$$

Further, we consider a lithium half cell with an ideal electrode material, reflected by a chemical potential function

$$f_\mathtt{A} = \ln \frac{y_\mathtt{A}}{1 - y_\mathtt{A}} \tag{184}$$

and similar for the SEI

$$f_{\mathtt{I}} = \ln \frac{y_{\mathtt{A}}}{1 - y_{\mathtt{A}}} \tag{185}$$

which entails $y_{\mathtt{I}} = y_{\mathtt{A}}$. Note that these specific material functions just serve for demonstration issues in order to decouple more complex effects which arise from the active material from our focus here on the SEI growth model. In section 4.3 we also consider more realistic chemical potential functions $f_{\mathtt{A}}$. Note that in all examples the SEI growth reaction depends self-consistently on the OCV of the electrode material via this contribution to the chemical potential function $\mu_{\mathtt{A}}$. If not state otherwise, cycling will occur between $E^{\mathsf{max}} = 0.2\,\mathrm{V}$ and $E^{\mathsf{min}} = 0\,\mathrm{V}$.

The ODE system can be solved with standard solvers for boundary value problems. Here, the following examples were computed using fifth-order Runge-Kutta methods, both in MATLAB with `ode45`, and in Python with `solve_ivp` from SciPy.

4.1 Charge and Rest

In this example, the initially lithium poor electrode is charged at constant current $i(t) = i^0$ (i.e. filled with lithium) until a certain threshold value E^{min} is reached, and then *stored* at $i(t) = 0$ for $t \to \infty$, where we compute the further time-evolution of all quantities. Hence, we consider as current

$$i(t) = \begin{cases} i^0\,, & t < t^* = \{\tau \in [0,T] | E(\tau) = E^{\mathsf{min}}\} \\ 0\,, & t \geq t^*\,. \end{cases} \tag{186}$$

We discuss essentially the variation of two parameters, (i) the forward reaction rate constant K^{fo} of the SEI formation reaction and (ii) of the initial electrolyte thickness $\ell^0_{\mathtt{E}}$.

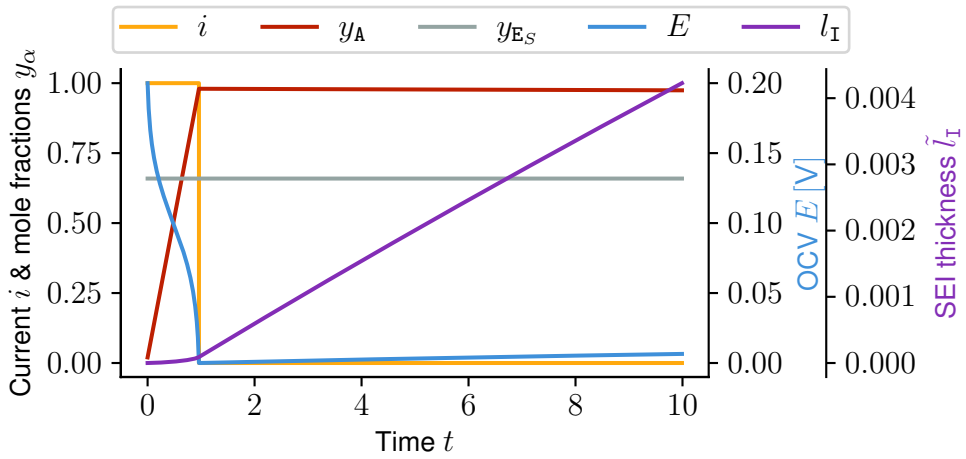

Figure 4: Time evolution of all variables for a *large* electrolyte domain $\tilde{\ell}^0_E = 100$ and a *small* reaction rate constant $\tilde{K}^{\mathsf{fo}} = 10^{-5}$.

For *large* electrolyte domains $\tilde{\ell}^0_E = 100$ (with respect to the domain size of the active phase) we find for small reaction rate constants $\tilde{K}^{\mathsf{fo}} = 10^{-5}$ of the formation reaction, after charging the electrode ($t > t^*$), almost constant values for $(y_{\mathtt{A}}(t), E(t), y_{\mathtt{E}_S}(t))$ as well as a very small (but linear) growth of SEI thickness $\ell_{\mathtt{I}}(t)$, see fig. 4. The SEI growth seems larger during storage than during charging, but rate of the formation reaction depends only on $y_{\mathtt{A}}$ and $y_{\mathtt{E}_S}$, making $\ell_{\mathtt{I}}$ continuously differentiable at the point of turning off the current, t^*. During storage, as the SEI continues to grow, the electrode is slowly discharged, and as a result, the OCV rises again.

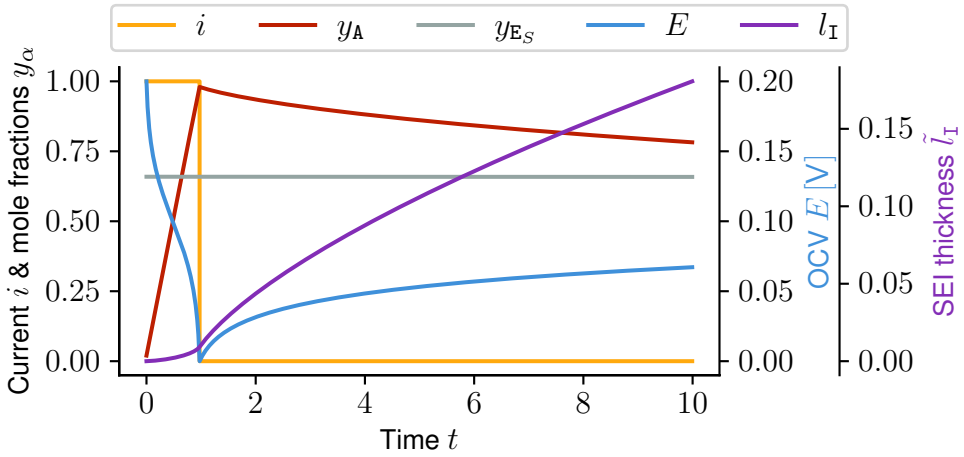

Figure 5: Time evolution of all variables for a *large* electrolyte domain $\tilde{\ell}_E^0 = 100$ and a *medium* reaction rate constant $\tilde{K}^{\mathrm{fo}} = 10^{-3}$.

For a *large* electrolyte domain and a *medium* reaction rate constant $\tilde{K}^{\mathrm{fo}} = 10^{-3}$, we find the SEI growth during charging to be comparatively slow to the growth during rest. This is due to the fact that affinity of the formation is largest in the fully charged state. After charging the electrode ($t > t^*$), a self-discharge of the electrode due to the SEI formation takes place, i.e. y_{A} decreases while the voltage $E(t)$ increases (see fig. 5). This coincides with the notion that the SEI growth consumes lithium, yielding the non-linear growth rate for $\ell_{\mathrm{I}}(t)$. Note that, since no external current (electrons) enter the electrode via an external circuit, the self-discharge of $\mathrm{C}\big|^{\mathrm{A}} \to \mathrm{C}^+\big|^{\mathrm{I}} + \mathrm{e}^-\big|^{\mathrm{I}}$ is *the* source of electrons and lithium ions in order to proceed with the SEI growth reaction[6] $\mathrm{C}\big|^{\mathrm{A}} + \mathrm{S}\big|^{\mathrm{E}} \rightleftharpoons \mathrm{B}\big|^{\mathrm{I}}$. Lithium ions from the electrolyte alone cannot grow the SEI.[7] As the reaction rate is larger than in the first case, more lithium is being consumed, resulting in a larger decrease in y_{A}. This in turn leads to a slower formation reaction as time goes on, leading to the nonlinear growth seen in fig. 5.

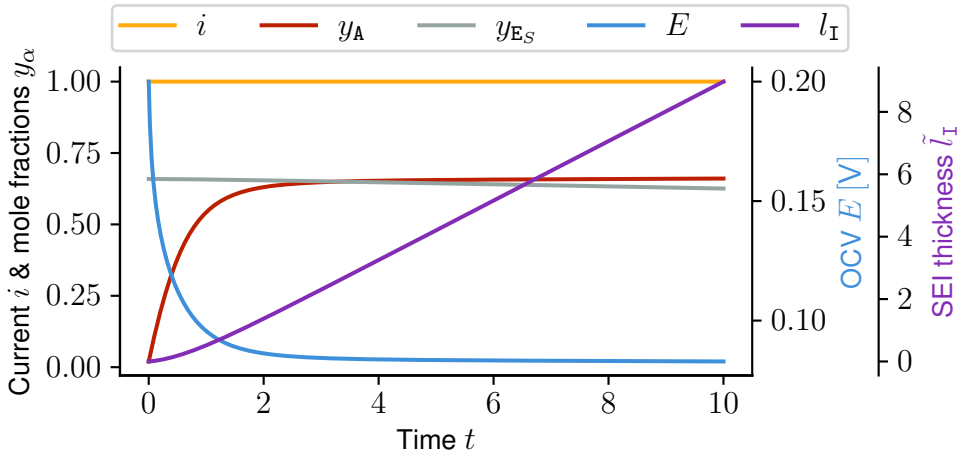

Figure 6: Time evolution of all variables for a *large* electrolyte domain $\tilde{\ell}_E^0 = 100$ and a *large* reaction rate constant $\tilde{K}^{\mathrm{fo}} = 10^{-1}$.

Finally, for a *large* electrolyte domain $\tilde{\ell}_E^0 = 100$ and a *large* reaction rate constant $\tilde{K}^{\mathrm{fo}} = 10^{-1}$, we

[6] Note that in equilibrium $\mathrm{C}^+\big|^{\mathrm{E}} \rightleftharpoons \mathrm{C}^+\big|^{\mathrm{I}} + \kappa_{\mathrm{E_C}}\mathrm{S}\big|^{\mathrm{E}}$ and $\mathrm{C}\big|^{\mathrm{A}} \to \mathrm{C}^+\big|^{\mathrm{I}} + \mathrm{e}^-\big|^{\mathrm{I}}$ whereby $\mathrm{C}^+\big|^{\mathrm{E}} + \mathrm{e}^-\big|^{\mathrm{I}} + \mathrm{S}\big|^{\mathrm{E}} \rightleftharpoons \mathrm{B}\big|^{\mathrm{I}} + \kappa_{\mathrm{E_C}}\mathrm{S}\big|^{\mathrm{E}}$ is equivalent to $\mathrm{C}\big|^{\mathrm{A}} + \mathrm{S}\big|^{\mathrm{E}} \rightleftharpoons \mathrm{B}\big|^{\mathrm{I}}$.

[7] If ions from the electrolyte together with electrons from the electrode (without connection to an external electron source) would grow the SEI, the electrode essentially would become positively charged, violating the electroneutrality condition.

find that the SEI formation reaction actually becomes the voltage determining process, whereby E^{min} actually cannot be reached for large electrolyte domains. While charging the electrode, $y_{\mathtt{A}}$ increases to about 0.6, which decreases correspondingly the OCV. However, we find that beyond about $t > 2$ the concentration saturates well below 1, i.e. before beeing entirely filled with intercalated cations (see Fig. 6). However, further *charging* of the electrode does not further change the mole fraction $y_{\mathtt{A}}$, whereby the entire current flows into the SEI growth. The resulting growth rate for the SEI is then again linear in time, however, due to another reason compared to the situation of Fig. 4.

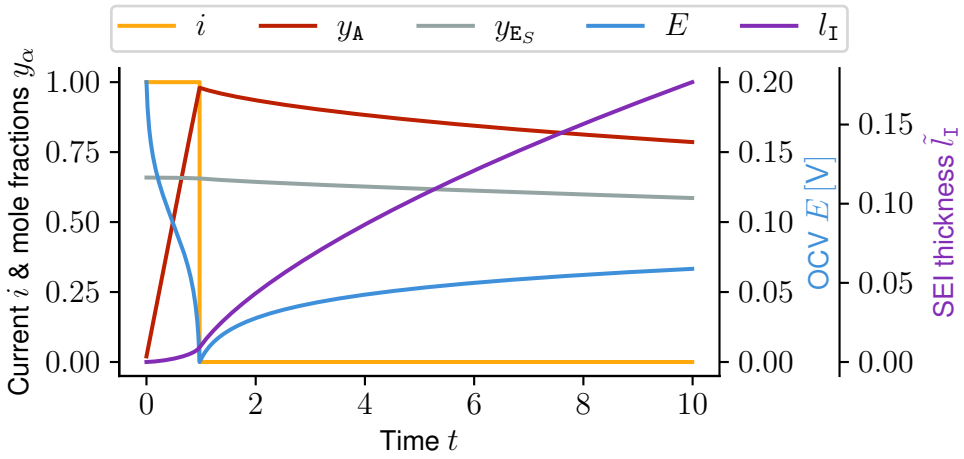

Figure 7: Time evolution of all variables for a *small* electrolyte domain $\tilde{\ell}_E^0 = 1$ and a *medium* reaction rate constant $\tilde{K}^{\text{fo}} = 10^{-3}$.

Next we discuss *small* electrolyte domains $\tilde{\ell}_E^0 = 1$. Since the SEI formation $\mathrm{C}\big|^{\mathtt{A}} + \mathrm{S}\big|^{\mathtt{E}} \rightleftharpoons \mathrm{B}\big|^{\mathtt{I}}$ consumes solvent species S, it changes the bulk solvent concentration (or mole fraction $y_{\mathtt{E}_S}$), see figs. 7 and 8. While for large electrolyte domains this variation is negligible, it becomes dominant for small electrolyte domains. For medium reaction rate constants $\tilde{K}^{\text{fo}} = 10^{-3}$ we find a linear decrease of the solvent concentration in time (cf. fig. 7), clearly showing the impact of the SEI reaction. Note that this effect could be more pronounced in small pores of porous media, where the pore size is actually in the order of the active phase particles. However, we find that the electrode is also self-discharging, whereby the lithium mole fraction $y_{\mathtt{A}}$ decreases non-linearly in time. The resulting SEI growth regime exhibits a square root like behavior. For the storage time plotted here, the difference between fig. 5 and fig. 7 is small; only the decrease in $y_{\mathtt{E}_S}$ is noticeably larger in the small electrolyte case. Until the solvent concentration has been noticeably reduced, the electrolyte domain size has no impact on the SEI growth. Under the OCV conditions considered here, the solvent transport does not influence the SEI formation.

For *large* reaction rate constant $\tilde{K}^{\text{fo}} = 10^{-1}$ and small electrolyte domains, the electrode no longer reaches the stop condition for the current, as the whole solvent is consumed before the OCV reaches $E^{\text{min}} = 0\,\mathrm{V}$. Both solvent concentration and SEI growth become nonlinear, and the SEI growth saturates (cf. fig. 8) once no more solvent is left to proceed with the reaction $\mathrm{C}\big|^{\mathtt{A}} + \mathrm{S}\big|^{\mathtt{E}} \rightleftharpoons \mathrm{B}\big|^{\mathtt{I}}$. Hence, the *origin* for the stop in SEI growth under these conditions is the vanishing concentration of solvent species $y_{\mathtt{E}_S}$. This stop in SEI growth occurs even though there is lithium in the active material and an external current present.

Overall we thus find that the SEI growth could *stop* for $t \to \infty$ when either the solvent or the intercalated cations are depleted, more precisely if $\frac{\lambda_{\mathtt{IE}}^{\text{fo}}}{k_{\mathrm{B}}T} \to 0$ (cf. eq. (171)), which is equivalent to

$$g(y_{\mathtt{E}_S}, y_{\mathtt{A}}) := (\ln(y_{\mathtt{E}_S}) - \ln(y_{\mathtt{E}_S}^0)) + f_{\mathtt{A}}(y_{\mathtt{A}}) - f_{\mathtt{A}}(y_{\mathtt{A}}^0) \overset{!}{\to} \Delta g^{\text{fo}}\,. \tag{187}$$

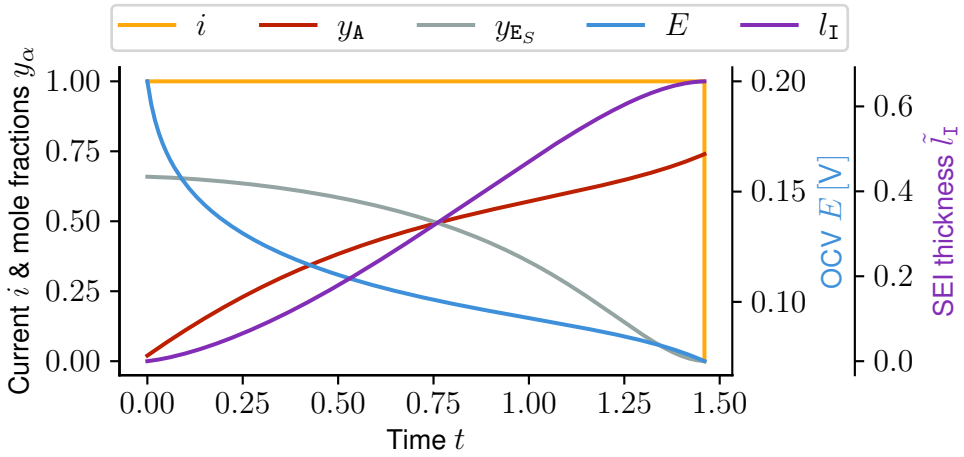

Figure 8: Time evolution of all variables for a *small* electrolyte domain $\tilde{\ell}_E^0 = 1$ and a *large* reaction rate constant $\tilde{K}^{\text{fo}} = 10^{-1}$.

The consumption of solvent $(\ln(y_{\mathrm{E}_S}) \to -\infty)$ and intercalated lithium $(f_{\mathrm{A}}(y_{\mathrm{A}}) \to -\infty)$ thus coincides with our notion of $\Delta g^{\text{fo}} \to -\infty$. Or stated the other way round: For a given Δg^{fo} the SEI growth can only stop if the solvent concentration $y_{\mathrm{E}_S}^\infty$ and the lithium concentration in the active phase y_{A}^∞ at t^∞ ensure $g(y_{\mathrm{E}_S}^\infty, y_{\mathrm{A}}^\infty) = \Delta g^{\text{fo}}$. However, since y_{E_S} and y_{A} are in general two independent variables, the condition $g(y_{\mathrm{E}_S}^\infty, y_{\mathrm{A}}^\infty) = \Delta g^{\text{fo}}$ forms a trajectory of $(y_{\mathrm{E}_S}^\infty, y_{\mathrm{A}}^\infty)$ values for which the SEI growth stops. Or, by the implicit function theorem, one might either write $y_{\mathrm{A}}^\infty = h_{\mathrm{A}}(\Delta g^{\text{fo}}, y_{\mathrm{E}_S}^\infty)$, where the lithium mole fraction (or SoC) is determined under which the SEI growth stops, for given values of $(\Delta g^{\text{fo}}, y_{\mathrm{E}_S}^\infty)$. Alternatively, $y_{\mathrm{E}_S}^\infty = h_{\mathrm{E}_S}(\Delta g^{\text{fo}}, y_{\mathrm{A}}^\infty)$ where $y_{\mathrm{E}_S}^\infty$ is determined as a function of the state of charge y_{A}. The latter might arise when electrodes are *stored* at constant voltage. However, in general both quantities are independent variables subject to their own evolution equations.

4.2 Periodic Cycling

Now let's consider periodic charging and discharging of the half-cell between E^{min} and E^{max} under constant current conditions. Note that due to the consumption of electrons in the SEI formation reaction, the cycle length is not constant between cycles. This is illustrated in fig. 9. For the n-th cycle, the time interval is denoted by $[t_n^{\text{max}}, t_{n+1}^{\text{max}}]$ and the cycle length by $t_n^{\text{cyc}} = t_{n+1}^{\text{max}} - t_n^{\text{max}}$, where $t_0^{\text{max}} = 0$.

We can then write the current $i(t)$ as

$$i(t) = \begin{cases} +i_0\,, & t \leq t_n^{\text{min}} = \{\tau \in [t_{n-1}^{\text{max}}, T] | E(t) = E^{\text{min}}\} \\ -i_0\,, & t_n^{\text{min}} < t \leq t_n^{\text{max}} = \{\tau \in [t_n^{\text{min}}, T] | E(\tau) = E^{\text{max}}\}\,. \end{cases} \tag{188}$$

and correspondingly the capacity q

$$q(t) = \int_0^t i(t')dt'\,. \tag{189}$$

Note, however, that for a constant charging cycle t^{cyc} we would find $q(t) \in [0, \frac{t}{t^{\text{cyc}}}]$. However, since t^{cyc} is not known *a priori*, we have to solve the ODE system, eq. (174), in the time interval $[0, T]$ and obtain t^{cyc} via the stopping condition $E(t) \geq E^{\text{max}}$. The determination of t_n^{cyc} is thus actually a part of solving the ODE system under the conditions of cycling between E^{min} and E^{max}, which yields the time-evolution of $q(t)$.

First, we consider a *large* electrolyte domain $\tilde{\ell}_E^0 = 100$ for both *small*, $\tilde{K}^{\text{fo}} = 10^{-5}$, and *medium*,

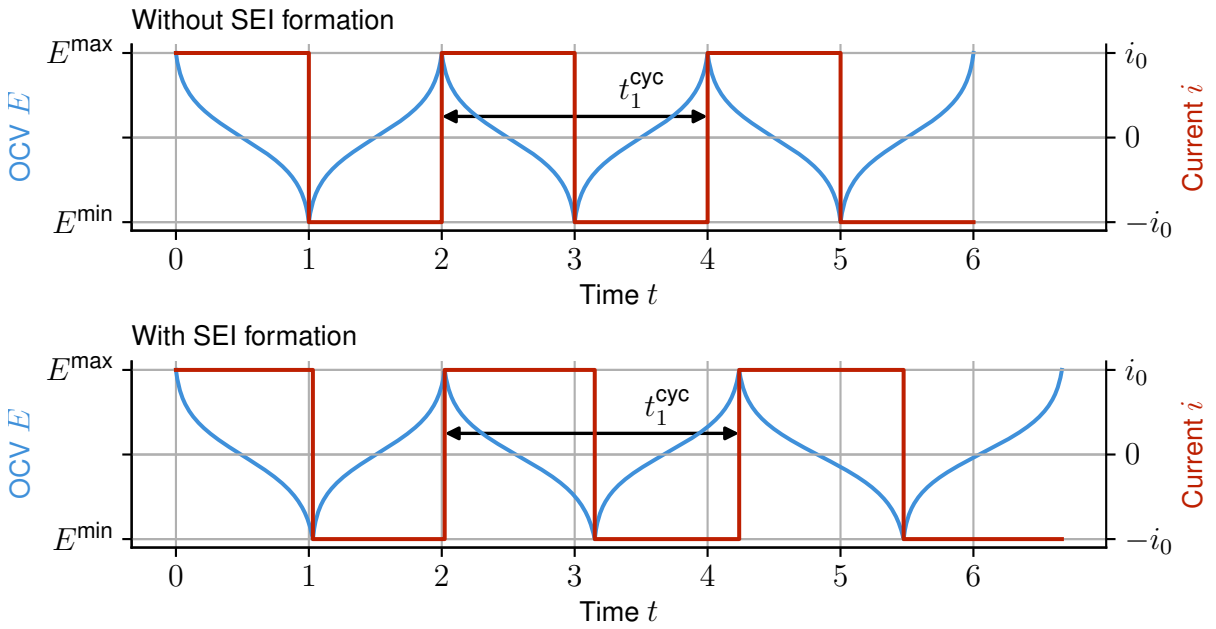

Figure 9: Current and OCV over time without SEI formation at the top, and with it at the bottom. Without SEI formation, the cycling time t_n^{cyc} is constant, but with SEI formation, the cycles become longer for the same charging rate.

$\tilde{K}^{\text{fo}} = 10^{-3}$, reaction rates. Figure 10 shows the evolution of the cell voltage for both systems over multiple cycles. For a *small* reaction rate the capacity remains almost constant, as only a negligible current flows into the SEI. Note that capacity q is not the amount of lithium that can be stored in the active material (which is assumed to be constant), but the time integral of the current, i.e. what would typically be measured during coulometry. For medium rates we find a clear right shift of the cell voltage E w.r.t. the capacity q, as well as a *widening* of the OCV curves. The right shift is a result of electrons being consumed by the formation reaction, leaving only a fraction of the overall current to (dis-)charge the electrode. The charge consumed by the SEI growth, $q_{\text{I}}(t) = \int_0^t e_0 R_{\text{IE}}^{\text{fo}}(t')\,\mathrm{d}t'$, is equal to the observed right shift. As the SEI grows, its capacity to store ions ($l_{\text{I}} n_{\text{I}_{\text{lat}}}$) is also increasing. Under the assumption of electroneutrality, there is an equal amount of electrons being stored alongside, causing the widening seen in fig. 10.

For large formation reaction rates, $\tilde{K}^{\text{fo}} = 10^{-1}$, the *shifting* and *stretching* of the cell voltage be-

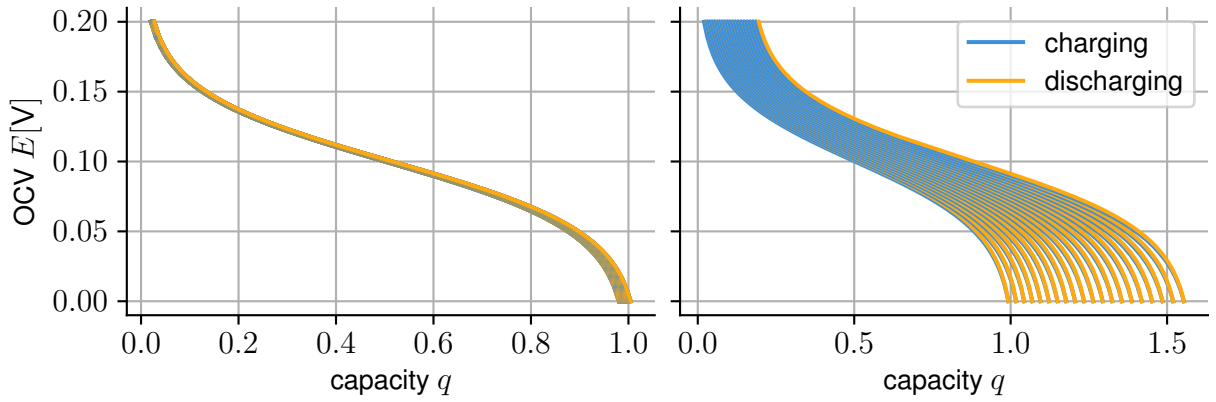

Figure 10: Evolution of the cell voltage E w.r.t. the capacity q for small (left) and medium (right) SEI formation rates.

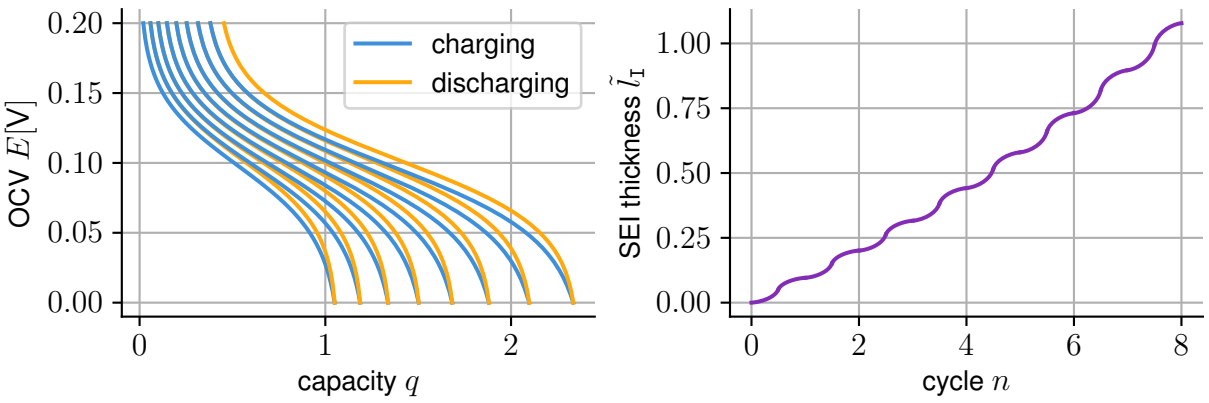

Figure 11: Computed behaviour of a half cell for large formation reaction rates, $\tilde{K}^{\mathrm{fo}} = 10^{-1}$. On the left the evolution of the cell voltage, and on the right the SEI thickness during cycling.

comes even more pronounced, cf. fig. 11. Since the formation reaction is treated as forward only (cf. section 3.4.4), the growth of the SEI is monotonic.

The formation reaction has an asymmetric influence on the charging and discharging times. During charging, some percentage of the external current current is used for supplying electrons to the SEI formation, rather than for the intercalation reaction that charges the active material. The charge cycle is therefore longer with SEI growth present than without it. During discharging, the formation reaction consumes electrons *in addition to* the external circuit, resulting in a faster discharge and therefore shorter discharge cycles.

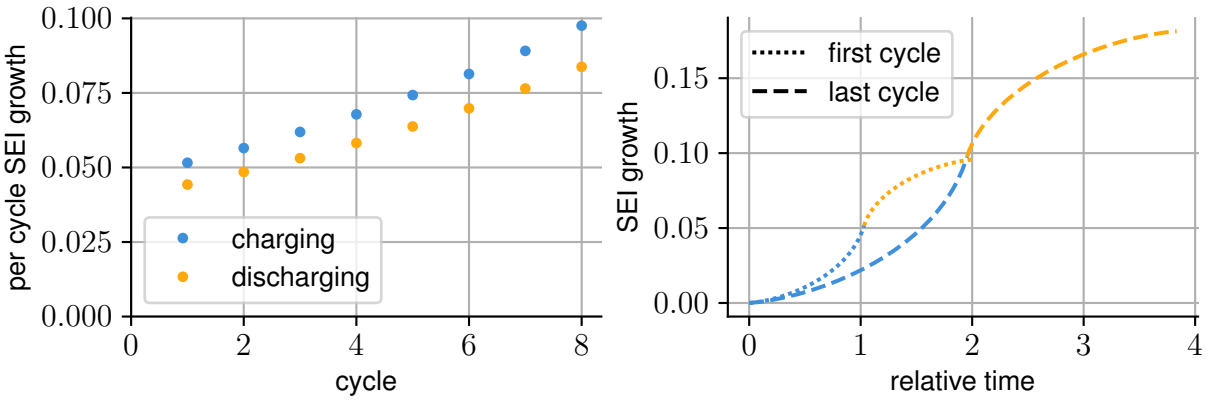

Figure 12: SEI growth per cycle is larger during charging than during discharging (left). The cycle length, and with it the SEI growth, become larger for later cycles (right). The growth rate is largest in the charged state ($y_{\mathrm{A}} \approx 1$) and lowest in the discharged state ($y_{\mathrm{A}} \approx 0$).

As a result of the different cycle lengths, the SEI growths more during charging than during discharging, as can be seen in fig. 12. In addition, as mentioned earlier, the cycles become longer overall due to the additional capacity of the SEI itself. If the electrolyte domain is large, the influence of the change in solvent concentration is negligible. In this case, the affinity of the formation reaction becomes very small as y_{A} returns to y_{A}^0. The derivative $\frac{\mathrm{d}l_\mathrm{I}(t)}{\mathrm{d}t}$ is therefore also close to zero when the electrode is empty. Conversely, the highest affinities and largest growth rates are observed when the electrode is fully charged.

The coulombic efficiency (CE) of an electrode relates the charge which is put into the electrode upon charging to the charge which can be withdrawn from the electrode upon discharging. When SEI growth

is considered, the CE η_n^{CE} is not constant amount cycles, but varies with the cycle number n, where

$$\eta_n^{\mathrm{CE}} := \frac{Q_n^{\mathrm{out}}}{Q_n^{\mathrm{in}}} \quad \text{with} \quad Q_n^{\mathrm{out}} = \int_{t_n^{\min}}^{t_n^{\max}} i(t')dt', \quad Q_n^{\mathrm{in}} = \int_{t_{n-1}^{\max}}^{t_n^{\min}} i(t')dt'. \tag{190}$$

We can compute the CE based on our model (c.f. 13 and 14) and and further examine the influence of depth of discharge on the SEI growth.

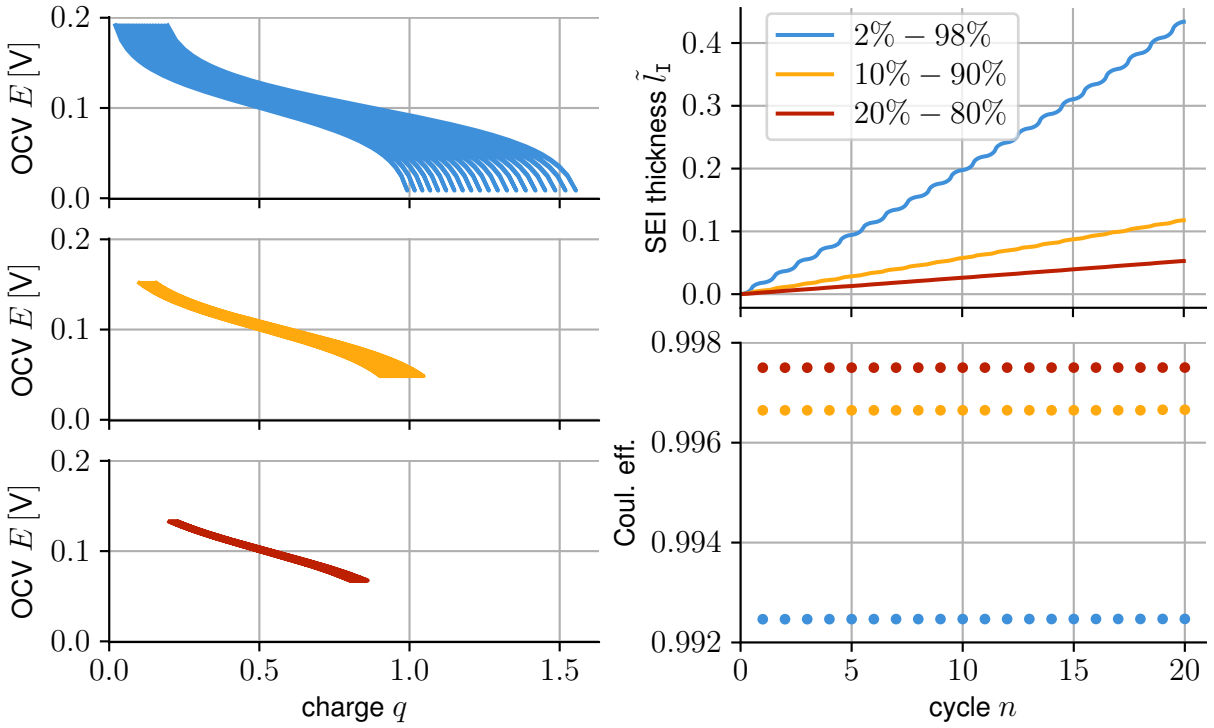

Figure 13: Evolution of the OCV curves, SEI thickness and coulombic efficiency for different cycling regimes. Shallower cycling results in less SEI growth and higher coulombic efficiency.

In fig. 13, the system behaviour over 20 cycles is shown for three different cycling regimes: $2\,\%$ to $98\,\%$, $10\,\%$ to $90\,\%$ and $20\,\%$ to $80\,\%$. The voltage range naturally decreases for shallower cycling. The SEI growth is much less pronounced for the shallower regimes, which consequently also results in less shift and stretch of the OCV curves. The coulombic efficiency stays constant over the cycles, as the large electrolyte domain means the solvent does not deplete significantly. For deeper cycling, more current is diverted into the irreversible SEI growth, causing lower efficiencies.

Lastly, we want to take a look at the behaviour over many cycles. In fig. 14, we can see the SEI growth and coulombic efficiency of the half-cell for different reaction rate coefficients of the formation reaction. These results are for an electrode with a small electrolyte domain, $\tilde{l}_{\mathrm{E}}^0 = 1$, where the consumption of solvent in the formation reaction leads to a slowing of the SEI growth at larger reaction rate coefficients and cycle numbers. This is directly related to the coulombic efficiency, as a reduction in SEI formation leaves a higher percentage of the current for charging and discharging of the active material.

4.3 Cycling with Experimental OCV Curves

The chemical potential function $\mu_{\mathrm{A}}(y_{\mathrm{A}})$ can be chosen to represent different materials. In the previous sections, we have assumed the non-constant part $f_{\mathrm{A}}(y_{\mathrm{A}})$ to be $\ln \frac{y}{1-y}$. Now, we will fit this function to experimental data from Smith et al. [61]. The experimental cells used MCMB graphite electrodes (92:4:4

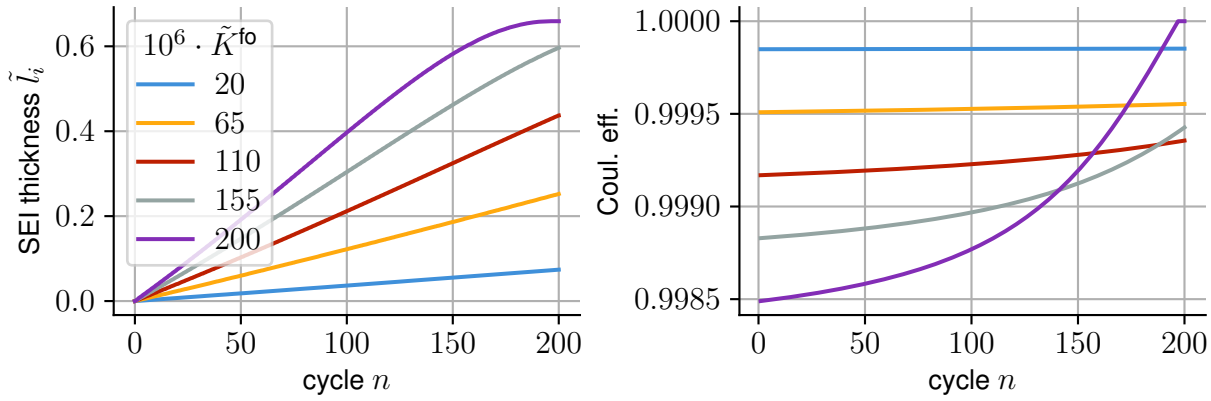

Figure 14: SEI growth for different reaction rate coefficients over 200 cycles of an electrode with a small electrolyte domain $\tilde{l}_{\text{E}}^0 = 1$. As the solvent is depleted, the formation reaction slows down, leading to a higher coulombic efficiency then during earlier cycles.

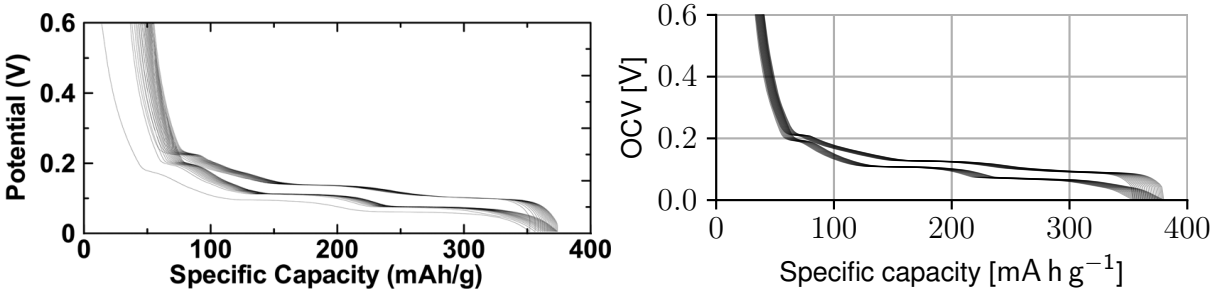

Figure 15: Comparison of experimental data from Smith et al. [61] (left) with computational results (right) based on fitted chemical potential functions.

weight ratio of active material:carbon black:PVDF binder) with 1 M $LiPF_6$ in ethylene carbonate:diethyl carbonate (1:2 v/v) electrolyte, cycled at C/20 and 30°C between 1.2 and 0.005 V. Their measurements demonstrated that SEI growth continues during cycling with the thickness increasing approximately proportional to $\sqrt{t}$, consistent with a parabolic growth law where the growth rate is inversely proportional to SEI thickness.

The cycling behaviour of the resulting model can be seen in fig. 15. It exhibits the shift and widening of the OCV curve in both experimental and numerical results. The simulation is unable to capture the initial formation cycle, where some of the assumptions made, such as the electroneutrality in the SEI, are unlikely to hold. Other degradation phenomena, such as lithium plating, mechanical degradation and electrolyte decomposition, are occurring simultaneously in the experiment, but are not captured in the model.

5 Summary and Conclusion

The growth and evolution of the solid electrolyte interphase (SEI) remains one of the primary factors driving lithium-ion battery degradation. While experimental studies have provided valuable insights into SEI structure and composition, they face inherent limitations due to SEI's nanoscale thickness, dynamic heterogeneity, and sensitivity to operating conditions. This complexity has motivated the development of mathematical models to complement experiments and predict long-term behaviour. This applies both to improved materials and manufacturing processes, but also to optimized charging

and storing conditions that take the SEI growth into account. Zero-dimensional SEI growth models, such as solvent limited (reaction or diffusion limited) and electron limited (migration or interstitial diffusion), capture individual limiting mechanisms but typically represent SEI as an idealised single layer at the electrode surface without resolving internal spatial gradients or explicitly identifying where growth occurs (electrode–SEI or SEI–electrolyte interface). In contrast, our model introduces a continuum-level framework based on non-equilibrium thermodynamics that explicitly resolves the SEI as a distinct domain rather than an interface layer, enabling spatial resolution of transport processes within the SEI itself. The SEI–electrolyte interface is represented as a moving boundary, the SEI is treated as a mixed ion–electron conductor, and the electrolyte reservoir is finite, enabling us to capture solvent consumption as a limiting factor for SEI growth. The general formulation consists of coupled PDEs for each domain, interface conditions between them, and an additional ODE for the SEI thickness. For open-circuit voltage (OCV) conditions, we derived a reduced ODE system with three independent variables: lithium concentration in the active material, solvent concentration, and SEI thickness.

Numerical experiments under charge & rest and cycling scenarios for the reduced model show that SEI growth is primarily governed by formation reaction kinetics and electrolyte reservoir size. Growth profiles such as linear or $\sqrt{t}$ emerge from different parameter values and loading patterns. Two distinct mechanisms for termination of SEI formation are predicted: depletion of active lithium or exhaustion of solvent species. The model also reproduces experimentally observed voltage shifts during cycling, which arise from current consumption by the formation reaction, as well as capacity expansion due to lithium storage within the SEI. Partial cycling shows much higher coulombic efficiency and associated lower SEI growth. The model handles hundreds of cycles, usually terminating when the solvent is depleted. As the solvent concentration decreases, the coulombic efficiency increases as the formation reaction slows down.

While the model successfully reproduces these observations, the current formulation makes several key simplifying assumptions. First, SEI growth is assumed to occur only at the SEI–electrolyte interface, neglecting potential contributions from electrode—SEI interface reactions or bulk SEI evolution. Second, the bulk SEI is represented by a single effective species, whereas experimental evidence indicates a multi-phase mosaic structure with distinct organic and inorganic layers. Third, only one component of the electrolyte is assumed to contribute to the formation reaction, though the framework can be extended to multi-component systems. Fourth, SEI growth is assumed to occur uniformly such that the electrolyte remains a single connected domain. Finally, the model assumes the preexistence of SEI; the initial formation during the first cycle may behave very differently. These simplifications may affect quantitative predictions of mechanical properties, porosity evolution, and the transition between dense inner and porous outer SEI regions. The numerical results presented here are for OCV conditions, which is not a limitation of the general model but rather of the reduced ODE system derived for computational efficiency.

Multiple opportunities for extension and improvement present themselves. For finite C-rates and fast charging, a numerical investigation of the behaviour of the system and its various parameters would be interesting; a follow-up paper is planned. With regard to faster, more practical simulations, homogenisation of the resulting system and integration of SEI growth into common pseudo-2D models is an important step; the manuscript for this approach is under preparation. Lastly, the interaction between SEI and electrode microstructure remains an open problem, e.g. how does SEI grow on non-spherical particles and how does it modify porosity and tortuosity?

In summary, our approach provides a thermodynamically consistent continuum framework that unifies several limiting mechanisms and explicitly accounts for solvent consumption and dynamic interface evolution, establishing a mechanistic foundation for improved lifetime prediction and optimized formation

protocols.

A Reproducibility

The code to reproduce all the figures in the paper, as well as the paper itself, has been published under the DOI 10.5281/zenodo.17952331.

B A Remark on the 1D Leibniz Rule

Consider the 1D PDE

$$\frac{\partial n_\alpha}{\partial t} = -\partial_x j_\alpha \qquad x \in [0, \ell(t)]\,, \tag{191}$$

$$+j_\alpha|_0 = R^1_\alpha\,, \tag{192}$$

$$-(j_\alpha - n_\alpha w)|_\ell = R^2_\alpha \quad \Rightarrow \quad j_\alpha = -R^2_\alpha + n_\alpha w\,, \tag{193}$$

where $w = \frac{\mathrm{d}\ell}{\mathrm{d}t}$. The 1D-Leibniz rule thus yields

$$\frac{\mathrm{d}}{\mathrm{d}t}\left(\int_0^{\ell(t)} n_\alpha(x,t)\ \mathrm{d}x\right) = n_\alpha(\ell(t),t)\frac{\mathrm{d}\ell}{\mathrm{d}t} + \int_0^{\ell(t)} \frac{\partial}{\partial t} n_\alpha(x,t)\ \mathrm{d}x\,. \tag{194}$$

Hence we obtain for

$$\int_0^{\ell(t)} \frac{\partial}{\partial t} n_\alpha(x,t)\,dx = -\int_0^{\ell(t)} \partial_x j_\alpha\,dx = j_\alpha|_{\mathtt{A}} - j_\alpha|_{\mathtt{SEI}} = R^1_\alpha + R^2_\alpha - n_\alpha w\,, \tag{195}$$

whereby

$$\frac{\mathrm{d}}{\mathrm{d}t}\Big(\int_0^{\ell(t)} n_\alpha(x,t)\ \mathrm{d}x\Big) = n_\alpha \cdot w + R^1_\alpha + R^2_\alpha - n_\alpha w = R^1_\alpha + R^2_\alpha\,. \tag{196}$$

A frequent quantity of interest is the mean value of some quantity. Consider thus

$$\bar{n}_\alpha := \frac{1}{\ell(t)}\int_0^{\ell(t)} n_\alpha(x,t)\ \mathrm{d}x\,, \tag{197}$$

for which we have

$$\frac{\mathrm{d}\bar{n}_\alpha}{\mathrm{d}t} = -\frac{\bar{n}_\alpha}{\ell(t)}\frac{\mathrm{d}\ell}{\mathrm{d}t} + \frac{1}{\ell(t)}\frac{\mathrm{d}}{\mathrm{d}t}\int_0^{\ell(t)} n_\alpha(x,t)\ \mathrm{d}x\,, \tag{198}$$

$$= -\frac{\bar{n}_\alpha}{\ell(t)}\frac{\mathrm{d}\ell}{\mathrm{d}t} + \frac{1}{\ell}(R^1_\alpha + R^2_\alpha)\,, \tag{199}$$

$$= \frac{1}{\ell(t)}\big(R^1_\alpha + R^2_\alpha - \bar{n}_\alpha w\big)\,. \tag{200}$$

Note that for $\bar{n} = \sum_\beta \bar{n}_\beta$ we obtain

$$\frac{\mathrm{d}\bar{n}}{\mathrm{d}t} = \frac{1}{\ell(t)}\big(\underbrace{\sum_\beta R^1_\beta}_{=:R^1} + \underbrace{\sum_\beta R^2_\beta}_{=:R^2} - \bar{n}w\big)\,. \tag{201}$$

Further quantities of interest are $y_\alpha = \frac{n_\alpha}{n}$ and $\bar{y}_\alpha$, which are somewhat ambigous to define. Consider

$$\bar{y}_\alpha := \frac{\bar{n}_\alpha}{\bar{n}}\,, \tag{202}$$

for which we can deduce

$$\begin{aligned}
\frac{\mathrm{d}}{\mathrm{d}t}\bar{y}_\alpha &= \frac{1}{\bar{n}}\frac{\mathrm{d}}{\mathrm{d}t}\bar{n}_\alpha - \frac{\bar{y}_\alpha}{\bar{n}}\frac{\mathrm{d}}{\mathrm{d}t}\bar{n}\,, && (203)\\
&= \frac{1}{\bar{n}}\frac{1}{\ell(t)}\big(R^1_\alpha + R^2_\alpha - \bar{n}_\alpha w\big) - \frac{\bar{y}_\alpha}{\bar{n}}\frac{1}{\ell(t)}\big(R^1 + R^2 - \bar{n}w\big)\,, && (204)\\
&= \frac{1}{\bar{n}}\frac{1}{\ell(t)}\big((R^1_\alpha - \bar{y}_\alpha R^1) + (R^2_\alpha - \bar{y}_\alpha R^2) - (\bar{n}_\alpha - \bar{y}_\alpha\bar{n})w\big)\,, && (205)\\
&= \frac{1}{\bar{n}}\frac{1}{\ell(t)}\big((R^1_\alpha - \bar{y}_\alpha R^1) + (R^2_\alpha - \bar{y}_\alpha R^2)\big)\,. && (206)
\end{aligned}$$

C List of Symbols

n_{ψ_α}	$\mathrm{mol\,m^{-3}}$	molar concentration of species α in phase ψ
$n_{\psi,\mathrm{tot}}$	$\mathrm{mol\,m^{-3}}$	total molar concentration in phase ψ
y_{ψ_α}	–	molar fraction of species α in phase ψ
g_{ψ_α}	J	Gibbs energy of species α in phase ψ
v_{ψ_α}	$\mathrm{m^3\,mol^{-1}}$	molar volume of species α in phase ψ
p_ψ	Pa	pressure in the phase ψ
p_{ref}	Pa	reference pressure
q_{E}	$\mathrm{C\,m^{-3}}$	charge density
e_0	C	elementary charge
k_{B}	$\mathrm{J\,K^{-1}}$	Boltzmann constant
T	K	temperature
z_α	–	charge number
$\boldsymbol{t}_{\mathrm{E}_C}$	–	cation transfer number
$\mathbf{v}$	$\mathrm{m\,s^{-1}}$	velocity
m_α	$\mathrm{kg\,mol^{-1}}$	molar mass
$\boldsymbol{J}_{\psi_\alpha}$	$\mathrm{mol\,m^{-2}\,s^{-1}}$	diffusive flux of α in ψ
$\boldsymbol{M}_{\alpha,\beta}$	$\mathrm{mol^2\,J^{-1}\,m^{-1}\,s^{-1}}$	mobility coefficients ?
$\boldsymbol{D}_{\alpha,\beta}$	$\mathrm{m^2\,s^{-1}}$	self-diffusion coefficients
$\boldsymbol{F}_{\alpha,\beta}$	$\mathrm{m^2\,s^{-1}}$	self-diffusion coefficients
$\boldsymbol{D}^{\mathrm{eff}}_{\psi_e}$	$\mathrm{m^2\,s^{-1}}$	effective diffusion coefficient
$\boldsymbol{D}^{0}_{\mathrm{A}}$	$\mathrm{m^2\,s^{-1}}$	diffusion coefficient in the active phase
$\boldsymbol{S}^{\mathrm{eff}}_{\psi_C}$	$\mathrm{C\,m^{-2}\,s^{-1}}$	effective conductivity parameter
μ_α	J	chemical potential of species α
φ_ψ	V	electric potential in the phase ψ
$\hat{\mu}_{\psi_\alpha}$	J	chemical potential for species α in phase ψ
Γ_ψ	–	thermodynamic factor
$\boldsymbol{\Lambda}_E$	$\mathrm{S\,m^{-1}}$	molar conductivity of the electrolyte
$\lambda^{\mathrm{in}}_{\mathrm{IE}}$, $\lambda^{\mathrm{fo}}_{\mathrm{IE}}$, $\lambda^{\mathrm{in}}_{\mathrm{AI}}$	J	surface affinity at the interfaces
$\boldsymbol{\sigma}^{\mathrm{eff}}_{\psi}$	$\mathrm{S\,m^{-1}}$	effective conductivity of phase ψ
$\boldsymbol{\sigma}_{\mathrm{A}}$	$\mathrm{S\,m^{-1}}$	conductivity of the active phase
γ_{A}	–	interaction parameter ?
ρ	$\mathrm{kg\,m^{-3}}$	density
χ	–	dielectric susceptibility
ψ	$\mathrm{J\,kg^{-1}}$	specific free energy
σ	$\mathrm{J\,K^{-1}\,m^{-3}\,s^{-1}}$	entropy production

References

[1] S. J. An et al. “The state of understanding of the lithium-ion-battery graphite solid electrolyte interphase (SEI) and its relationship to formation cycling”. In: *Carbon* 105 (2016), pp. 52–76. DOI: 10.1016/j.carbon.2016.04.008.

[2] P. M. Attia, W. C. Chueh, and S. J. Harris. “Revisiting the $t^{0.5}$ dependence of SEI growth”. In: *Journal of The Electrochemical Society* 167.9 (2020), p. 090535. DOI: 10.1149/1945-7111/ab8ce4.

[3] P. M. Attia, S. J. Harris, and W. C. Chueh. “Benefits of fast battery formation in a model system”. In: *Journal of The Electrochemical Society* 168.5 (2021), p. 050543. DOI: 10.1149/1945-7111/abff35.

[4] P. M. Attia et al. “Electrochemical Kinetics of SEI Growth on Carbon Black: Part I. Experiments”. In: *Journal of The Electrochemical Society* 166.4 (2019), E97–E106. DOI: 10.1149/2.0231904jes.

[5] D. Aurbach. “Review of selected electrode–solution interactions which determine the performance of Li and Li ion batteries”. In: *Journal of Power Sources* 89.2 (2000), pp. 206–218. DOI: 10.1016/S0378-7753(00)00431-6.

[6] C. R. Birkl et al. “Degradation diagnostics for lithium ion cells”. In: *Journal of Power Sources* 341 (2017), pp. 373–386. DOI: 10.1016/j.jpowsour.2016.12.011.

[7] F. Brosa Planella et al. “A continuum of physics-based lithium-ion battery models reviewed”. In: *Progress in Energy* 4.4 (2022), p. 042003. DOI: 10.1088/2516-1083/ac7d31.

[8] F. Degen and O. Krätzig. “Modelling large scale manufacturing of automotive battery cells–Impact of new technologies on production economies”. In: *Available at SSRN 4019171* (2021). DOI: 10.2139/ssrn.4019171.

[9] D. Diddens et al. “Modeling the solid electrolyte interphase: Machine learning as a game changer?” In: *Advanced Materials Interfaces* 9.8 (2022), p. 2101734. DOI: 10.1002/admi.202101734.

[10] W. Dreyer, C. Guhlke, and M. Landstorfer. “A Mixture Theory of Electrolytes Containing Solvation Effects”. In: *Electrochemistry Communications* 43 (2014), pp. 75–78. DOI: 10.1016/j.elecom.2014.03.015.

[11] W. Dreyer et al. “New insights on the interfacial tension of electrochemical interfaces and the Lippmann equation”. In: *European Journal of Applied Mathematics* 29.4 (2018), pp. 708–753. DOI: 10.1017/S0956792517000341.

[12] W. Dreyer, C. Guhlke, and R. Müller. “Bulk-Surface Electrothermodynamics and Applications to Electrochemistry”. In: *Entropy* 20.12 (2018), p. 939. DOI: 10.3390/e20120939.

[13] W. Dreyer, C. Guhlke, and R. Müller. “A new perspective on the electron transfer: recovering the Butler-Volmer equation in non-equilibrium thermodynamics”. In: *Physical Chemistry Chemical Physics* 18 (2016), pp. 24966–24983. DOI: 10.1039/C6CP04142F.

[14] W. Dreyer, C. Guhlke, and R. Müller. “Modeling of electrochemical double layers in thermodynamic non-equilibrium”. In: *Physical Chemistry Chemical Physics* (2015), pp. 27176–27194. DOI: 10.1039/C5CP03836G.

[15] W. Dreyer, C. Guhlke, and R. Müller. “Overcoming the shortcomings of the Nernst-Planck model”. In: *Physical Chemistry Chemical Physics* 15 (2013), pp. 7075–7086. DOI: 10.1039/C3CP44390F.

[16] F. Duffner et al. “Large-scale automotive battery cell manufacturing: Analyzing strategic and operational effects on manufacturing costs”. In: *International Journal of Production Economics* 232 (2021), p. 107982. DOI: 10.1016/j.ijpe.2020.107982.

[17] J. S. Edge et al. “Lithium ion battery degradation: what you need to know”. In: *Physical Chemistry Chemical Physics* 23.14 (2021), pp. 8200–8221. DOI: 10.1039/d1cp00359c.

[18] H. Ekström and G. Lindbergh. “A Model for Predicting Capacity Fade due to SEI Formation in a Commercial Graphite/$LiFePO_4$ Cell”. In: *Journal of The Electrochemical Society* 162.6 (2015), A1003–A1007. DOI: 10.1149/2.0641506jes.

[19] T. F. Fuller, M. Doyle, and J. Newman. “Simulation and Optimization of the Dual Lithium Ion Insertion Cell”. In: *Journal of The Electrochemical Society* 141.1 (1994), pp. 1–10. DOI: 10.1149/1.2054684.

[20] Y. Gao and B. Zhang. “Probing the mechanically stable solid electrolyte interphase and the implications in design strategies”. In: *Advanced Materials* 35.18 (2023), p. 2205421. DOI: 10.1002/adma.202205421.

[21] M. Gauthier et al. “Electrode–electrolyte interface in Li-ion batteries: current understanding and new insights”. In: *The Journal of Physical Chemistry Letters* 6.22 (2015), pp. 4653–4672. DOI: 10.1021/acs.jpclett.5b01727.

[22] S. de Groot and P. Mazur. *Non-Equilibrium Thermodynamics*. Dover Publications, 1984.

[23] C. Guhlke. “Theorie der elektrochemischen Grenzfläche”. PhD thesis. TU Berlin, 2015. DOI: 10.14279/depositonce-4342.

[24] A. A. Habib et al. “Lithium-ion battery management system for electric vehicles: constraints, challenges, and recommendations”. In: *Batteries* 9.3 (2023), p. 152. DOI: 10.3390/batteries9030152.

[25] S. K. Heiskanen, J. Kim, and B. L. Lucht. “Generation and evolution of the solid electrolyte interphase of lithium-ion batteries”. In: *Joule* 3.10 (2019), pp. 2322–2333. DOI: 10.1016/j.joule.2019.08.018.

[26] M. Herstedt et al. “X-ray photoelectron spectroscopy of negative electrodes from high-power lithium-ion cells showing various levels of power fade”. In: *Electrochimica Acta* 49.28 (2004), pp. 5097–5110. DOI: 10.1016/j.electacta.2004.06.021.

[27] W.-C. Huang, Q. Zhang, and F. You. “Impacts of battery energy storage technologies and renewable integration on the energy transition in the New York State”. In: *Advances in Applied Energy* 9 (2023), p. 100126. DOI: 10.1016/j.adapen.2023.100126.

[28] J. Newman, K. Thomas. *Electrochemical Systems*. John Wiley & Sons, 2014.

[29] N. Kamyab, J. W. Weidner, and R. E. White. “Mixed mode growth model for the solid electrolyte interface (SEI)”. In: *Journal of The Electrochemical Society* 166.2 (2019), A334. DOI: 10.1149/2.1101902jes.

[30] P. Keil et al. “Calendar aging of lithium-ion batteries”. In: *Journal of The Electrochemical Society* 163.9 (2016), A1872. DOI: 10.1149/2.0411609jes.

[31] L. Köbbing, A. Latz, and B. Horstmann. “Growth of the solid-electrolyte interphase: Electron diffusion versus solvent diffusion”. In: *Journal of Power Sources* 561 (2023), p. 232651. DOI: 10.1016/j.jpowsour.2023.232651.

[32] L. von Kolzenberg, A. Latz, and B. Horstmann. “Solid–electrolyte interphase during battery cycling: Theory of growth regimes”. In: *ChemSusChem* 13.15 (2020), pp. 3901–3910. DOI: 10.1002/cssc.202000867.

[33] L. von Kolzenberg et al. “A four parameter model for the solid-electrolyte interphase to predict battery aging during operation”. In: *Journal of Power Sources* 539 (2022), p. 231560. DOI: 10.1016/j.jpowsour.2022.231560.

[34] M. Landstorfer, C. Guhlke, and W. Dreyer. “Theory and structure of the metal-electrolyte interface incorporating adsorption and solvation effects”. In: *Electrochimica Acta* 201 (2016), pp. 187–219. DOI: 10.1016/j.electacta.2016.03.013.

[35] M. Landstorfer. “A Discussion of the Cell Voltage during Discharge of an Intercalation Electrode for Various C-Rates Based on Non-Equilibrium Thermodynamics and Numerical Simulations”. In: *Journal of The Electrochemical Society* 167.1 (2019), p. 013518. DOI: 10.1149/2.0182001jes.

[36] M. Landstorfer. “Boundary Conditions for Electrochemical Interfaces”. In: *Journal of The Electrochemical Society* 164.11 (2017), E3671–E3685. DOI: 10.1149/2.0641711jes.

[37] M. Landstorfer et al. “A modelling framework for efficient reduced order simulations of parametrised lithium-ion battery cells”. In: *European Journal of Applied Mathematics* 34.3 (2023), pp. 554–591. DOI: 10.1017/s0956792522000353.

[38] R. Li et al. “Modelling solvent consumption from SEI layer growth in lithium-ion batteries”. In: *Journal of The Electrochemical Society* 169.6 (2022), p. 060516. DOI: 10.1149/1945-7111/ac6f84.

[39] X. Lin et al. “A comprehensive capacity fade model and analysis for Li-ion batteries”. In: *Journal of The Electrochemical Society* 160.10 (2013), A1701. DOI: 10.1149/2.040310jes.

[40] J. Liu and L.-W. Fan. “Atomistic insights into the thermal transport properties of inorganic components of solid electrolyte interphase (SEI) in lithium-ion batteries”. In: *International Journal of Heat and Mass Transfer* 221 (2024), p. 125069. DOI: 10.1016/j.ijheatmasstransfer.2023.125069.

[41] J. Liu et al. “Aging behavior and mechanisms of lithium-ion battery under multi-aging path”. In: *Journal of Cleaner Production* 423 (2023), p. 138678. DOI: 10.1016/j.jclepro.2023.138678.

[42] K. Manmi et al. “A Comparison of Standard SEI Growth Models in the Context of Battery Formation”. In: *Journal of The Electrochemical Society* 171.10 (2024), p. 100530. DOI: 10.1149/1945-7111/ad8548.

[43] S. G. Marquis. “Long-term degradation of lithium-ion batteries”. PhD thesis. Oxford University, 2020.

[44] J. D. McBrayer et al. “Mechanical studies of the solid electrolyte interphase on anodes in lithium and lithium ion batteries”. In: *Nanotechnology* 32.50 (2021), p. 502005. DOI: 10.1088/1361-6528/ac17fe.

[45] I. Müller. *Thermodynamics*. Pitman, 1985.

[46] R. Müller and M. Landstorfer. “Galilean Bulk-Surface Electrothermodynamics and Applications to Electrochemistry”. In: *Entropy* 25.3 (2023). DOI: 10.3390/e25030416.

[47] J. Newman. “The Polarized Diffuse Double Layer”. In: *Transactions of the Faraday Society* (1965). DOI: 10.1039/TF9656102229.

[48] A. Örüm Aydin et al. “Lithium-Ion Battery Manufacturing: Industrial View on Processing Challenges, Possible Solutions and Recent Advances”. In: *Batteries* 9.11 (2023), p. 555. DOI: 10.3390/batteries9110555.

[49] G. Pasini, G. Lutzemberger, and L. Ferrari. “Renewable electricity for decarbonisation of road transport: batteries or E-fuels?” In: *Batteries* 9.2 (2023), p. 135. DOI: 10.3390/batteries9020135.

[50] E. Peled, D. Golodnitsky, and G. Ardel. “Advanced model for solid electrolyte interphase electrodes in liquid and polymer electrolytes”. In: *Journal of the Electrochemical Society* 144.8 (1997), p. L208. DOI: 10.1149/1.1837858.

[51] E. Peled and S. Menkin. “Review—SEI: Past, Present and Future”. In: *Journal of The Electrochemical Society* 164.7 (2017), A1703–A1719. DOI: 10.1149/2.1441707jes.

[52] M. B. Pinson and M. Z. Bazant. “Theory of SEI Formation in Rechargeable Batteries: Capacity Fade, Accelerated Aging and Lifetime Prediction”. In: *Journal of The Electrochemical Society* 160.2 (2012), A243–A250. DOI: 10.1149/2.044302jes.

[53] F. B. Planella and W. D. Widanage. “A Single Particle Model with Electrolyte and Side Reactions for degradation of lithium-ion batteries”. In: *Applied Mathematical Modelling* 121 (2023), pp. 586–610. DOI: 10.1016/j.apm.2022.12.009.

[54] T. Rahman and T. Alharbi. “Exploring lithium-Ion battery degradation: A concise review of critical factors, impacts, data-driven degradation estimation techniques, and sustainable directions for energy storage systems”. In: *Batteries* 10.7 (2024), p. 220. DOI: 10.3390/batteries10070220.

[55] P. Ramadass et al. “Development of First Principles Capacity Fade Model for Li-Ion Cells”. In: *Journal of The Electrochemical Society* 151.2 (2004), A196. DOI: 10.1149/1.1634273.

[56] M. Safari et al. “Multimodal Physics-Based Aging Model for Life Prediction of Li-Ion Batteries”. In: *Journal of The Electrochemical Society* 156.3 (2008), A145. DOI: 10.1149/1.3043429.

[57] A. Sanfeld. *Introduction to the thermodynamics of charged and polarized layers*. Wiley, 1968.

[58] F. Schomburg et al. “Characterization of the solid–electrolyte interphase growth during cell formation based on differential voltage analysis”. In: *Energy Technology* 11.5 (2023), p. 2200688. DOI: 10.1002/ente.202200688.

[59] F. Single, B. Horstmann, and A. Latz. “Revealing SEI morphology: in-depth analysis of a modeling approach”. In: *Journal of The Electrochemical Society* 164.11 (2017), E3132. DOI: 10.1149/2.0121711jes.

[60] F. Single, A. Latz, and B. Horstmann. “Identifying the mechanism of continued growth of the solid–electrolyte interphase”. In: *ChemSusChem* 11.12 (2018), pp. 1950–1955. DOI: 10.1002/cssc.201800077.

[61] A. J. Smith et al. “A High Precision Coulometry Study of the SEI Growth in Li/Graphite Cells”. In: *Journal of The Electrochemical Society* 158.5 (2011), A447. DOI: 10.1149/1.3557892.

[62] M. Tang, S. Lu, and J. Newman. “Experimental and theoretical investigation of solid-electrolyte-interphase formation mechanisms on glassy carbon”. In: *Journal of The Electrochemical Society* 159.11 (2012), A1775. DOI: 10.1149/2.025211jes.

[63] L. Timilsina et al. “Battery degradation in electric and hybrid electric vehicles: A survey study”. In: *IEEE Access* 11 (2023), pp. 42431–42462. DOI: 10.1109/access.2023.3271287.

[64] P. Verma, P. Maire, and P. Novák. “A Review of the Features and Analyses of the Solid Electrolyte Interphase in Li-ion Batteries”. In: *Electrochimica Acta* 55.22 (2010), pp. 6332–6341. DOI: 10.1016/j.electacta.2010.05.072.

[65] J. Vetter et al. “Ageing mechanisms in lithium-ion batteries”. In: *Journal of Power Sources* 147.1-2 (2005), pp. 269–281. DOI: 10.1016/j.jpowsour.2005.01.006.

[66] A. Wang et al. “Review on modeling of the anode solid electrolyte interphase (SEI) for lithium-ion batteries”. In: *NPJ Computational materials* 4.1 (2018), p. 15. DOI: 10.1038/s41524-018-0064-0.

[67] Y. Wang et al. “Theoretical studies to understand surface chemistry on carbon anodes for lithium-ion batteries: reduction mechanisms of ethylene carbonate”. In: *Journal of the American Chemical Society* 123.47 (2001), pp. 11708–11718. DOI: 10.1021/ja017073i.

[68] P. J. Weddle et al. “Continuum-level modeling of Li-ion battery SEI by upscaling atomistically informed reaction mechanisms”. In: *Electrochimica Acta* 468 (2023), p. 143121. DOI: 10.1016/j.electacta.2023.143121.

[69] D. L. Wood, J. Li, and S. J. An. “Formation challenges of lithium-ion battery manufacturing”. In: *Joule* 3.12 (2019), pp. 2884–2888. DOI: 10.1016/j.joule.2019.11.002.

[70] H. Wu et al. “Recent progress in understanding solid electrolyte interphase on lithium metal anodes”. In: *Advanced Energy Materials* 11.5 (2021), p. 2003092. DOI: 10.1002/aenm.202003092.

[71] J. Wu et al. “Understanding solid electrolyte interphases: Advanced characterization techniques and theoretical simulations”. In: *Nano Energy* 89 (2021), p. 106489. DOI: 10.1016/j.nanoen.2021.106489.

[72] R. Xiong et al. “Lithium-ion battery aging mechanisms and diagnosis method for automotive applications: Recent advances and perspectives”. In: *Renewable and Sustainable Energy Reviews* 131 (2020), p. 110048. DOI: 10.1016/j.rser.2020.110048.

[73] X.-G. Yang et al. “Modeling of lithium plating induced aging of lithium-ion batteries: Transition from linear to nonlinear aging”. In: *Journal of Power Sources* 360 (2017), pp. 28–40. DOI: 10.1016/j.jpowsour.2017.05.110.

[74] H.-L. Zhang et al. “New Insight into the Solid Electrolyte Interphase with Use of a Focused Ion Beam”. In: *The Journal of Physical Chemistry B* 109.47 (2005), pp. 22205–22211. DOI: 10.1021/jp053311a.